UNIVERSITEIT VAN PRETORIA
UNIVERSITY OF PRETORIA
YUNIBESITHI YA PRETORIA

Stearate intercalated layered double hydroxides: methods and applications

by

Edith Phyllis Landman

Submitted in partial fulfilment of the requirements for the degree

Philosophiae Doctor

in the Faculty of Natural and Agricultural Sciences, University of Pretoria

May 2005

Declaration

I, Edith Phyllis Landman, declare that this thesis is my own work, except where specifically acknowledged in the text. I also declare that neither this thesis nor any part thereof has been submitted by me for degree purposes at any other university.

……..

E.P. Landman

Acknowledgements

My sincerest thanks go to the following people:

- Prof. W.W. Focke, for his guidance and trust in my abilities.
- My loving husband, Andreas Landman, for reading all my articles and thesis, helping with fine-tuning and for putting up with my moods when things went wrong.
- Pravina Maharaj, for doing administrative tasks on my behalf, keeping my hands free to do the research.
- Mila Maksa, for doing so many thermal analyses.
- Maria Atanasova, and the Council for Geoscience (South Africa) for the X-ray diffraction analyses.
- Bram Dekkers, for making some films and doing paper coating experiments.
- Ndebo Mokaloba, for doing some intercalation experiments.
- This work was supported by a grant from the Technology and Human Resources for Industry Programme (THRIP); a partnership programme funded by the Department of Trade and Industry (DTI) and managed by the National Research Foundation (NRF).
- The financial assistance of the Department of Labour (DoL) towards this research is hereby acknowledged. Opinions expressed and conclusions arrived at, are those of the author and are not necessarily to be attributed to the Department of Labour.
- The author also wishes to thank African Products (Pty) Ltd and the University of Pretoria for financial support.

Abstract

Stearate anions were successfully intercalated into the layered double hydroxide $Mg_4Al_2(OH)_{12}CO_3{\cdot}3H_2O$ (LDH-CO_3) by several methods to form LDH-SA. The intercalation method which involved the acid-base reaction between emulsified stearic acid (SA) and the carbonate anions in aqueous media was studied for the first time. This method led to the formation of more LDH-SA than well known methods such as melting the carboxylic acid in the presence of the LDH, allowing the interlayer region to swell in the presence of glycerol and reconstructing the calcined LDH in the presence of aqueous sodium stearate. Other literature methods involve ion-exchange of Cl^- in LDH-Cl with stearate in aqueous sodium stearate, usually under N_2 atmosphere. The methods developed in this study are more industrially viable because the more easily produced LDH-CO_3 is used and no N_2 atmosphere is necessary.

The LDH-SA was successfully used to intercalate sodium polyvinyl sulphonate by an ion exchange with the intercalated stearate, without the need for a N_2 atmosphere. This method of production could be useful for the production of nanocomposites in general, for example anionic polymer chains (such as DNA) and anionic clays.

The same intercalation reaction was allowed to take place *in situ* during the formation of dextrin-alginate-glycerol film solutions in water-ethanol media. The stearate intercalated as a bilayer in the interlayer region of the LDH. The SA to LDH ratio was varied from 100% SA to 100% LDH. Around the middle of the series a minimum water vapour permeability (WVP) was obtained, which corresponded to an 80% reduction in WVP in comparison to the reference (blank) film. Around the middle of the series a maximum increase in Young's modulus, corresponding to a 213% increase in comparison to the blank film, was obtained. Around the middle of the series a reduction in the intensity of the basal reflection and interlayer distance showed that some exfoliation (delamination) took place.

Samevatting

Verskeie metodes om stearaatione tussen die hidroksiedlae van $Mg_4Al_2(OH)_{12}CO_3{\cdot}3H_2O$ (LDH-CO_3) te laat inskuif, was getoets. Die metode wat gebaseer is op die suur-basis inskuifreaksie tussen geemulgeerde stariensuur (SA) en die karbonaatanione in watermedium is vir die eerste keer getoets. Hierdie metode het gelei tot die vorming van meer LDH-SA as welbekende metodes soos smelting van die karboksielsuur in die teenwoordigheid van die LDH, die swelling van die interlaagruimte deur middel van gliserol asook die herkonstruksie van die gekalsineerde LDH in die teenwoordigheid van waterige natriumstearaat. Ander literatuurmetodes behels die ioonuitruiling van die Cl^- van LDH-Cl met stearaat in waterige natriumstearaat, gewoonlik onder `n stikstofatmosfeer. Die metodes wat tydens hierdie studie ontwikkel is, is meer industrieel toepasbaar omdat die maklik produseerbare LDH-CO_3 benut word en ook geen stikstofatmosfeer vereis word nie.

Die LDH-SA is suksesvol aangewend om die inskuif van natriumpolivinielsulfonaat te bewerkstellig deur `n ioonuitruilmeganisme met die geinterkaleerde stearaatione, sonder dat `n stikstofatmosfeer benodig is. Hierdie metode kan in die algemeen aangewend word om nano-saamgestelde materiale te vervaardig vanuit enige anioniese polimeer (bv. DNS) en anioniese kleie.

Dieselfde inskuifreaksie is toegelaat om plaas te vind tydens die vorming van `n dekstrien-alginaat-gliserol gebaseerde filmvormende oplossing in `n water-etanol medium. `n Dubbellaag stearaat het in die LDH tussenlaagruimte ingeskuif. Die hoeveelheid SA tot LDH was gevarieer van 100% SA tot 100% LDH. `n 80% verlaging in waterdamp permeabiliteit was verkry in die middel van die reeks in vergelyking met die verwysingsfilm (kontrole). In daardie omgewing is ook `n maksimum toename in Young's modulus van ongeveer 213% van die kontrole film waargeneem asook `n daling in die intensiteit van die basale refleksie en interlaagafstand, wat aandui dat die LDH-SA in `n mate ontblaar het.

1 Corinthians 2:2

For I determined not to know any thing among you, save Jesus Christ, and him crucified.

1 Corinthians 1:17-21

For Christ sent me not to baptize, but to preach the gospel: not with wisdom of words, lest the cross of Christ should be made of none effect. For the preaching of the cross is to them that perish foolishness; but unto us which are saved it is the power of God. For it is written, I will destroy the wisdom of the wise, and will bring to nothing the understanding of the prudent. Where *is* the wise? where *is* the scribe? where *is* the disputer of this world? hath not God made foolish the wisdom of this world? For after that in the wisdom of God the world by wisdom knew not God, it pleased God by the foolishness of preaching to save them that believe.

Table of Contents

List of Figures

List of Tables

List of Equations

Nomenclature and Abbreviations as used by the Author

Term	Abbreviation	Explanation
Hydrotalcite	HT	The layered double hydroxide of composition $Mg_6Al_2(OH)_{16}CO_3.4H_2O$.
Layered double hydroxide	LDH	Anionic clay minerals consisting of $Mg(OH)_2$ like layers which contains both divalent and trivalent cations in different ratios.
Interlayer		The region between the two hydroxide layers in which the charge balancing anions and crystal water lie.
Sand-rose morphology		Particles consisting of many intergrown smaller particulates which reduce the surface area.
Intercalation		Process in which atoms, ions or molecules are trapped between layers in a crystal lattice without the formation of a formal chemical bond [1].
Intercalate (verb)		Diffusion of atoms, ions or molecules into the interlayer region of a layered compound.
Intercalate (noun) or Intercalation compound		A compound in which atoms, ions or molecules are trapped between layers in a crystal lattice [1].
Adsorption		Formation of (a) layer(s) of gaseous, liquid or solid molecules on the surface of a molecule, held by chemical or physical forces [1].
Stearic acid	SA	A solid saturated fatty acid, $CH_3(CH_2)_{16}COOH$ [1].
Carboxylic acid		Organic compounds containing the group –COOH [1].

Fatty acid	FA	An organic compound consisting of a hydrocarbon chain and a terminal carboxyl group [1].
Ion exchange		The exchange of ions of the same charge between a solution and a solid in contact with it [1].
Anionic exchange capacity	AEC	The amount of exchangeable anions available within the crystal structure of an adsorbent material, expressed in mmol/g or mmol/100 g adsorbent.
Brønsted acid/base		A Brønsted-Lowry acid is a substance that donates a proton and a Brønsted-Lowry base is a substance that accepts a proton [2].
Lewis acid/base		A Lewis acid is a substance that accepts an electron pair, and a Lewis base is a substance that donates an electron pair [2].
Carbonate layered double hydroxide	LDH-CO_3	A layered double hydroxide into which the carbonate anion has intercalated.
Chloride layered double hydroxide	LDH-Cl	A layered double hydroxide into which the chloride anion has intercalated.
Stearate layered double hydroxide	LDH-SA	A layered double hydroxide into which the stearate anion has intercalated.
Emulsion		A kinetically stable dispersion of two immiscible liquids, stabilized by the presence of a surfactant at the interface.
Emulsifier		A surfactant that resides at the interface of two immiscible liquids in order to stabilize the mixture of the two liquids.

Micro-emulsion		A thermodynamically stable mixture of two immiscible liquids, stabilized by a high concentration of surfactant and a co-surfactant.
Surfactant		Molecules with both hydrophilic and hydrophobic parts.
Sodium dodecyl sulfate	SDS	An anionic surfactant, $CH_3(CH_2)_{11}SO_4Na$
Calcine		Heat a substance to an elevated temperature to facilitate a reaction, for example decomposition reaction. In the case of the LDHs used in this study, the calcination facilitates the dehydration, decarbonation and dehydroxilation reactions which can collectively be described as decomposition reactions.
Reconstruction		Rehydration of a calcined LDH in the presence of an aqueous solution of an anion.
Layered double oxide	LDO	Calcined LDH.
Poly(sodium vinylsulfonate)	PVS	The sodium salt of a polymer consisting of vinyl sulfonic acid monomeric units.
Polyanion or anionic polymer		A polymer consisting of anionic (negatively charged) monomeric units.
Polyelectrolyte		A polymer consisting of positively or negatively charged monomers
Cross linkage		A short side chain of atoms (or a charged moiety) linking two longer chains in a polymeric material [1].
Sodium alginate		The sodium salt of alginic acid, a polysaccharide occurring in the cell walls of brown algae [1].

Dextrin	An intermediate polysaccharide resulting from the hydrolysis of starch by amylase enzymes or acids [1].
Polysaccharide	Polymers consisting of long chains of monosaccharide (simple-sugar) molecules [1].
Plasticizer	Materials incorporated into plastic resins to change workability, flexibility, flow and impact resistance [3], for example glycerol.
Glycerol	1,2,3-trihydroxypropane, used as a plasticizer in thermoplastic starch [3].
Defoamer	A substance (usually petroleum oil based) that prevents a surfactant from creating foam in a mixture.
Filler	Solid inert material added to a polymeric matrix to change its physical properties or to dilute it for economy [1].
Composite material	A material consisting of two or more substances.
Nanocomposite	A composite material in which one of the constituents have at least one dimension which is lower than 100 nm.
Foliate	With regard to polymer chains or layered compounds, whereby polymer chains line up or the individual layers are stacked together.
Exfoliate	Polymer chains or individual inorganic layers that are dispersed randomly within a composite.

Exfoliation		Process whereby polymer chains that were aligned or stacked inorganic layers are pushed apart into a random pattern.
Viscosity		A measure of the resistance to flow that a fluid offers when it is subjected to shear stress [1].
Water vapour permeability	WVP	The mass of water vapour that moves through a film of certain thickness per unit time, unit area and unit difference in water vapour pressure.
Young's modulus		Synonym for the modulus of elasticity, namely the ratio of the unit stress to the unit strain [4].
Tensile strength		Synonym for ultimate strength, namely the maximum ordinate to the stress-strain curve [4].
Percentage strain (elongation) at break		The increase in length of the gage after fracture divided by the initial gage length and multiplied by 100 [4].
Retrogradation		A process which happens during the ageing of starch in which the starch chains lose water and form intermolecular hydrogen bonds.
Crystalline		Used to indicate that a chemical species has long-range structure.
Amorphous		Used to indicate that a chemical species does not have long-range structure. This does, however, not preclude the existence of short-range structure.
X-ray diffraction	XRD	Diffraction of X-rays by a crystal due to the comparable size of the wavelengths of X-rays and the distances between atoms in crystals [1].

X-ray fluorescence	XRF	The emission of X-rays from excited atoms produced by the impact of high-energy electrons, particles or a primary beam of X-rays. The wavelengths of the fluorescent X-rays are measured by an X-ray spectrometer as a means of chemical analysis [1].
Scanning electron microscopy	SEM	A beam of primary electrons scans the specimen surface and those that are reflected, together with secondary electrons emitted, are collected to form a visual image [1].
Transmission electron microscopy	TEM	A sharply focused electron beam passes through a thin section of metal-coated specimen onto a fluorescent screen to form a visual image [1].
Freeze drying		A process used to dehydrate heat sensitive substances whereby the product is deep-frozen and the ice is sublimed by reducing the pressure [1].
Freeze fracturing		A process whereby a material is embrittled by freezing it in liquid nitrogen and broken to obtain a clean surface without smearing.
Microscopic structure		The shape of a particle as observed with a microscope, using either an optical or an electron microscope.
Fourier Transform infrared spectroscopy	FTIR	Fourier transformations are done on infrared spectroscopic data by a computer to enable the intensity against wave number to be plotted with high sensitivity [1].

Thermogravimetry	TG	The mass of a sample in a controlled atmosphere is recorded continuously as a function of temperature or time [5].
Derivative of the thermogravimetric trace	DTG	Derivative of the thermogravimetric curve

References

1 Oxford Dictionary of Chemistry, Third edition, J. Daintith (ed.), Oxford University Press, Oxford, ISBN: 0-19-280031-0, 1996.

2 McMurry J., Organic Chemistry, Fourth edition, Brooks/Cole Publishing Company, Pacific Grove, p. 50-58, 1996.

3 Penguin Dictionary of Chemistry, Second edition, D.W.A. Sharp (ed.), Penguin Books, London, ISBN: 0 14 051.232 2, 1990.

4 W.A. Nash, Strength of Materials, Second edition, SI (Metric) edition, McGraw-Hill Book Company, New York, p. 3-6, 1977.

5 D.A. Skoog, F.J. Holler, T.A. Nieman, Principles of Instrumental Analysis, Fifth Edition, Saunders College Publishing, Philadelphia, p. 798, 1998.

Preface

The research done for this PhD study is joined in this book in the form of 3 extended self-contained articles (Chapters 2-4) featuring different aspects of the research. Chapter 1 is an introduction to the general concepts dealt with in this research as well as an outline of the aims and importance of this research. Chapter 5 is a general concluding chapter, with some ideas on future research in this field. The abbreviated versions of the articles were submitted to different journals. A list of publications, patents and conference proceedings emanating from this research are given in Appendix A.

Chapter 1

Introduction

Some general, overall aims and objectives of this study, as well as some introductory topics are described. More specific aims and introductions are stated within each draft article, which forms the chapters of this thesis.

1.1. The evolution of this project

The first and foremost aim of this project was to use the cheaper carbonate layered double hydroxide (LDH-CO_3) as a starting reagent in producing fatty acid intercalated LDHs, in stead of the more expensive and cumbersome to prepare chloride LDH. Ion exchange between the highly charged CO_3^{2-} and the sodium salt of a carboxylic (fatty) acid is not a viable process [1,2]. The fatty acid was used as starting reagent in stead of its salt. The pK_a values of carbonic acid are 6,35 and 10,33 at 25 °C respectively for the two protonation steps [3,4], which are higher than that of the fatty acids (4,8 at 25 °C [5]). The carbonate anion should be protonated by the fatty acid because an acid will donate a proton to the conjugate base of any acid with a higher pK_a [6]. CO_2 gas will subsequently be released. Hibino *et al*. [7] found that in LDHs with Mg/Al ratio of 2, no leaching of Mg^{2+} cations took place in acideous aqueous paramolybdate solutions, whereas substantial leaching of Mg^{2+} took place for LDHs with Mg:Al ratios of 3 and 4. Therefore one does not expect Mg^{2+} ions to leach during the intercalation reaction involving stearic acid and the LDH $Mg_4Al_2(OH)_{12}CO_3{\cdot}3H_2O$.

In the current study the intercalation reaction between stearic acid and the LDH was hampered by lump formation. Surfactants (such as SDS) were consequently added to adsorb onto the LDH surface and to emulsify the stearic acid. The performance of polymeric surfactants or polyelectrolytes such as poly(vinyl sulfonate) was tested and led to the discovery of a new route to intercalate

polymers into the LDHs. Finally, the biodegradable film forming polyelectrolyte sodium alginate was used in the role of surfactant for the intercalation reaction. This led to the development of films with desirable physical and water vapour barrier properties.

1.2. The aims of this research

- To develop new techniques for intercalating organic anions (especially fatty acid anions, such as stearate) into LDH-CO_3 and to compare the new techniques to existing techniques in literature. The new technique should not use calcination steps or N_2 atmosphere.
- To develop new techniques for intercalating anionic polymers into LDH-CO_3 in order to produce nanocomposites.
- To use the modified LDH as a filler in thermoplastic starch composites in order to reduce the water vapour permeability of starch.

Chapter 2 describes the intercalation method we used in comparison to existing literature methods. Chapters 3 and 4 describe some applications of these stearate intercalated LDHs, namely as a starting reagent to easily intercalate anionic polymers and as a filler in starch-based composites.

References

1 E.L. CREPALDI, J. TRONTO, L.P. CARDOSO and J.B. VALIM, *Colloids Surf. A* **211** (2002) 103.

2 S. CARLINO, *Solid State Ionics* **98** (1997) 73.

3 Dissociation constants of inorganic acids and bases, "Handbook of Physics and Chemistry", 79th edition, edited by D.R. Lide (CRC Press, Boca Raton, 1998) p. ***8***-44.

4 D.D. PERRIN, Ionization constants of inorganic acids and bases in aqueous solutions, Second edition, (Pergamon, Oxford, 1982).

5 J.F. MEAD, R.B. ALFIN-SLATER, D.R. HOWTON, G. POPJÁK, Lipids: chemistry, biochemistry, and nutrition, (Plenum Press, New York, 1986) p. 24-26.

6 J. McMURRY, Organic Chemistry, Fourth edition, (Brooks/Cole Publishing Company, Pacific Grove, 1996) p. 50-58.

7 T. HIBINO and A. TSUNASHIMA, *Chem. Mater.* **9** (1997) 2082.

Chapter 2

Stearate intercalated layered double hydroxides: a comparison of methods

Expanded version of article submitted to *Journal of Materials Science*.

Abstract

Calcined and uncalcined layered double hydroxides (LDH-CO_3) of the composition $Mg_4Al_2(OH)_{12}CO_3 \cdot 3H_2O$ were intercalated with stearate anions. Molten stearic acid (SA) in water was reacted with the carbonate anions of the interlayer. The presence of a surfactant, used to emulsify the SA and to disperse the LDH, did not significantly enhance the efficiency of intercalation, but prevented lump formation and facilitated the purification of the stearate intercalated LDH (LDH-SA) by removing unreacted SA during washing with water. Glycerol caused the removal of more carbonate anions possibly through intercalation of glycerolate anions, without facilitating stearate intercalation. Melting SA with LDH-CO_3 formed less LDH-SA than when the reaction took place in an aqueous medium. Reconstruction of calcined LDH in the presence of aqueous sodium stearate led to monolayer intercalation, whereas the methods entailing molten SA in aqueous media with LDH-CO_3 led to bilayer intercalation. Thermogravimetry was used for the first time to quantify the LDH-SA phase. The % mass loss in the temperature region 400-430 °C had a linear relationship to the relative amount of intercalated phase as determined by the internal standard method of XRD ($I_{50Å}/I_{9,3\ Å}$).

Keywords: layered double hydroxide, hydrotalcite, intercalation, stearic acid, glycerol, surfactant, calcinations, reconstruction, melt intercalation, infrared spectroscopy, thermogravimetry, X-ray diffraction

2.1. Introduction

Hydrotalcite is an anionic clay mineral with the composition $Mg_6Al_2(OH)_{16}CO_3.4H_2O$, and the layered structure of brucite [$Mg(OH)_2$], in which some of the Mg^{2+} ions are substituted by Al^{3+} ions. The presence of the Al^{3+} ions leads to a residual positive charge in the layers. This positive charge is balanced by anions such as CO_3^{2-}, Cl^- and NO_3^- or organic anions in the interlayer [1]. For the CO_3^{2-} containing structure, the d-spacing of the (003) and (006) planes are 7,8 Å and 3,9 Å respectively [2]. A range of compositions are possible in terms of bivalent and trivalent cations and of their relative amounts. These types of compounds are generally referred to as layered double hydroxides (LDHs). They will be referred to as LDH-CO_3, LDH-Cl or LDH-SA (stearic acid), depending upon the anions residing in the interlayer region. Carlino [3] reviewed the different methods that are employed to intercalate carboxylic acids into LDHs. The relevant methods will be highlighted in the following paragraphs.

Due to the strong electrostatic and hydrogen-bond interactions, the carbonate anions in the interlayer are difficult to ion exchange. When the LDH-CO_3 is dehydroxylated and decarbonated at 400 - 500°C to form a layered double oxide (LDO) and subsequently reconstructed in an aqueous solution of a carboxylic acid (or its salt) or anionic surfactant, intercalation of the acid or the surfactant can be achieved. The hydrophobic interaction between the hydrocarbon chains, contribute to the stability of the intercalated product. The mechanism of this intercalation is believed to consist of the fast rehydration of the oxide and intercalation of OH^- anions, followed by the slow anion exchange of OH^- anions by the carboxylate anions [4].

Dimotakis *et al.* [5] developed a method of intercalating carboxylic acids or surfactants into LDH-CO_3 in the presence of glycerol as swelling agent, thereby improving the OH^- exchange in the interlayer. $[Mg_6Al_2(OH)_{16}](OH)_2{\cdot}xH_2O$ can be prepared from $[Mg_6Al_2(OH)_{16}]CO_3{\cdot}xH_2O$ by calcination and reconstruction in pure water (one volume equivalent) under nitrogen atmosphere. Upon addition of two volume equivalents glycerol, extensive swelling occurs. A glycerated phase, with basal spacing in excess of 40 Å, forms. In the presence of carboxylate anions, facile exchange of OH^- takes place

at room temperature. According to Hansen *et al.* [6], LDH-CO_3 can be swollen in glycerol liquid or glycerol vapour resulting in a basal spacing of 9,6 Å or 14,4 Å respectively. Subsequently, the CO_3^{2-} can be exchanged by dissolved nitrate, chloride or sulphate anions. It is believed that the glycerol in the interlayer decreases the electrostatic and H-bond forces acting on the carbonate, making the carbonate more exchangeable with other anions. Another possibility is that glycerolate anions ($CH_2OH–CHOH–CH_2O^-$) are intercalated and exchanged [6].

Carlino *et al.* [7,8] developed a method in which molten sebacic acid (decane-1,10-dicarboxylic acid) and phenylphosphonic acid are intercalated into LDH-CO_3 in the absence of any solvents. The intimate mixture of the acid and LDH-CO_3 are heated slowly to above the melting point of the acid and kept there for 8 to 10 hours. Depending upon the molar ratio of acid to LDH, an intercalated phase or a salt (e.g. magnesium salt) of the acid formed. The products were biphasic because of the presence of unreacted LDH-CO_3 together with the intercalated phases [7,8].

Borja *et al*. [9] developed a method in which the Cl^- anions in LDH-Cl were ion-exchanged by the fatty acid anion in ethanolic solutions of lauric, meristic and palmitic acids. Literature procedures for the intercalation of specifically stearate anions into LDHs, mostly involve the anion exchange of Cl^- anions in LDH-Cl by stearate anions in aqueous solutions of sodium stearate under nitrogen atmosphere [10,11]. Depending on the amount of stearate present and the temperature employed, a monolayer or bilayer of stearate can be intercalated (Fig.1). The interlayer distance is about 32 Å for the monolayer and 52-53 Å for the bilayer [10,11]. Crepaldi *et al*. [12] developed a method of intercalating terephthalate ions into LDH-DS (dodecylsulphate) by salt formation between the intercalated DS^- and CTA^+ (N-cetyl-N,N,N-trimethylammonium). The salt is extracted into chloroform.

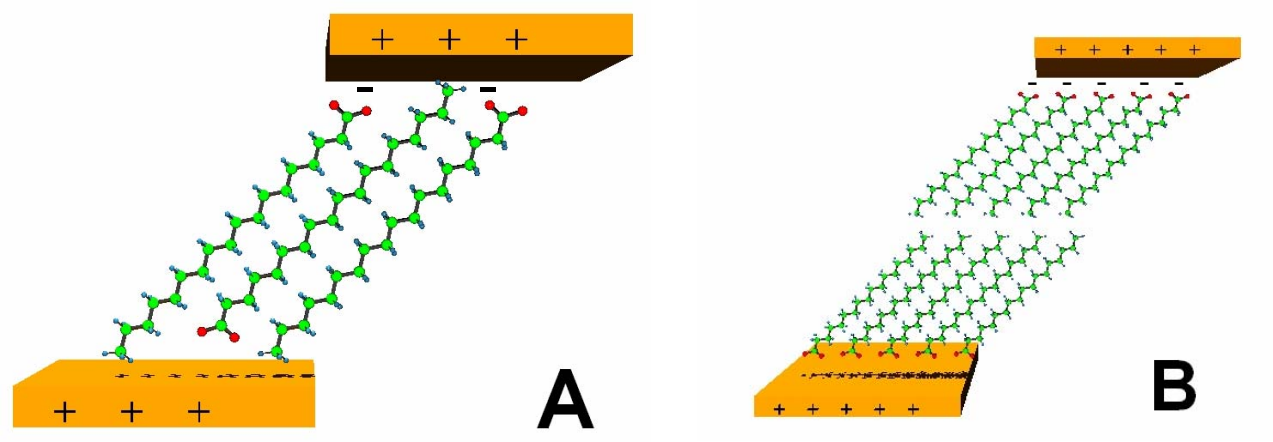

Figure 2-1 Monolayer (A) and bilayer (B) arrangement of stearate intercalated LDH (LDH-SA).

Organically modified layered compounds or clays such as LDH-SA can be used to form nanocomposites by being exfoliated within polymer matrices [13] or to protect and carry pharmaceuticals or genes [14] into cells due to its membrane-like structure or as stationary phases for chromatography [15]. Therefore, it would be beneficial to develop methods of intercalation that is time and energy efficient as well as environmentally friendly. In these respects, the starting reagent should be LDH-CO_3, which is easier to produce on large scale than, for example, the LDH-Cl. Furthermore, the use of water, in stead of volatile organic solvents, low temperatures (no calcinations) and no N_2 atmosphere would be beneficial. These aspects are explored in this work.

The aim of this work was to intercalate SA into LDH-CO_3 with the formula $Mg_4Al_2(OH)_{12}CO_3{\cdot}3H_2O$ by a wide range of methods to form LDH-SA. The methods entailed reacting both LDH-CO_3 and LDO with SA in aqueous or ethanolic media or mixtures thereof. In the aqueous media the acidic SA is envisaged to react with and replace the CO_3^{2-} of the interlayer. To the best of our knowledge the use of SA and water to intercalate LDH-CO_3 has not been studied before. The effect of adding sodium dodecylsulphate (SDS) to the water was also tested. This surfactant-mediated method has, to the best of our knowledge, also not been studied previously. The use of 2:1 (v/v) glycerol/water mixtures with molten SA (similar to the method developed by Dimotakis

et al. [5] for nonanoic acid) was also tested as well as reacting the LDH-CO_3 with molten SA in the absence of solvents (similar to the method developed by Carlino *et al.* [7,8] for sebacic acid). Reconstruction of the LDO in the presence of aqueous sodium stearate was also performed. This research was aimed at determining the most efficient method for the intercalation of SA into LDH-CO_3 and developing thermogravimetry (TG) as a quick and easy tool for quantifying the LDH-SA phase.

2.2. Experimental procedure

2.2.1. Sample preparation

The layered double hydroxide (LDH) used in this study had the chemical formula $Mg_4Al_2(OH)_{12}CO_3{\cdot}3H_2O$ (LDH-CO_3), and was supplied by Chamotte Holdings (Pty) Ltd, South Africa. The amount of crystalline water was determined from TG analysis. The mole ratio of Mg:Al was 2.01:1 as determined by XRF analysis (Appendix B). The particle size distribution as determined by the Mastersizer 2000 (Malvern Instruments) was d(0,1): 0,694 μm; d(0,5): 5,062 μm and d(0,9): 23,925 μm. The theoretical anionic exchange capacity of this LDH-CO_3 was calculated to be 213 meq/100 g.

According to Itoh *et al.* [10] stearate anions can intercalate up to about 225% of the AEC. Therefore, stearic acid (SA, AR, 65-90%, Bio-Zone Chemicals) was used at 200% of the theoretical anionic exchange capacity (AEC) of the LDH. The intercalation of the LDH-CO_3 by SA was performed by 10 different methods (Table 2-1). A reference sample was also prepared in which no reaction took place (mixture of SA and LDH-CO_3 powders). The naming of methods in Table 2-1 are exemplified by the following: A sample or method name of *Calcined-SDS-water* refers to a sample or method in which LDH-CO_3, calcined at 500 °C, was reacted with SA in the presence of sodium dodecylsulphate (SDS) and water; the sample *Glycerol-water* was prepared by reacting the LDH-CO_3 and SA in the presence of a glycerol-water mixture. SDS was used to adsorb onto LDH surface to disperse it and to emulsify the SA. Deionised water, Glycerol (99%, UNILAB®), sodium dodecylsulphate (SDS, Empicol LZ/D, Akulu Marchon), sodium stearate (chemically pure, minimum 40%, UNILAB®) and ethanol (96% rectified, Dana Chemicals) were used. In methods where LDO was used 2 g of the

LDH-CO_3 was weighed, calcined at 500 °C for 2 h and the residue was added to the reaction mixtures. The mixtures were heated and stirred with a magnetic heater/stirrer at 70 °C for 2 h, unless specified as reacted for 24 h. All experiments were carried out in air in order to determine the efficiency of intercalation that one could expect under industrial conditions, where N_2 atmospheres would not be viable. Samples were washed with deionised water to remove excess SDS or glycerol; unreacted SA was not washed out. Mass yields of the LDH-SA were not determined because of the mixed nature of the product (containing SA, LDH-CO_3 and LDH-SA). Therefore, the relative amount of LDH-SA formed and unreacted LDH-CO_3 in the different methods was determined by XRD. Samples were filtered, except in the case of *SDS-water* methods in which the product was separated by centrifugation.

2.2.2. Characterization

2.2.2.1. *Fourier Transform Infrared spectroscopy (FTIR)*

A Perkin Elmer Spectrum RX I FT-IR System was used to scan the infrared transmittance through a KBr (Uvasol, potassium bromide, Merck) pellet 32 times at a resolution of 2 cm^{-1}. The averaged spectrum was background-corrected using a pure KBr pellet run under similar conditions. The pellets were prepared with approximately 2 mg of sample and 100 mg of KBr.

2.2.2.2. *Thermogravimetry (TG)*

15 mg of the powder sample was placed in a 70 μl alumina pan. It was heated from 25 °C to 700 °C at a rate of 10 °C/min in air with no lid in a Mettler Toledo STAR^e System. The first derivatives of the thermogravimetric traces were used because it is more intuitive.

Table 2-1 Experimental details on the intercalation methods investigated.

Method name and details	**Notes**
1. Water. 4,6 g SA, 2 g LDH-CO_3, 150 ml *water*. SA is melted but not dissolved. Filter, dry and grind product.	Gelation after ca. 20 minutes and later changed into lumpy agglomerates.
2. Calcined-Water. 4,6 g SA, LDO*, 150 ml *water*. SA is melted but not dissolved. Filter, dry and grind product.	Lumpy agglomerates formed.
3. Ethanol. 4,6 g SA, 2 g LDH-CO_3, 150 ml *ethanol.* SA is dissolved in ethanol. Filter and dry product. No washing.	No lumps formed.
4. Ethanol-water. 2 g LDH-CO_3 reacted with 4,6 g SA in a 1:1 v/v *water/ethanol* mixture.	Small globules formed (ca. 1 mm diameter).
5. SDS-water**. 4,6 g SA, 2 g LDH-CO_3, 150 ml *water*, 2,5 g *SDS*. SA emulsified by SDS. Centrifuge, wash and dry product.	Well dispersed product.
6. Calcined-SDS-water**. 4,6 g SA, LDO*, 150 ml *water*, 2,5 g *SDS*. SA emulsified by SDS. Centrifuge, wash and dry product.	Well dispersed product.
7. Glycerol-water. 4,6 g SA, 2 g LDH-CO_3, 50 ml *water*, 100 ml *glycerol*. SA is melted within the liquid mixture, not dissolved. Filter, wash and dry product.	Spherical soft lumps formed.
8. Calcined-glycerol-water. 4,6g SA, LDO*, 50 ml *water*, 100 ml *glycerol*. SA is melted within the liquid mixture, not dissolved. Filter, wash and dry product.	A soft gel formed and transformed into soft lumps.
9. Calcined-Na stearate-water**. LDO* reacted with 5,22 g *sodium stearate* (2 times AEC) dissolved in 150 ml *water*. 150 ml hot deionised water added after reaction and before centrifugation to retard rate of gelling of sodium stearate. Washed again with hot deionised water.	No lumps formation.
10. Carlino melt. 2 g LDH-CO_3 reacted with 4,6 g *molten* SA at 70 °C for 8 h. No solvents present. In air.	Soft mixture showing channels through which CO_2 gas escaped.
11. Reference. *No reaction*. 2 g LDH-CO_3 powder mixed with 4,6 g SA powder.	-

* Residue after 2 g of LDH-CO_3 was calcined at 500 °C in air for 2 h.
** 24 h reactions was also performed and denoted, for example, as *SDS-water-24 h.*

2.2.2.3. *Powder X-ray diffraction (XRD)*

The XRD analyses were done on a Siemens D500 X-ray system equipped with a 2.2 kW Cu long fine focus tube, variable slit and secondary graphite monochromator (to eliminate K_β radiation and reduce fluorescent radiation). The system is computer controlled using SIEMENS DIFFRAC ^{Plus} software. The goniometer was set to reflection mode. Samples were scanned from 1 to 40° 2θ with Cu K_α radiation (1,5418 Å) at a speed of 0,02° 2θ, with a recording time of 2 s per step and generator settings of 40 kV and 30 mA. For quantitative XRD analyses the internal standard method [16] was used whereby 20 % m/m talc powder (< 10 micron, Sigma-Aldrich, $3MgO.4SiO_2.H_2O$) was added to the obtained products. Sample preparation was done in standard sample holders by a single person in a repetitive way. Phases were quantified by determining the ratios of the intensities of the basal reflections to that of the 9,3 Å reflection of the talc.

2.2.2.4. *Scanning electron microscopy (SEM)*

Small amounts of the powder products or pristine LDH were placed onto carbon tape on a metal sample holder. The excess powder was removed by compressed air. A small piece of the gel-like mixture obtained during the *Calcined-glycerol-water* method was placed onto a carbon stub of approximately 5 mm diameter. It was frozen in a Reichert KF80 plunge freezer (Vienna, Austria). The frozen sample was dried in a custom built high vacuum freeze drier (Pretoria Technicon, South Africa). All samples were coated with chromium in a high resolution ion beam coater, Gatan model 681 (Warrendale, PA, USA) and studied with the JSM-6000F field emission scanning electron microscope (JEOL, Tokyo, Japan).

2.3. Results and discussion

Table 2-1 gives a summary of some of the observations made during the reactions.

2.3.1. Results and discussion of the different intercalation methods

2.3.1.1. *Reference* sample

During the thermogravimetric (TG) analysis of the reference sample, the stearic acid (SA) melted and intercalated to form the LDH-SA product with decomposition peak around 412 °C (Fig. 2-2). At the higher temperatures (during the temperature program), SA probably also reacted with the hydroxyl groups of the LDH layers, leading to the formation of thermally more stable products (decomposition temperatures of 441 °C and 473 °C, Fig. 2-2). Unreacted SA acid with a decomposition peak around 252 °C was present. The pure SA showed a decomposition peak at around 280 °C. The intercalation mechanism is similar to that of the method developed by Carlino *et al*. [7] in which the LDH and carboxylic acid powders were mixed and the acid allowed to melt. FTIR and XRD analysis showed the presence of only unreacted SA and LDH.

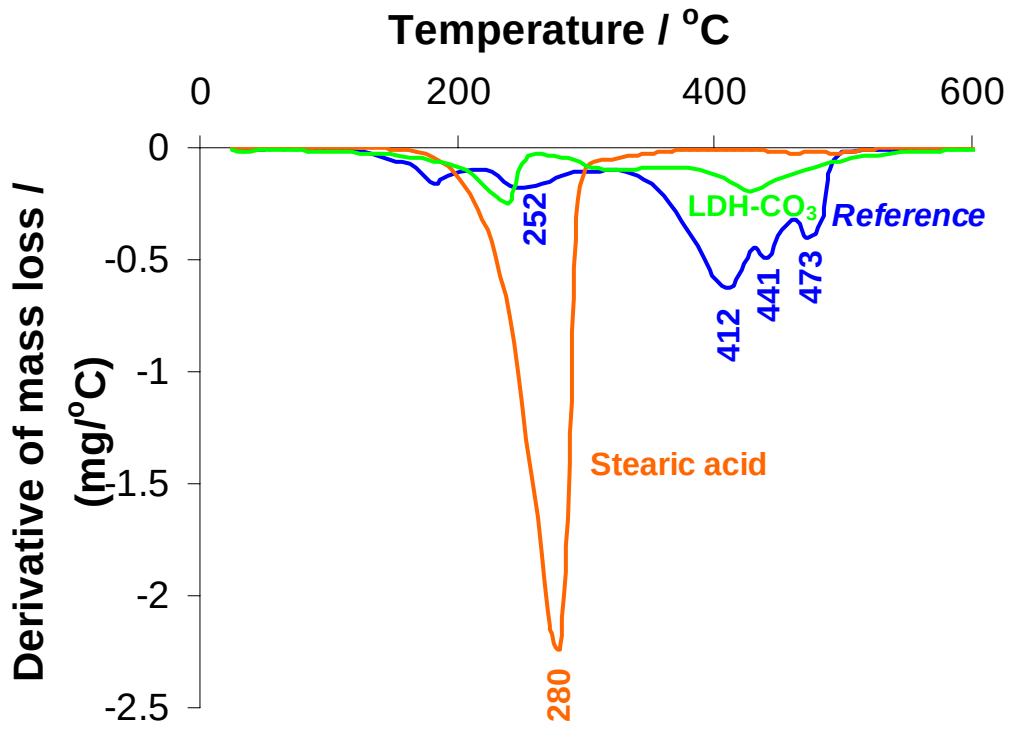

Figure 2-2 Derivatives of the thermogravimetric traces (DTG) of the LDH-CO_3, SA and the *Reference* mixture of LDH-CO_3 and SA, showing that SA intercalated during the analysis.

2.3.1.2. *Ethanol and Ethanol-water* methods

In pure ethanolic solution the intercalation could not take place because the SA was not ionized and, therefore, could not react with the carbonate of the LDH-CO_3 (Fig. 2-3, raw data in Appendix C). The amount of LDH-CO_3 present, were anomalously high with respect to the *Reference* sample (Fig. 2-4) because the SA stayed in solution and was not part of the solid product, leaving only a SA coating on the LDH-CO_3. The presence of 50% v/v ethanol (*Ethanol-water* method) did not reduce the efficiency of intercalation much (in terms of amount of LDH-SA formed) in comparison to the *Water* method (Fig. 2-3). The presence of the 50% v/v ethanol prevented the agglomeration that took place in the *Water* method. Agglomerated spheres of less than 1 mm diameter formed.

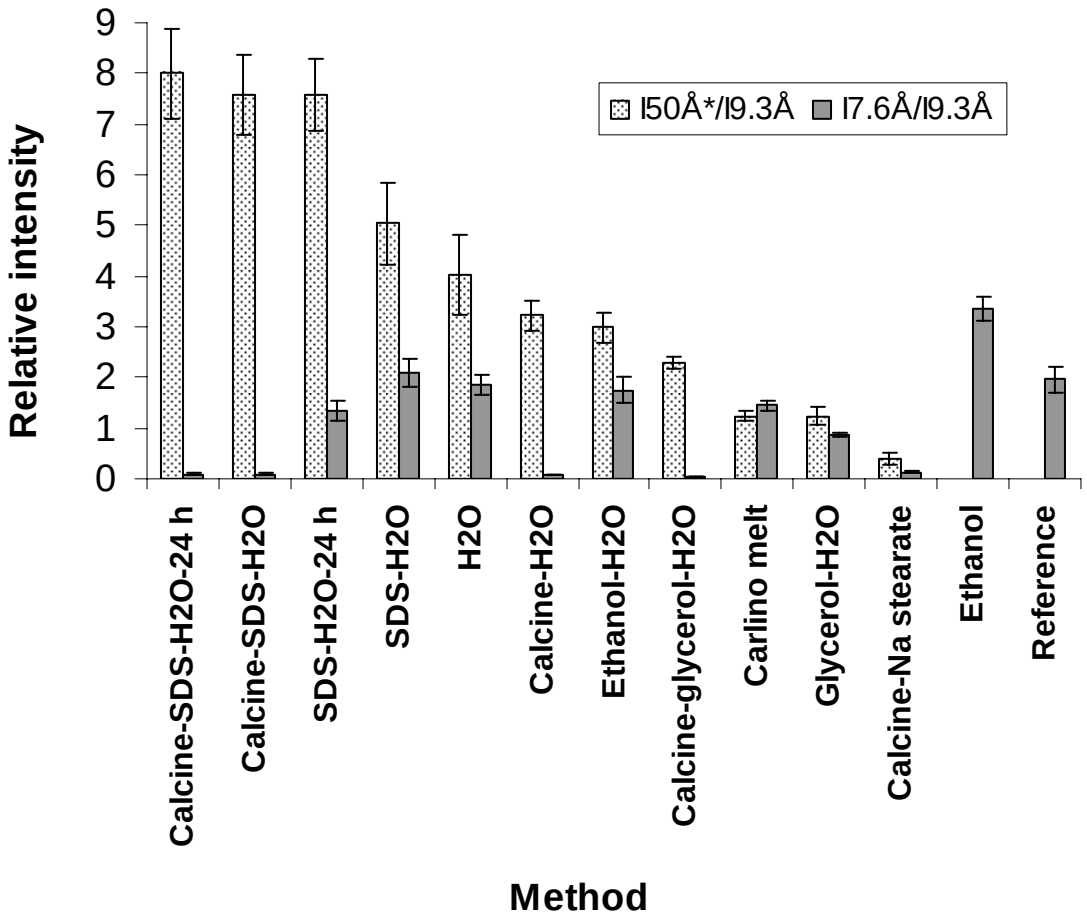

Figure 2-3 Relative amounts of the LDH-SA and LDH-CO_3 phases in the samples of different intercalation methods as determined by the internal standard XRD method. The raw data are given in Appendix C.

* Reflection in the region of 50 Å.

2.3.1.3. *Glycerol-water and Calcined-glycerol-water* methods

The relative amount of LDH-CO_3 phase diminished drastically in the presence of glycerol in comparison to the other methods (Fig. 2-3 and Fig. 2-4), and that without any calcination. The carbonate vibration at 1365 cm^{-1} was drastically reduced and a small peak at 1384 cm^{-1} remained. According to Hansen *et al.* [6] this could be attributed to the weakening of the H-bonds between the water and carbonate in the interlayer region by glycerol or even the intercalation of glycerolate anions. Therefore, one would expect more SA intercalation because of the removal of the carbonate counter-ions. However,

less of the LDH-SA product formed in comparison to most methods (Fig. 2-3), a phenomenon which could be attributed to several factors. First, less SA was in the ionized state because the medium consisted of only about 33 % water. Second, FTIR spectra of these samples (Fig. 2-4) indicated a more amorphous structure (broad, unresolved peaks) in comparison to that of the *Water* method. The amorphous LDH-SA would be undetectable by XRD. The weak peak at 1725 cm^{-1} (Fig. 2-4), also seen by Borja *et al.* [9] at 1720 cm^{-1}, could be attributed to the intercalation of the acid (COOH) itself.

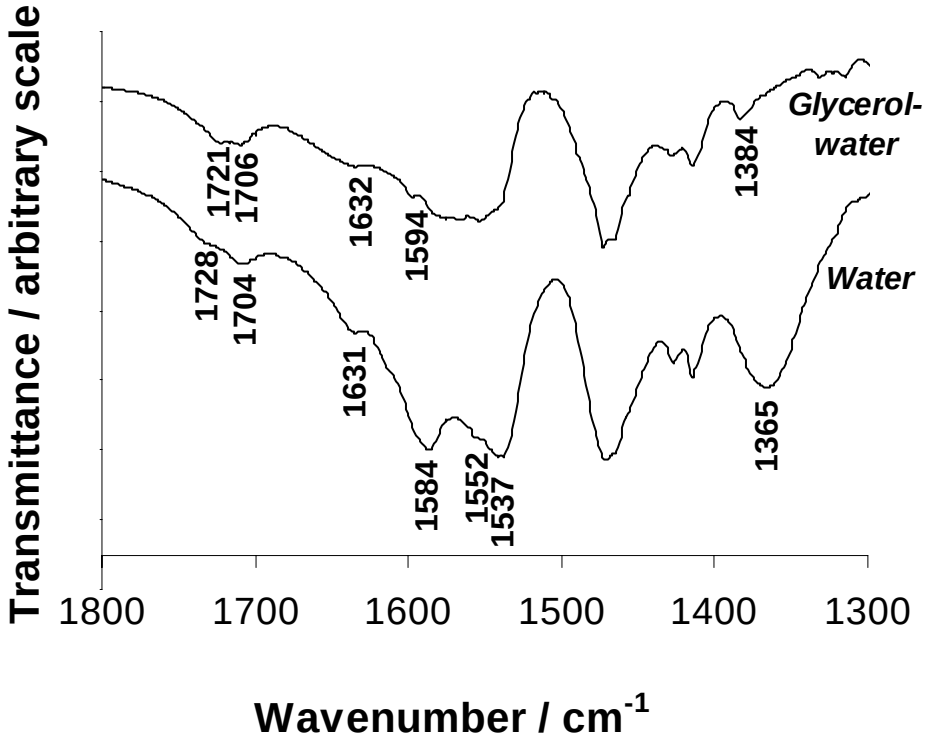

Figure 2-4 FTIR spectra of the *Water* and *Glycerol-water* methods, showing that the presence of glycerol caused the removal of carbonate from the LDH (large carbonate vibration at 1365 cm^{-1} vs. small one at 1384 cm^{-1}) as well as a more amorphous arrangement of the stearate species (broad, overlapping carboxylate asymmetric stretching vibrations around 1550 cm^{-1}).

LDH particles usually have sand-rose structures (Fig. 2-5 A). The particles consist of many intergrown smaller particulates which reduce the surface area [17]. This sand-rose structure broke down under the influence of the SA to form plate-like structures of large surface area (approximately 10 μm diameter, 200-500 nm thickness, Figs. 5 C and D), and gelling occurred. The thickening or "gelling" of the reaction mixture could be attributed to the house of cards arrangement of the plates (Figs. 5 C and D). The structure of the crystals looked much the same as the LDH-SA obtained by Itoh *et al*. [10] The formation of these gels seemed to depend upon the stirring conditions because in the case of the *Calcined-glycerol-water* method, the gel only formed during a large scale experiment (with overhead stirring) and not during the small scale experiment. When the gel of *Calcined-glycerol-water* was diluted and washed with water, dried and ground, neither the plate-like product, nor the sand-rose morphology of the original LDH persisted (Fig. 2-5 B).

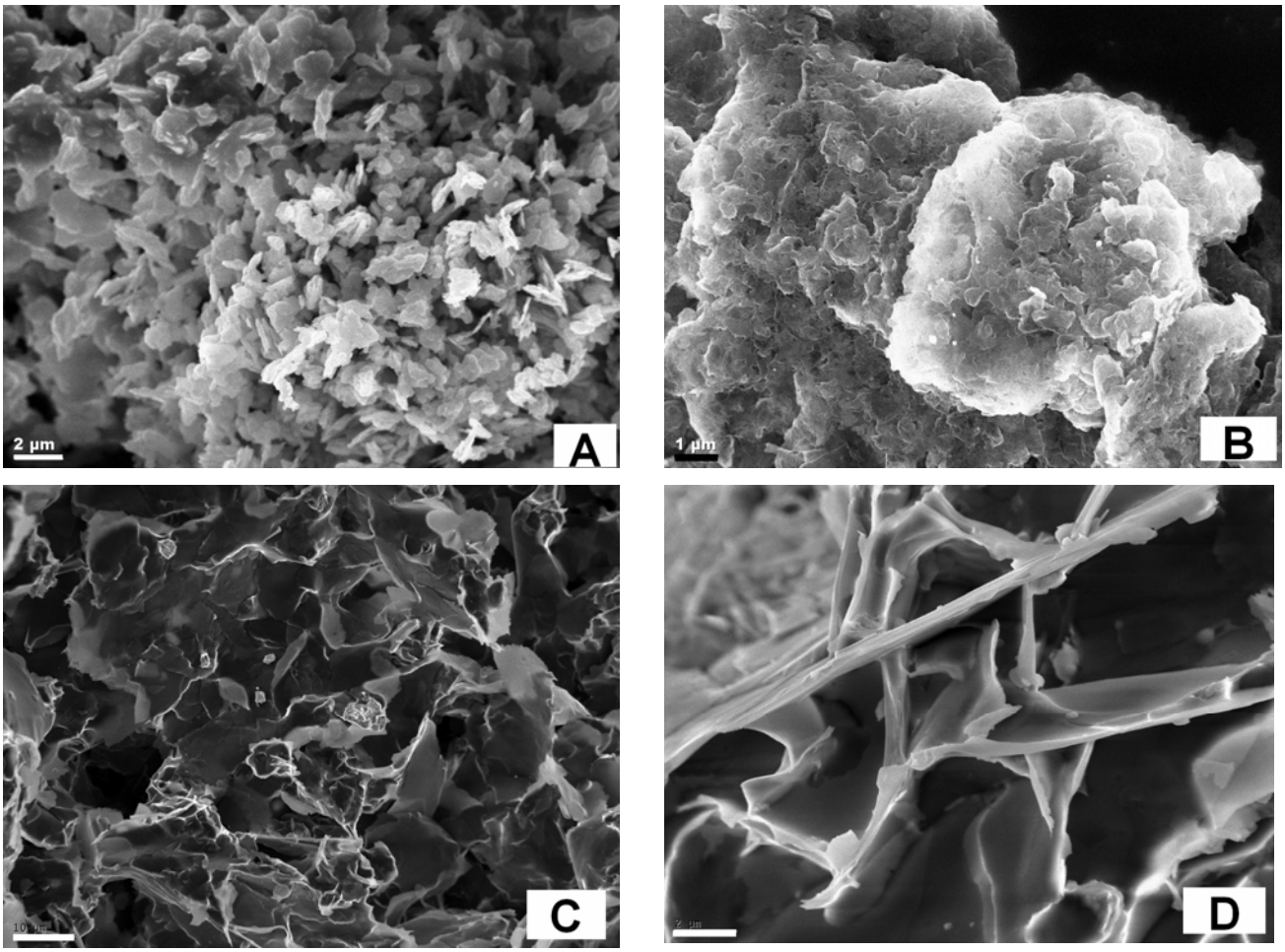

Figure 2-5 Scanning electron micrographs of the LDH-CO_3 showing the sand-rose microscopic structure (A), the powder product (B) and the gel of *Calcined-glycerol-water* (C and D). The bar in A is 2 μm, in B 1 μm, in C 10 μm and in D 2 μm.

2.3.1.4. *Water, Calcined-water, SDS-water and Calcined-SDS-water* methods

The FTIR spectrum of the LDH-SA obtained from the *SDS-water* method (Fig. 2-6) revealed the following: All the stearic acid reacted because the ν(C=O) stretching vibration at 1702 cm^{-1} was absent. The carboxylate (COO^-) asymmetric stretching vibrations were at 1539 cm^{-1}, 1555 cm^{-1}, 1586 cm^{-1} and 1635 cm^{-1}, which correlates well with the carboxylate asymmetric stretching vibrations (1542 cm^{-1}, 1557 cm^{-1}, 1589 cm^{-1} and 1637 cm^{-1}) obtained by Borja *et al.* [9] for meristate intercalated Mg_3Al-LDH. The carboxylate asymmetric stretching vibrations are different from that of magnesium stearate (Fig. 2-6). The hydroxyl groups of the layers of the Mg_2Al-LDH are probably not

strong enough Brønsted bases to react with the SA (due to the Lewis acidity of the Al^{3+}). Leaching of Mg^{2+} from the Mg_2Al-LDH used in this study (due to the presence of the acidic SA) is not expected because Hibino *et al*. [18] found that no leaching of Mg^{2+} cations took place in LDHs with Mg/Al ratio of 2 when treated with aqueous paramolybdate solutions (low pH), whereas substantial leaching took place in LDHs with Mg/Al ratios of 3 and 4. There is, furthermore, stoichiometrically not enough SA present for the salt (magnesium stearate) to form. The presence of the peak at 1362 cm^{-1}, attest to the fact that all the carbonate counter-ions did not react (Fig. 2-6). Longer reaction times and higher SA concentrations might be required for the complete conversion of the carbonate ions. The sulphate peak of SDS (1217 cm^{-1}, [19]) was not present, indicating that SDS did not co-intercalate (Fig. 2-6), probably because SDS has a different chain length from SA, the stearate intercalated LDH were more stable, the SDS was present in lower concentration than the SA, the SA alone satisfied the anionic exchange capacity and the SDS was not reactive toward the carbonate.

When LDHs are calcined at temperatures around 400 °C, a Mg-Al oxide with MgO-like structure forms [20]. MgO and SA are used to produce magnesium stearate [21]. Therefore, it was not surprising that the product of *Calcined-water* was similar to magnesium stearate in terms of the carboxylate asymmetric stretching vibrations (around 1575 cm^{-1}, Fig. 2-6) and the higher decomposition temperature (446 °C vs. 414 °C for *Water* method, Fig. 2-7). However, when SDS or glycerol was present in the system the products did not resemble magnesium stearate (Fig. 2-8). Therefore, these compounds adsorbed onto the basic sites of the LDO, protecting the carboxylic acid group of the SA from attack by the O^{2-} Lewis bases and the LDH-SA intercalates with lower decomposition temperatures formed (Fig. 2-8).

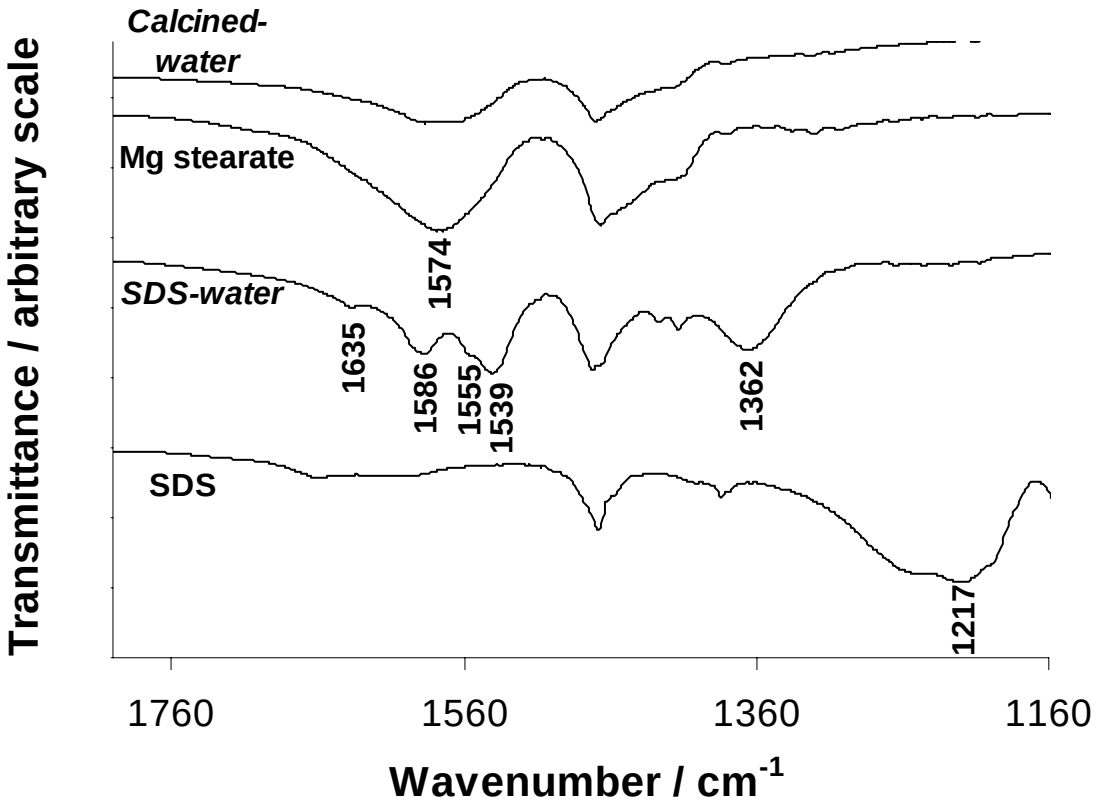

Figure 2-6 FTIR spectra of SDS, *SDS-water* product, magnesium stearate and *Calcined-water* product, showing that magnesium stearate did not form in *SDS-water* method, that SDS did not co-intercalate and that the product of *Calcined-water* were similar to magnesium stearate in the carboxylate asymmetric stretching vibrations (around 1575 cm^{-1}).

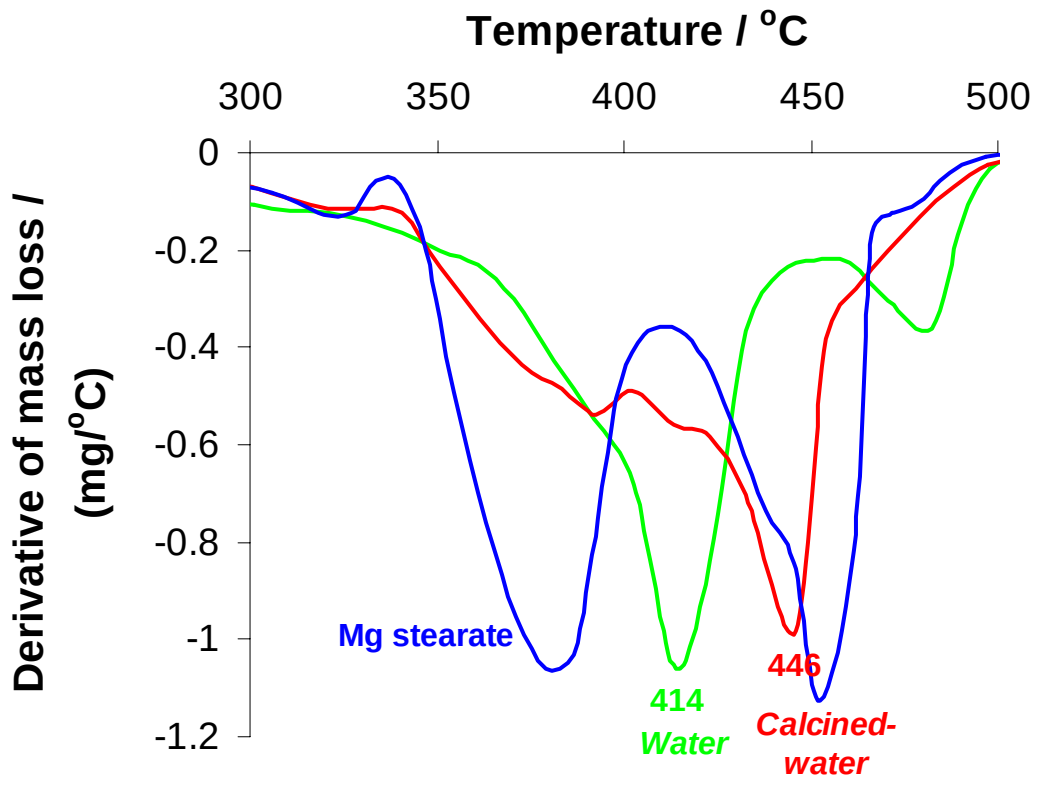

Figure 2-7 DTG traces of magnesium stearate, sample *Water* and sample *Calcined-Water*, showing that *Calcined-water* formed a product similar to magnesium stearate.

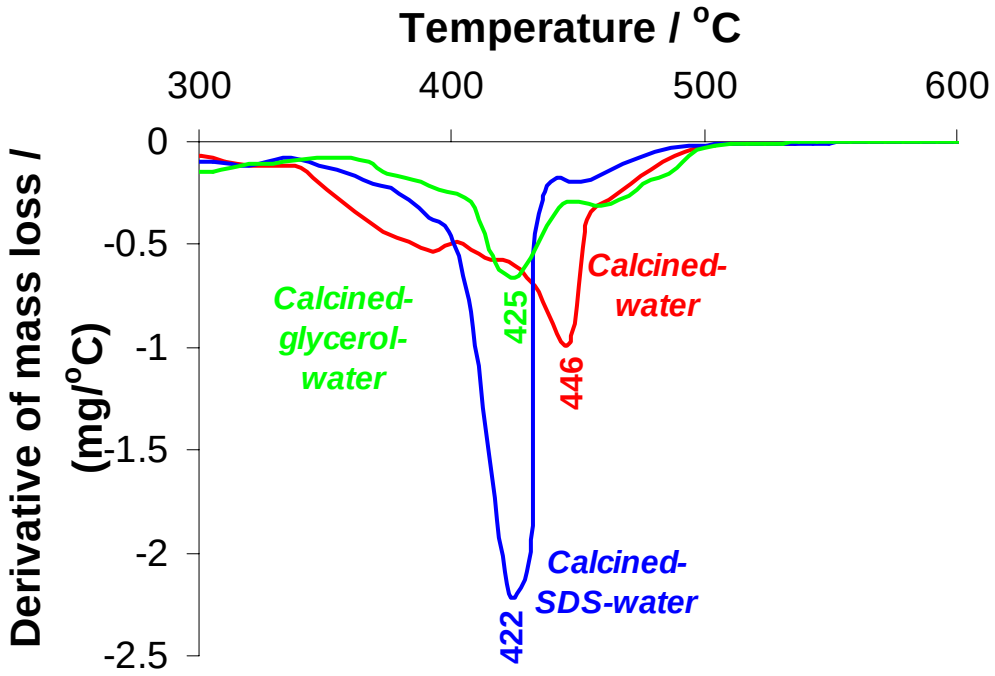

Figure 2-8 DTG traces of *Calcined-water*, *Calcined-SDS-water* and *Calcined-glycerol-water*, showing that the presence of SDS or glycerol protected the LDO from reacting with SA to form an Mg/Al stearate type salt; LDH-SA being the main product.

The reflections at 49,52 Å, 25,43 Å, 17,11 Å and 10,34 Å in Fig. 2-9 can be attributed to the bilayer intercalated LDH-SA. The pattern of the relative intensities of these 4 peaks (high, low, high, and low) is reminiscent of that obtained by Borja *et al*. [9] for the ion exchange of Cl^- in LDH-Cl by meristic acid in ethanol. Itoh *et al*. [10] attributed the reflection at 53 Å as the basal reflection of stearate intercalated LDH (bilayer) with the chains at approximately a 29° angle from the normal of the layers. This phase was present in the samples of all methods (with varying interlayer distances due to varying angles or degrees of interpenetration of the chains) except the *Ethanol* and *Calcined-Na stearate-water* methods. Monolayer intercalated LDH-SA was also present in sample *Calcined-SDS-water* as a minor phase (reflections at 30,35 Å and 15,43 Å, Fig. 2-9) but in none of the other methods (except *Calcined-Na stearate-water*). For SDS intercalation one would expect reflections at 26 Å, 36 Å or 47 Å depending on the mode of

intercalation [22]. The absence of these reflections (Fig. 2-9) indicates that no SDS intercalated, as was seen by FTIR analyses as well.

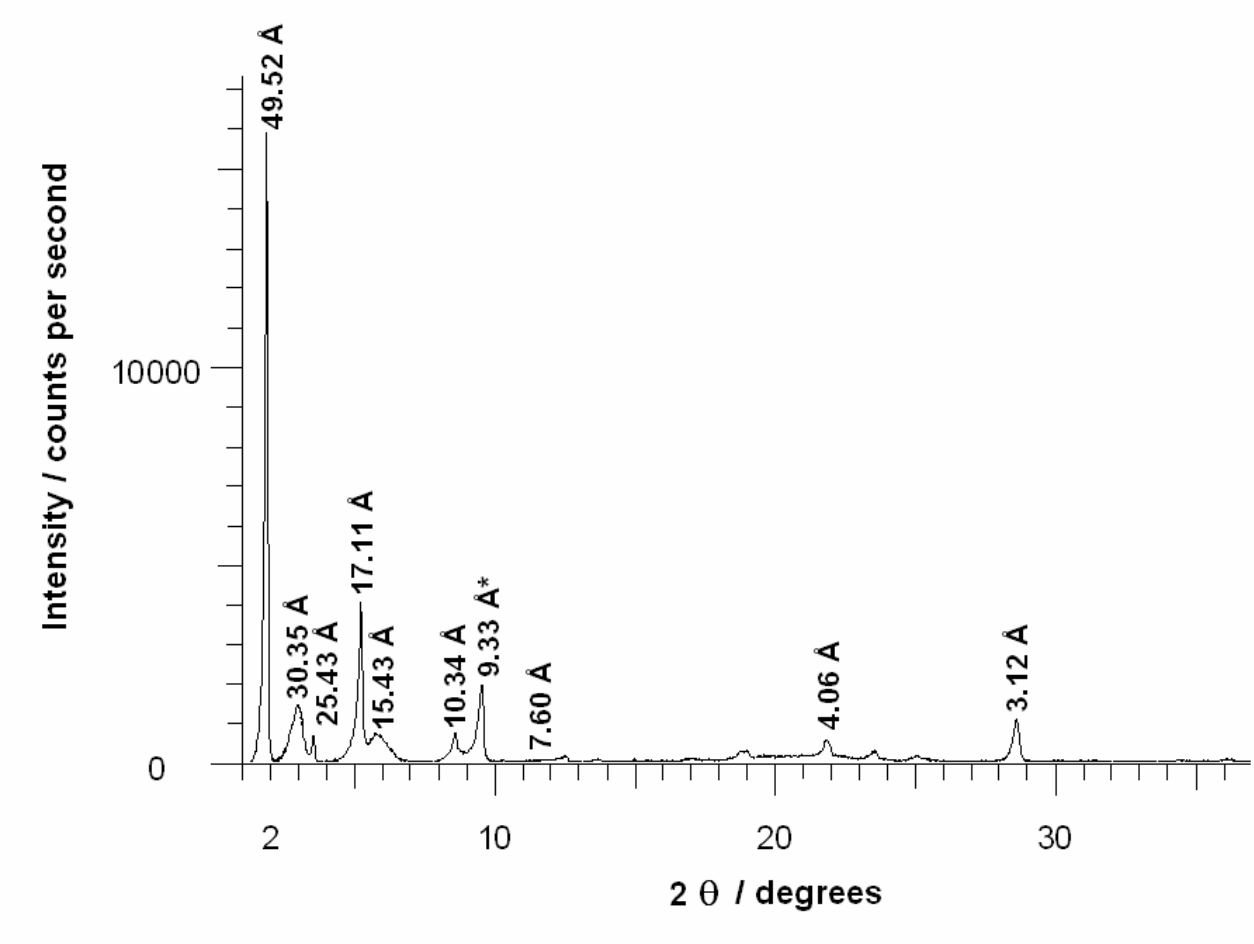

Figure 2-9 X-ray diffractogram of method *Calcined-SDS-water-24 h.* Reflections due to bilayer (49,52 Å, 25,43 Å, 17,11 Å and 10,34 Å) and monolayer (30,35 Å and 15,43 Å) intercalated LDH-SA were present.
* Reflection of internal standard (talc).

Unreacted SA was removed together with the SDS during washing with water; consequently the product was enriched in the LDH-SA and unreacted LDH-CO_3 phases. This explains why there were (anomalously) somewhat more LDH-CO_3 present than in the reference sample (Fig. 2-3). The relative amount of LDH-CO_3, however, decreased from 2,1 ± 0,3 to 1,3 ± 0,2 when comparing a 2 h reaction with a 24 h reaction.

In a preliminary study it was found that the amount of surfactant did play a role in the amount of stearate that intercalated. For the same relative amounts of LDH and SA, the higher the SDS concentrations, the higher the yield (mass) of the LDH-SA after thorough washing with water and acetone. The internal standard method of XRD (Fig. 2-3) was not sensitive enough to capture these differences (compare *Water* and *SDS-water*). The correlation between the amount of surfactant and amount of stearate intercalation could possibly be attributed to the droplet size of the molten stearic acid as well as the surfactant adsorbing onto the LDH surface, preventing the side-reaction whereby the stearic acid reacts with the surface OH groups of the LDH.

Gelling occurred after 20 minutes of reaction in the *Water* method (as in *Calcined-glycerol-water* method), but in none of the other methods described in this paper. The gel was, however, too weak to withstand the preparation methods for SEM analysis, but it is believed to have the same microscopic structure as depicted in Figs. 5 C and D. Upon vicious shaking, the gel broke and the mixture could be stirred for the remainder of the time. Lumps of growing size started to form, which made magnetic stirring increasingly difficult (especially around and after 2 h of reaction), which possibly inhibited further diffusion of SA into the interlayer regions.

2.3.1.5. *Calcined-Na stearate-water* method

The carboxylate asymmetric stretching vibration region of sample *Calcined-Na stearate-water* looked almost identical to that of pure sodium stearate (Fig. 2-10). Therefore, at first it seemed as if no intercalation took place. However, reflections due to monolayer intercalation (31,90 Å and 15,69 Å) as well as a minor reflection at 45-48 Å due to bilayer intercalation were seen in XRD (Fig. 2-11). The decomposition temperature (T_{peak}) was lower (334 °C) than that of the bilayer intercalated products (about 420 °C). The reaction mixtures' tendency to gel makes the sodium stearate method less attractive.

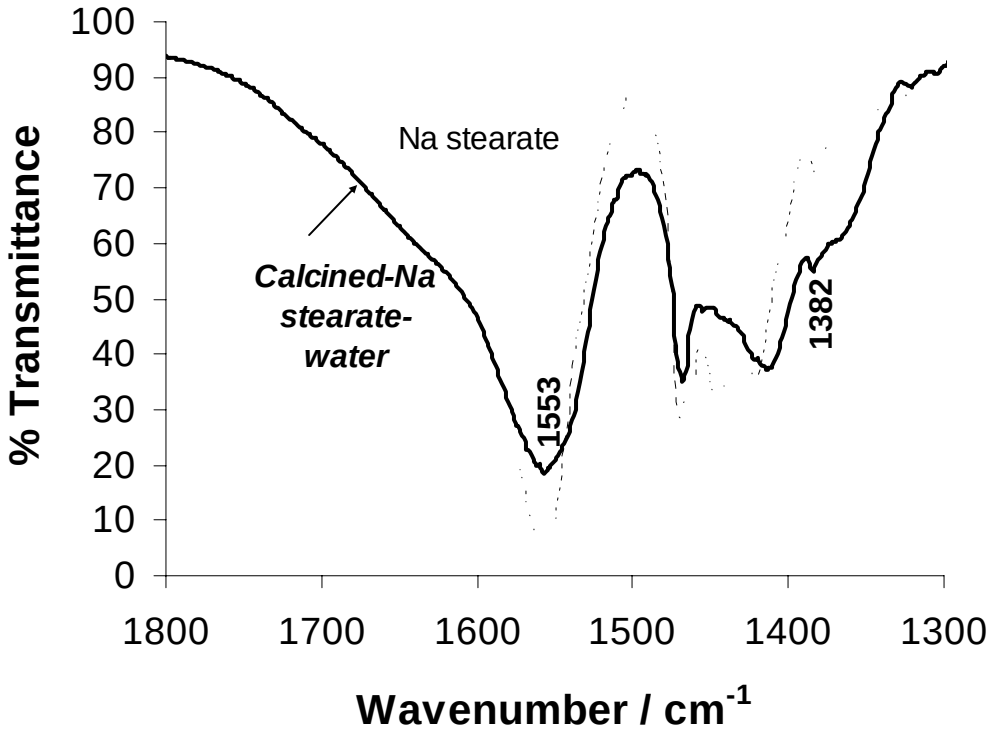

Figure 2-10 FTIR spectra of sodium stearate and sample *Calcined-Na stearate-water*, showing that the carboxylate asymmetric stretching vibrations of sodium stearate did not change much after intercalation (only some broadening seen).

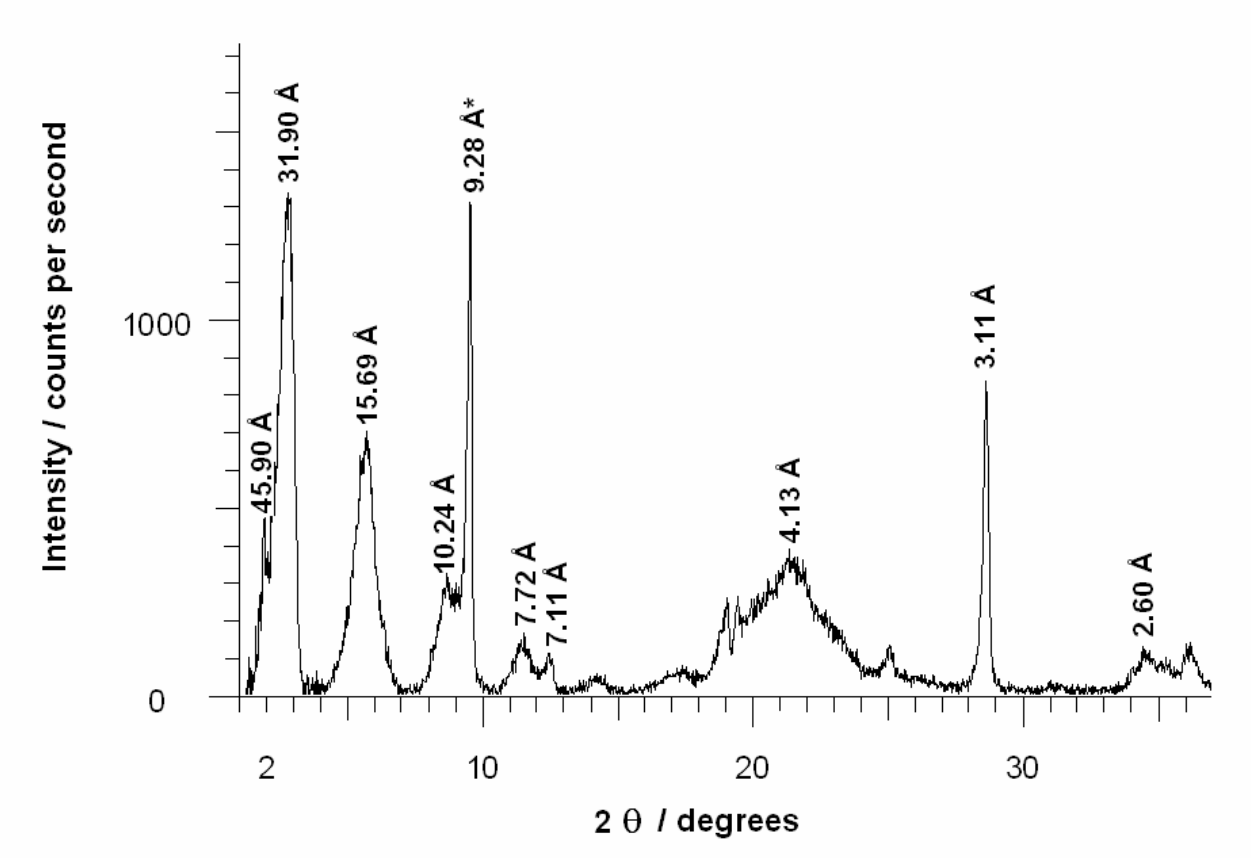

Figure 2-11 X-ray diffractogram of method *Calcined-Na stearate-water-24 h.* Monolayer intercalation with reflections at 31,90 Å and 15,69 Å were obtained together with a minor phase of near bilayer intercalation (45,90 Å).

* Reflection of internal standard (talc).

2.3.1.6. *Carlino melt* method

In the case of the *Carlino melt* method less of the LDH-SA phase seemed to form even though more of the LDH-CO_3 disappeared (Fig. 2-3) with respect to the *Water* and *SDS-water* methods. One would expect, however, that more LDH-CO_3 have reacted because of the longer reaction time (8 h vs. 2 h). The low amount of LDH-SA could possibly be ascribed to the following factors: mixing was not as efficient as in the case of stirring in the presence of a solvent, the SA is less ionized due to the absence of water or the LDH-SA is less crystalline and could mostly not be detected by XRD. FTIR results also attested to the formation of a less crystalline product due to the broad overlapping

carboxylate asymmetric stretching vibrations. (Fig. 2-12) The relative heights of the peaks at 1550 cm^{-1} and 1583 cm^{-1} differed significantly from that of the other methods described in this work (Figs. 4 and 6, which correlated well with the relative heights seen by Borja *et al.* [9]). This is indicative that the carboxylates were present in different amounts in the different environments in comparison to the methods where water was present. There was also some unreacted SA (1706 cm^{-1}) left in the *Carlino melt* sample.

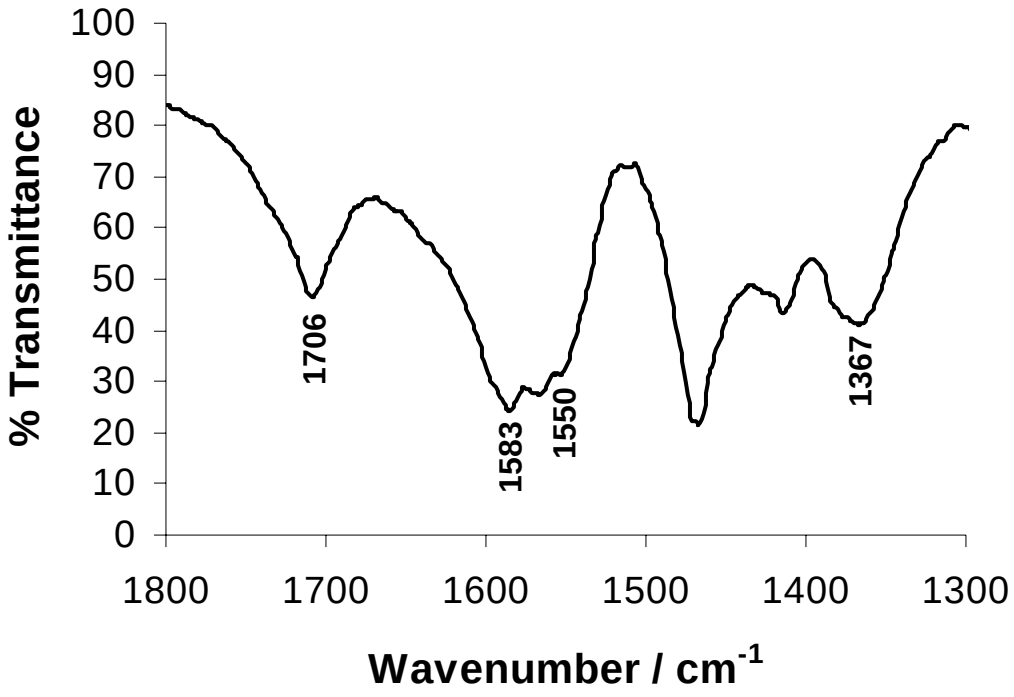

Figure 2-12 FTIR spectrum of the *Carlino melt* product showing different relative intensities of the carboxylate asymmetric stretching vibrations than the *Water* (Fig. 2-4) and *SDS-water* (Fig. 2-6) methods.

2.3.2. The effect of reaction time

The observed interlayer distances (basal reflections) ranged from 47-54 Å. There are indications that intercalated SA reached approached an equilibrium state with increasing reaction time because the interlayer distances decreased: Compare *SDS-water* with *SDS-water-24 h* as well as *Calcined-SDS-water* with *Calcined-SDS-water-24 h* in Table 2-2. The *Carlino melt* sample (which was reacted for 8 h) had an interlayer distance of only 47,04 Å. The solvents and other constituents may also have an effect on the observed interlayer distances (angle of the chains or extent of interpenetration of the chains). The decomposition peak temperature also increased with time (from about 420°C to about 438-446°C, Table 2-2). The higher decomposition temperatures can be due to the fact that the product reached a state closer to equilibrium (optimum Van der Waals interactions between chains) or reaction with hydroxyl groups might have occurred following the displacement of the carbonate anions by the carboxylates.

2.3.3. Correlation between TG and XRD data

The DTG curves of magnesium stearate and the intercalated LDH-SA phase cross each other at 400 and 430 °C (Fig. 2-7) It was thought that the mass loss between these two temperatures could be a quantitative measure of the amount of LDH-SA because it more or less excludes any Mg stearate like salts that might have formed. The mass loss of the uncalcined samples in the region 400-430 °C was indeed directly proportional to the relative amount of the intercalated LDH-SA phase as determined by the XRD internal standard method (R^2 = 0,9923, Table 2-3). The correlation was good because the basic LDH structure is unchanged. In Table 2-3 one can also see that the relative amount of LDH-SA that formed was dependent on the amount of water present in the medium. In the light of the time-dependent results given in Table 2-2, it is important to apply the TG quantization method only for samples reacted for the same time (e.g. 2 h) because the decomposition temperature (T_{peak}) shifted to temperatures above 430 °C at longer reaction times. When the calcination methods were added to the regression, the correlation coefficient decreased to 0,8563, because the reconstruction of the LDO in the presence of substances such as glycerol or SDS was affected due to adsorption onto the reforming crystals. When the *Carlino melt* and *Calcined-Na stearate-water*

methods were added to the equation, the correlation coefficient dropped to 0,7515, probably because the intercalation mechanisms at work are so different.

Table 2-2 Interlayer distances of samples prepared by different methods and peak temperatures (T_{peak}) for the decomposition of the LDH-SA phase.

Method	Interlayer distance of bilayer / Å	Interlayer distance of monolayer / Å	LDH-SA decomposition T_{peak} / °C
Water	49,96-50,86	-	412-414
Calcined-water	48,25-50,37	-	441-446
Ethanol-water	49,52	-	418
Ethanol	-	-	-
SDS-water	48,94-50,86	-	418
SDS-water-24 h	47,02	-	438
Calcined-SDS-water	54,48	30,74 (minor phase)	422
Calcined-SDS-water-24 h	49,52	30,35 (minor phase)	446
Glycerol-water	48,25-49,94	-	431-438
Calcined-glycerol-water	48,25-49,97	-	408-425
Calcined-Na stearate-water	48,25 (minor phase)	31,90	334
Calcined-Na stearate-water-24 h	45,90 (minor phase)	31,90	328
Carlino melt	47,04	-	410

Table 2-3 Correlation between XRD and TG data for the quantization of the LDH-SA phase.

Method	$I_{50\ Å}/I_{9,3\ Å}$ *	% Mass loss from 400-430 °C	Equation	Correlation coefficient (R^2)
SDS-water	5,0	28	y = 4,3661x + 4,9846	0,9923
***Water* (100% water)**	4,2	22		
***Ethanol-water* (50% water)**	3,0	17		
***Glycerol-water* (33% water)**	1,1	10		
***Ethanol* (no water)**	0	5		
Calcined-SDS-water	7,5	30	y = 3,3693x + 7,5653	0,8563
Calcined-glycerol-water	2,4	22		
Calcined - Water	3,2	15		
Carlino melt	1,2	20	y = 3,3755x + 7,8328	0,7515
Calcined -Na stearate	0,4	3		

* Relative amount of LDH-SA phase in region of 50 Å.

2.3.4. Recommendations for future work

It would be interesting to study the effect of varying the ratio of glycerol to water in the *Glycerol-water* method because the more glycerol present, the more carbonate will be removed, but the more water present, the more SA will intercalate due to ionization of the SA. A more thorough study of the time-dependent changes in interlayer distance and

basal reflection intensity should be conducted in future, for all methods described in this work. The shift in decomposition temperature should also be followed with time of reaction to learn more about the intercalation mechanism and product.

2.4. Conclusions

This article described a direct method for intercalating fatty acids into LDH-CO_3, due to a reaction between the carbonate and the ionized SA in aqueous media. In general, such a direct method of intercalation does not work with anions which are unreactive towards the carbonate. Even though the current experiments were carried out in air, virtually no LDH-CO_3 phase reformed in the cases where LDOs were used (Fig. 2-3). Therefore, the bilayer intercalated stearate anions has greater stability than LDH-CO_3, probably because of the stabilising effect of hydrophobic interactions between the chains [11,23]. Large scale production of the LDH-SA would, therefore, be easy because a N_2 atmosphere is not necessary.

Interestingly, XRD and FTIR analyses of the samples of these water-based methods remarkably resembled those obtained by Borja *et al.* [9] for the ion exchange of Cl^- in LDH-Cl and the fatty acid in ethanolic media. Therefore, as concluded by Borja *et al.* [9], the fatty acid intercalated in both the dissociated (COO^-) and undissociated (COOH) form. Itoh *et al*. [10] also obtained bilayer intercalated LDH-SA by exchanging the Cl^- in LDH-Cl by stearate in aqueous sodium stearate solutions (24 h, 80 °C). It is clear from Fig. 2-11, however, that reconstruction of the LDO in the presence of aqueous sodium stearate led to the intercalation of a monolayer of stearate. Therefore, when using LDH-CO_3 as a starting reagent, molten SA in aqueous medium should be used to obtain bilayer intercalation.

The reaction mixtures of method *Water* and *Calcined-Water* could not be stirred for 24 h because large lumps (> 1 cm) tended to form, making stirring difficult. The lump formation did not drastically decrease the rate of LDH-SA formation within the first 2 h in comparison to the *SDS-water* and *Calcined-SDS-water* methods and it is unknown whether the rate of reaction is inhibited upon longer stirring times. Sodium dodecyl

sulphate (SDS) not only prevented this agglomeration, but also kept the unreacted SA in emulsion; therefore removing it from the final product. A purer LDH-SA end-product resulted with less effort. The surfactant-mediated methods of intercalation are, therefore, environmentally friendly because the SDS solutions should be recyclable and no volatile or flammable organic solvents (such as ethanol) are needed to free the product from SA. In the case of the *Water* methods the products were hard lumps, whereas in the surfactant-mediated methods the products were soft and easy to grind to a fine powder. Therefore, the surfactant played a role in terms of ease of stirring and ease of purification and grinding of the product and not in facilitating the reaction. The relative amounts of LDH-SA formed in the *SDS-water-24 h*, *Calcined-SDS-water* and *Calcined-SDS-water-24 h* methods (Fig. 2-3) were similar. The *Calcined-SDS-water* method was the most time efficient and the amount of LDH-SA formation seemed to have reached a plateau within the 2 hours. The *SDS-water* method should be tested at more time intervals to determine when a plateau is reached. The thermal history of the LDH-SA (whether it was calcined or not) could have an influence on the performance of the products within a given application and should be tested. When exposing the LDO to aqueous SA, however, a thermally more stable Mg/Al stearate type salt formed and much less of the desired LDH-SA in comparison to *Calcined-SDS-water* (Fig. 2-3). In the presence of glycerol, the CO_3^{2-} of the LDH-CO_3 were removed and probably replaced by glycerolate anions, without facilitating the intercalation of SA because the 2:1 glycerol/water does not allow ionization of as much SA as do pure water.

In this study it was found that TG could be used for quantification of the LDH-SA phase (especially for uncalcined samples) because the % mass loss in the region 400-430 °C correlated with the relative amount of LDH-SA phase as determined by XRD (internal standard method). Quantitative XRD needs more sample as well as the addition of an internal standard. Furthermore, sample preparation needs to be done meticulously and repetitively to prevent orientation of the LDH-SA crystals. If preferred orientation occurs, the intensity of the interlayer distance reflection is artificially enhanced [24] and the intensity could, therefore, be subject to erroneous quantification. TG analysis, on the other hand, requires only a few milligrams of sample and no special sample preparation

techniques to prevent preferred orientation of the crystals. The gradient of the linear equation (Table 2-2) indicated that the TG analysis was 3-4 times more sensitive than XRD to the amount of LDH-SA present.

References

1 S. MIYATA and T. KUMURA, *Chem. Lett.* (1973) 843.

2 J. OLANREWAJU, B.L. NEWALKAR, C. MANCINO and S. KOMARNENI, *Mater. Lett.* **45** (2000) 307.

3 S. CARLINO, *Solid State Ionics* **98** (1997) 73.

4 E.L. CREPALDI, J. TRONTO, L.P. CARDOSO and J.B. VALIM, *Colloids Surf. A* **211** (2002) 103.

5 E.D. DIMOTAKIS and T.J. PINNAVAIA, *Inorg. Chem.* **29** (1990) 2393.

6 H.C.B. HANSEN and R.M. TAYLOR, *Clay Miner.* **26** (1991) 311.

7 S. CARLINO and M.J. HUDSON, *J. Mater. Chem.* **4** (1994) 99.

8 S. CARLINO, M.J. HUDSON, S. WAQIF HUSAIN and J.A. KNOWLES, *Solid State Ionics* **84** (1996) 117.

9 M. BORJA and P.K. DUTTA, *J. Phys. Chem.* **96** (1992) 5434.

10 T. ITOH, N. OHTA, T. SHICHI, T. YUI and K. TAKAGI, *Langmuir* **19** (2003) 9120.

11 T. KANOH, T. SHICHI and K. TAKAGI, *Chem. Lett.* (1999) 117.

12 E.L. CREPALDI, P.C. PAVAN and J.B. VALIM, *J. Mater. Chem*. **10** (2000) 1337.

13 H.R. FISCHER and L.H. GIELGENS, USP 6 372 837, Nanocomposite material, 16 April 2002.

14 J.-H. CHOY, S.-Y. KWAK, J.-S. PARK, Y.-J. JEONG and J. PORTIER, *J. Am. Chem. Soc.* **121** (1999) 1399.

15 M. JACUPKA and P.K. DUTTA, *Chem. Mater.* **7** (1995) 989.

16 J. ANWAR, in “Industrial Applications of X-ray Diffraction”, edited by F.H. Chung and D.K. Smith (Marcel Dekker, Inc., New York, 2000) p. 545.

17 M. ADACHI-PAGANO, C. FORANO and J.-P. BESSE, *Chem. Commun.* (2000) 91.

18 T. HIBINO and A. TSUNASHIMA, *Chem. Mater.* **9** (1997) 2082.

19 E.L. CREPALDI, P.C. PAVAN, J. TRONTO and J.B. VALIM, *J. Colloid Interface Sci.* **248** (2002) 429.

20 F. MILLANGE, R.I. WALTON and D. O'HARE, *J. Mater. Chem.* **10** (2000) 1713.

21 P. BRACCONI, C. ANDRÈS and A. NDIAYE, *Int. J. Pharm.* **262** (2003) 109.

22 A. CLEARFIELD, M. KIEKE, J. KWAN, J.L. COLON and R.C. WANG, *J. Inclusion Phenom. Mol. Recognit. Chem.* **11** (1991) 361.

23 K. TAKAGI, T. SHICHI, H. USAMI and Y. SAWAKI, *J. Am. Chem. Soc.* **115** (1993) 4339.

24 G.T.D. SHOULDICE, P.Y. CHOI, B.E. KOENE, L.F. NAZAR and A. RUDIN, *J. Polym. Sci. Part A: Polym. Chem.* **33** (1995) 1409.

Chapter 3

Poly(vinyl sulfonate) intercalation into stearate intercalated layered double hydroxides

Expanded version of article submitted to *Journal of Colloid and Interface Science*.

Abstract

Poly(vinyl sulfonate), PVS, was intercalated into a carbonate layered double hydroxide (LDH-CO_3), after an intercalative reaction with stearic acid in a one-pot reaction. The intercalated stearate ion exchanged with the PVS to form sodium stearate and LDH-PVS. Within an hour at 78 °C all the carbonate anions reacted. The PVS intercalated material had low crystallinity and features an interlayer distance of 13,91 Å attributed by Oriakhi *et al.* [1] to a bilayer intercalation.

Keywords: layered double hydroxides; carbonate hydrotalcite; intercalation; stearate; poly(vinyl sulfonate); ion exchange

3.1. Introduction

Intercalation of polymers into layered inorganic minerals has recently received a lot of attention [2]. The composites display physical properties, due to the molecular level interactions, that cannot be achieved by the polymer or filler alone. For instance, the polymer could be protected from UV degradation, the mineral could act as flame retardant or the thermal stability of the composite could be enhanced above that of the separate constituents [2,3].

Hydrotalcite [$Mg_6Al_2(OH)_{16}CO_3{\cdot}4H_2O$] is an anionic clay. It is a member of the family of layered double hydroxides (LDH). LDHs have the same stacked sheet structure as brucite [$Mg(OH)_2$] but are distinguished by the partial replacement of Mg^{2+} with Al^{3+} ions in the sheets and the presence of charge balancing anions, for example CO_3^{2-}, Cl^-, NO_3^- or stearate, in the interlayer [4]. The corresponding compounds are referred to as LDH-CO_3, LDH-Cl, LDH-NO_3 or LDH-SA.

Several methods have been employed [1,5,6,7] to intercalate polymers into LDHs and other layered minerals or clays. Anionic polymers such as poly(styrenesulfonate), poly(acrylic acid) and poly(vinylsulfonate) have been intercalated by synthesizing the LDH in the presence of the polymer [1,5]. The products obtained were amorphous but hydrothermal treatment improved the crystallinity [5]. The polymers only intercalated under N_2 atmosphere. When the procedure was attempted in air, the carbonate intercalated LDH (LDH-CO_3) was obtained [1]. Choy *et al.* [6] successfully intercalated DNA (deoxyribonucleic acid, an anionic polymer) into Mg_2Al-NO_3 LDH by ion exchange. The key to intercalation into layered species is usually to modify the interlayer region by surfactants with hydrophobic tails [2]. This surfactant-mediated method was successfully used by Kerr *et al.* [7] to intercalate poly(*p*-phenylene) into MoO_3. The polymer chains are preferentially adsorbed into the hydrophobic interlayer region from the polar solution.

Due to the strong electrostatic and hydrogen-bond interactions, the carbonate anions in the interlayer are difficult to ion exchange. When the LDH-CO_3 is dehydroxylated and decarbonated at 400 - 500°C to form a layered double oxide (LDO) and subsequently reconstructed in an aqueous solution of a carboxylic acid (or its salt) or anionic surfactant, intercalation of the acid or the surfactant can be achieved [8]. Fatty acids such as stearic acid, however, can be intercalated into uncalcined LDH-CO_3 (unpublished results). The stearate anions intercalate as a bilayer into the interlayer of the LDH (Fig. 3-1) with an interlayer distance in the region of 50 Å. The aim of this study was to intercalate stearate anions into the interlayer region of $Mg_4Al_2(OH)_{12}CO_3{\cdot}3H_2O$ (LDH-CO_3) by using molten stearic acid (SA) emulsified by poly(vinyl sulfonate) in a water-ethanol medium. Possibly the stearate bilayer would facilitate the intercalation of the PVS. This would represent an easy and environmentally friendly method of intercalating an anionic polymer into the cheap LDH-CO_3, without the need for energy intensive calcination.

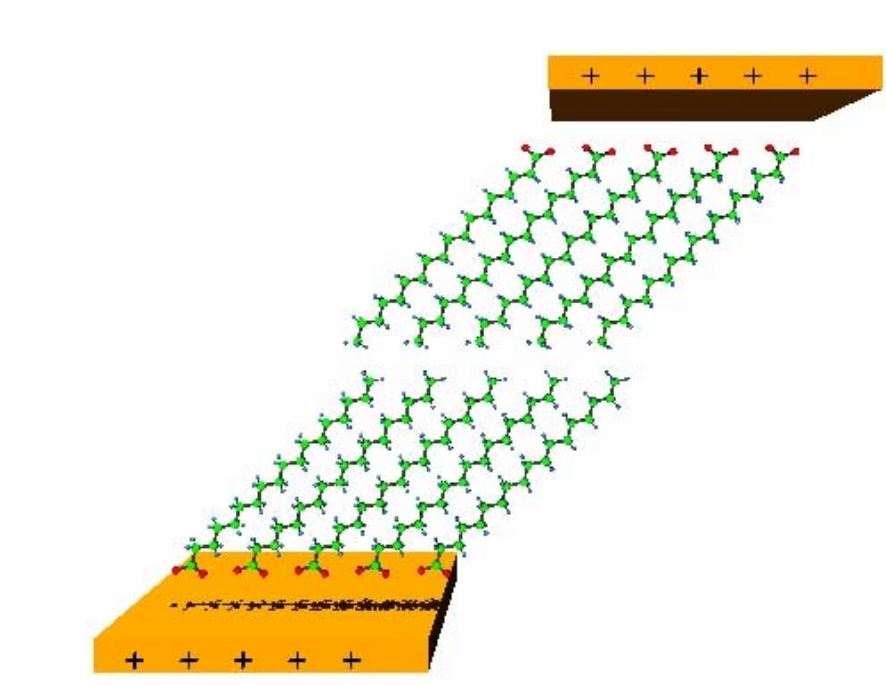

Figure 3-1 Bilayer arrangement of stearate intercalated LDH (LDH-SA).

3.2. Materials and methods

3.2.1. Materials

The layered double hydroxide used in this study had the chemical composition $Mg_4Al_2(OH)_{12}CO_3{\cdot}3H_2O$. The mole ratio of Mg:Al was determined from XRF analysis as 2.01:1 (Appendix B). The LDH was received from the local manufacturer Chamotte Holdings (Pty) Ltd. The particle size distribution as determined by a Mastersizer 2000 (Malvern Instruments) was d(0,1): 0,694 μm; d(0,5): 5,062 μm and d(0,9): 23,925 μm. The theoretical anionic exchange capacity of this LDH-CO_3 was calculated to be 213 meq/100 g.

25% m/m poly(vinyl sulfonate, sodium salt) solution in water (PVS, Mw 70 000, Sigma-Aldrich), stearic acid ($C_{18}H_{36}O_2$, Merck, 85% pure) and ethanol (96% rectified, Dana Chemicals) were used. Reactions were carried out in deionized water. Deionized water, tap water or solutions of $CaCl_2.2H_2O$ (UNIVAR®, Saarchem) in deionized water (20 volume equivalents) were used to dilute the reacted mixtures (1 volume equivalent).

3.2.2. Intercalation method

8 g of the 25% m/m sodium-PVS solution in water was added to 57 ml deionised water to obtain a solution consisting of approximately 2 g of PVS in 60 ml water. This solution was heated to 78 °C. 0,7 g stearic acid (SA) was dissolved in 30 ml ethanol and heated to approximately 60 °C. The SA solution was slowly added to the PVS solution and the temperature allowed to reach 78 °C. 0,34 g of the LDH powder was added to the solution and stirred for 1 h. Itoh *et al.* [9] found that stearate is capable of intercalating up to about 225% of the anionic exchange capacity (AEC) of the LDH and therefore a level of 200% SA in relation to the AEC was used. The reaction mixture will be referred to as the PVS-SA-LDH mixture.

3.2.3. Characterization

3.2.3.1. *Fourier Transform Infrared spectroscopy (FTIR)*

A Perkin Elmer Spectrum RX I FT-IR System was used to scan the infrared transmittance through a KBr (Uvasol, potassium bromide, Merck) pellet 32 times at a resolution of 2 cm^{-1}. The averaged spectrum was background-corrected using a pure KBr pellet run under similar conditions. The pellets were prepared with approximately 2 mg of sample and 100 mg of KBr. The 2 mg powder samples were obtained by diluting the cooled down reaction mixture with a 20-fold excess of deionised or tap water or $CaCl_2$ solution, in order to release (flocculate) the insoluble reaction products, which were subsequently centrifuged off, washed again (to remove any unreacted PVS or salts), dried and ground.

3.2.3.2. *Powder X-ray Diffraction (XRD)*

The XRD analyses were performed on a Siemens D500 X-ray system equipped with a 2.2 kW Cu long fine focus tube, variable slit and secondary graphite monochromator (to eliminate K_β radiation and reduce fluorescent radiation). The system is computer controlled using SIEMENS DIFFRAC ^{Plus} software. The goniometer was set to reflection mode. Samples were scanned from 1 to 35° 2θ with Cu K_α radiation (1,5418 Å) at a speed of 0.02° 2θ, with a recording time of 2 s per step and generator settings of 40 kV and 30 mA. Part of the reacted mixture was cast onto an aluminium sample holder and the solvent was allowed to evaporate. This was repeated a few times to obtain enough material to mask the aluminium. One would expect the intercalated LDH phases to be highly oriented within these holders and the interlayer distances to be preferentially enhanced [10].

3.2.3.3. *Scanning Electron Microscopy (SEM)*

A small disc of the clear and white parts of the gel was placed onto carbon stubs of approximately 5 mm diameter. It was frozen in a Reichert KF80 plunge freezer (Vienna, Austria). A drop of the gel that was diluted with deionized water was also placed on a stub and was frozen in the same way. The frozen samples were

dried in a custom-built high vacuum freeze drier (Pretoria Technicon, South Africa). A drop of the gel that was diluted with deionized water was also allowed to air dry on a stub. These were coated by chromium in a high resolution ion beam coater, Gatan model 681 (Warrendale, PA, USA) and studied with a JSM-6000F field emission scanning electron microscope (JEOL, Tokyo, Japan).

3.2.3.4. *Transmission Electron Microscopy (TEM)*

The mixture (before onset of gelling) was diluted with deionised or tap water. A droplet of the solution containing white suspended particles was placed onto a carbon coated formvar grid, the excess water was removed by the capillary action of filter paper and it was allowed to dry in air. The Philips EM301 (Eindhoven, Netherlands) Transmission electron microscope was used.

3.3. Results and discussion

3.3.1. General

After the addition of the LDH-CO_3 to the SA-PVS emulsion, CO_2 gas was released. Some particles settled to the bottom after the reaction, but most of the particles were suspended. In time a small amount of clear solution collected at the top. Within a few days both the clear phase and the reaction mixture as a whole had gelled. Upon shaking, the gel broke but reformed in time. Experiments showed that the sodium PVS solutions did not gel in the presence of Mg^{2+}, Al^{3+}, Ca^{2+} or H^{+} ions as some other anionic polymers do. The gelling mechanism is, therefore, unknown.

Before the onset of the gelling, some of the mixture was diluted with water. Upon addition of 20 volumes of deionized water, a suspension of white fluffy particles (> 10-20 μm, Fig. 3-7E) formed. After centrifuging, the sediment particles went back into suspension upon the least disturbance, probably due to electrostatic repulsion. The white particles have been unchanged and in suspension for more than a year at the time of writing. Upon dilution with tap water, however, the suspension became unstable and the fluffy particles collected at the top. With

time the particles formed heavy white globules, which settled to the bottom. After 2 to 3 months the solution and the sediment became yellow due to oxidation of the PVS (Fig. 3-2).

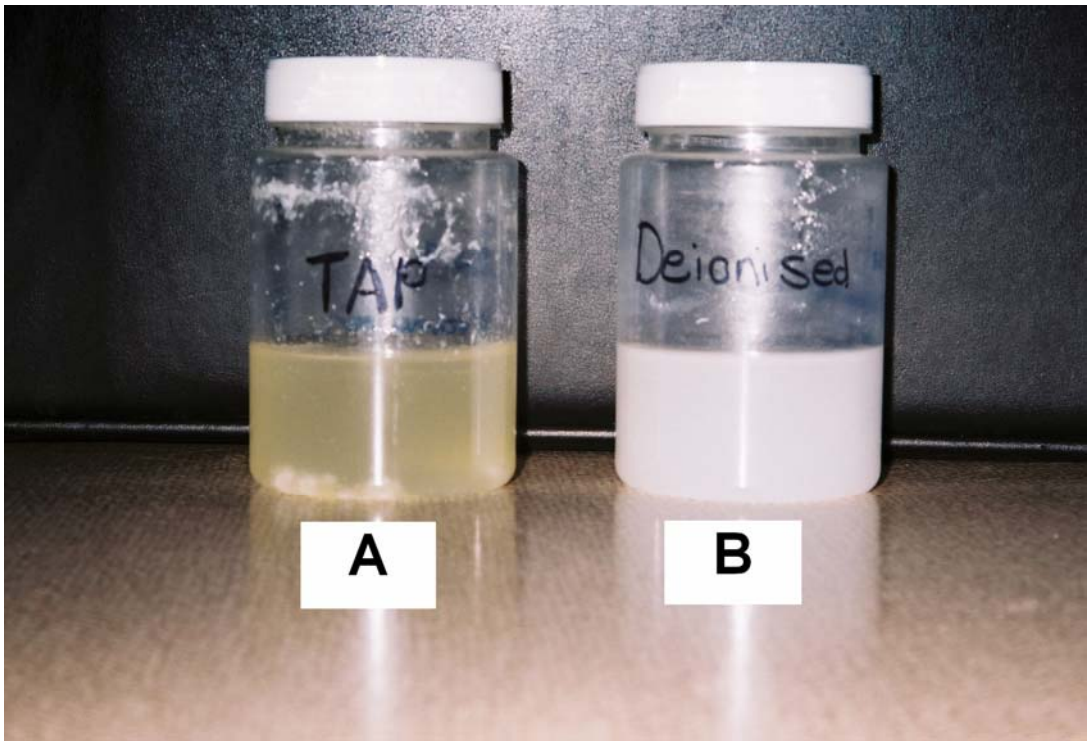

Figure 3-2 The reaction mixture diluted with tap water (A) and deionized water (B), showing that the suspension is destabilized by the divalent cations in tap water, leading to PVS release and decomposition.

3.3.2. FTIR results

When PVS was not present in the system, the reaction between LDH-CO_3 and SA could not proceed to completion under the conditions employed (78 °C, 1 h) as evidenced by the presence of unreacted carbonate (1367 cm^{-1}) and unreacted carboxylic acid (1703 cm^{-1}) in Fig. 3-3A. In the presence of other surfactants, such as sodium dodecyl sulfate (SDS), the reaction also does not go to completion, even in 24 hours. In the presence of PVS, however, the reaction proceeded to completion under the same conditions (only 1 hour). Only a small carbonate vibration peak remained at 1383 cm^{-1} (Fig. 3-3B). The LDH platelets

were still intact, because the OH stretching vibration (3440 cm^{-1}) and the O-M-O bending vibration (446 cm^{-1}) were present (Fig. 3-4) [11]. If the hydroxide layers had reacted to form an Mg/Al type stearate salt, these vibrations would no longer be present. The PVS is intercalated (refer to Section 3.3.3): In spite of extensive washing, the sulfonate peak around 1176-1181 cm^{-1} remains (Figs. 3 and 4B).

When heating and melting SA in the presence of PVS, no acid-base reaction can occur because sodium PVS is a weak conjugated base of the strong polyvinyl sulfonic acid. Therefore, one does not expect sodium stearate and polyvinyl sulfonic acid to form. Upon cooling, the SA crystallizes out of the emulsion. When the PVS-SA-LDH reaction product was diluted with tap water or $CaCl_2$ solution, the observable peaks in the carboxylate asymmetric stretching region were different from when it was diluted with deionized water. The peak at 1558 cm^{-1}, which corresponds to that of sodium stearate, decreased in intensity and peaks at 1572 and 1539 cm^{-1}, which corresponds to that of calcium stearate, appeared (Figs. 3B and C). Therefore, sodium stearate formed during the PVS-SA-LDH-CO_3 reaction. In comparison, when PVS is absent, the vibration peaks in the carboxylate asymmetric stretching region were typical of stearate intercalated LDHs (Fig. 3-3A and [12]).

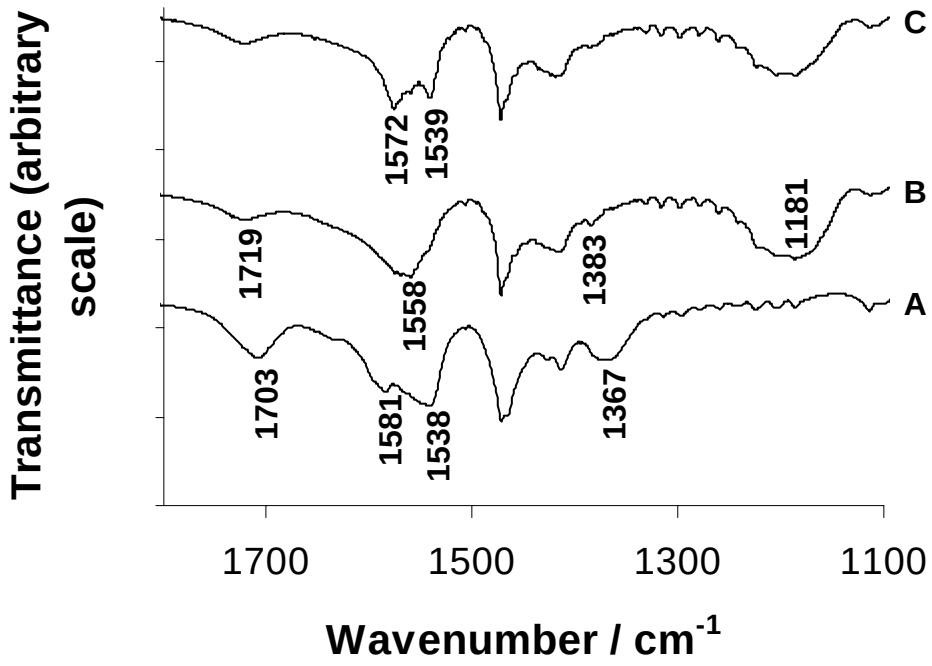

Figure 3-3 FTIR spectra of the LDH-SA (A), PVS-SA-LDH product (B) and the PVS-SA-LDH product isolated from tap water (C), showing that sodium stearate (1558 cm^{-1}) formed, which changed to calcium stearate (1572 cm^{-1}, 1539 cm^{-1}) in tap water in contrast to the typical LDH-SA bands at 1538 cm^{-1} and 1581 cm^{-1} (A).

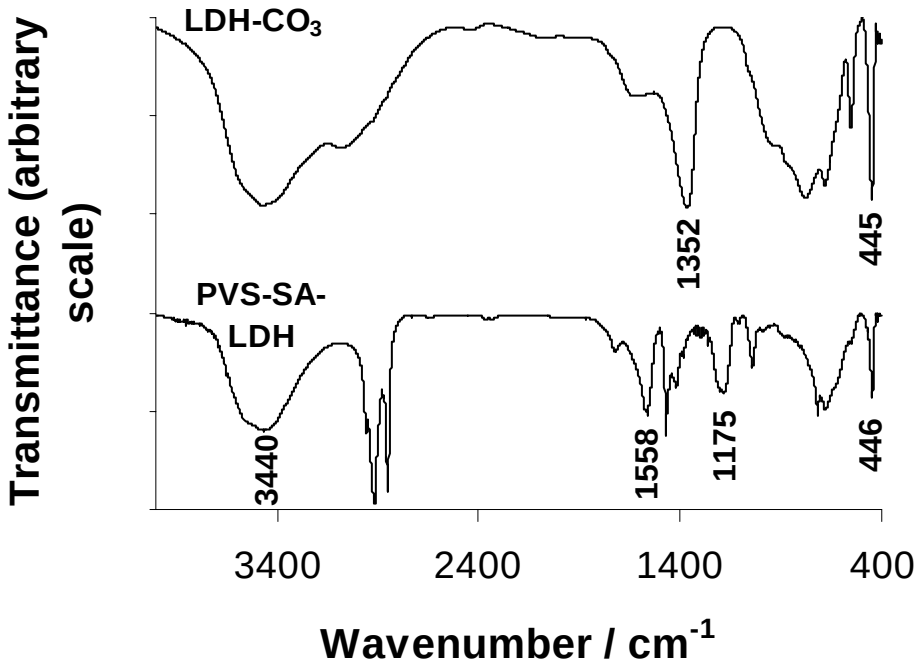

Figure 3-4 FTIR spectra of the PVS-SA-LDH reaction mixture (bottom) and the LDH-CO_3 (top), showing that the PVS intercalated and that the LDH platelets were intact (O-M-O bending vibration at 445 cm^{-1}).

It is supposed that the mechanism of intercalation of the PVS into the LDH consists of two steps. First, the acid-base reaction between SA and the interlayer carbonate anions takes place, releasing H_2CO_3 and eventually CO_2, with the stearate anions being intercalated as bilayers. Second, the sodium PVS ion exchange with the stearate ions, releasing sodium stearate and the PVS intercalates. The entropy gain due to the release of the bilayer-intercalated stearates is probably larger than the entropy loss due to the intercalation of the PVS. The sodium stearate probably stabilized the suspended particles through electrostatic repulsion, but in tap water calcium stearate formed, which precipitated and, hence, could not stabilize the suspension.

3.3.3. XRD results

The X-ray diffractogram (Fig. 3-5) of the reaction product obtained in the absence of PVS showed the presence unreacted SA (39,20 Å, 13,17 Å, 4,12 Å and 3,11 Å), unreacted LDH-CO_3 (7,60 Å, 3,79 Å and 2,57 Å) and bilayer intercalated LDH-SA (49,52 Å, 25,43 Å, 17,11 Å, 10,29 Å). The product obtained in the presence of PVS was amorphous (broad, low intensity reflections, Fig. 3-6). The reflections at 13,91 Å (and 6,94 Å, second order) are due to intercalation of a bilayer of PVS [1] and it correlates well with the value of 13,1 Å observed by Oriakhi *et al.* [1]. The reflection at 45,17 Å is probably the remnant of bilayer intercalated LDH-SA which was too stable to allow for exchange with PVS chains because of the high degree of interpenetration of the two stearate layers. There was only a small reflection left at 7,81 Å, indicating that most of the LDH-CO_3 reacted. When stirring the LDH-CO_3 and PVS together under the same conditions but in the absence of SA, the diffractogram of the LDH-CO_3 was unchanged (not shown). This is due to the stability of the LDH-CO_3 and the slow diffusion of the polymer chains [1]. The intercalated stearate anions destabilize the layered structure and allows for the PVS chains to intercalate.

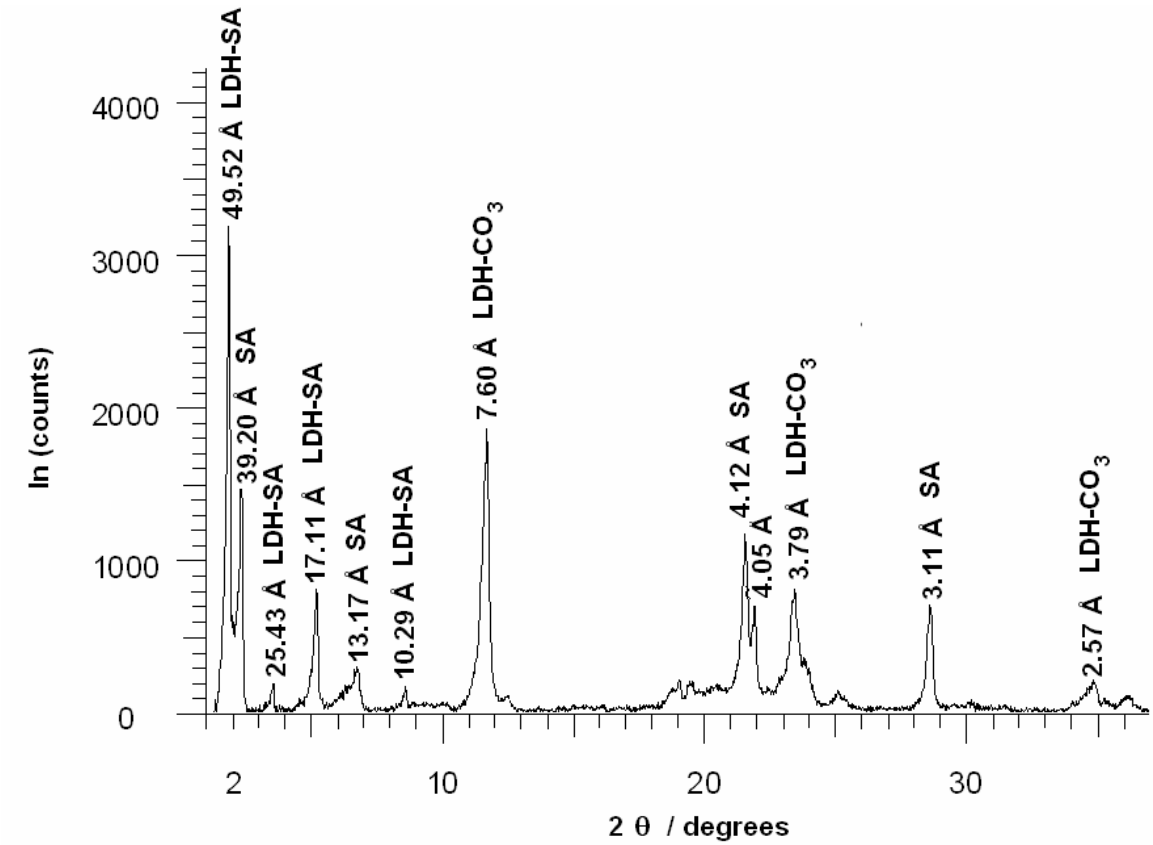

Figure 3-5 X-ray diffractogram of the LDH-SA product formed in the absence of PVS, showing that it is highly crystalline.

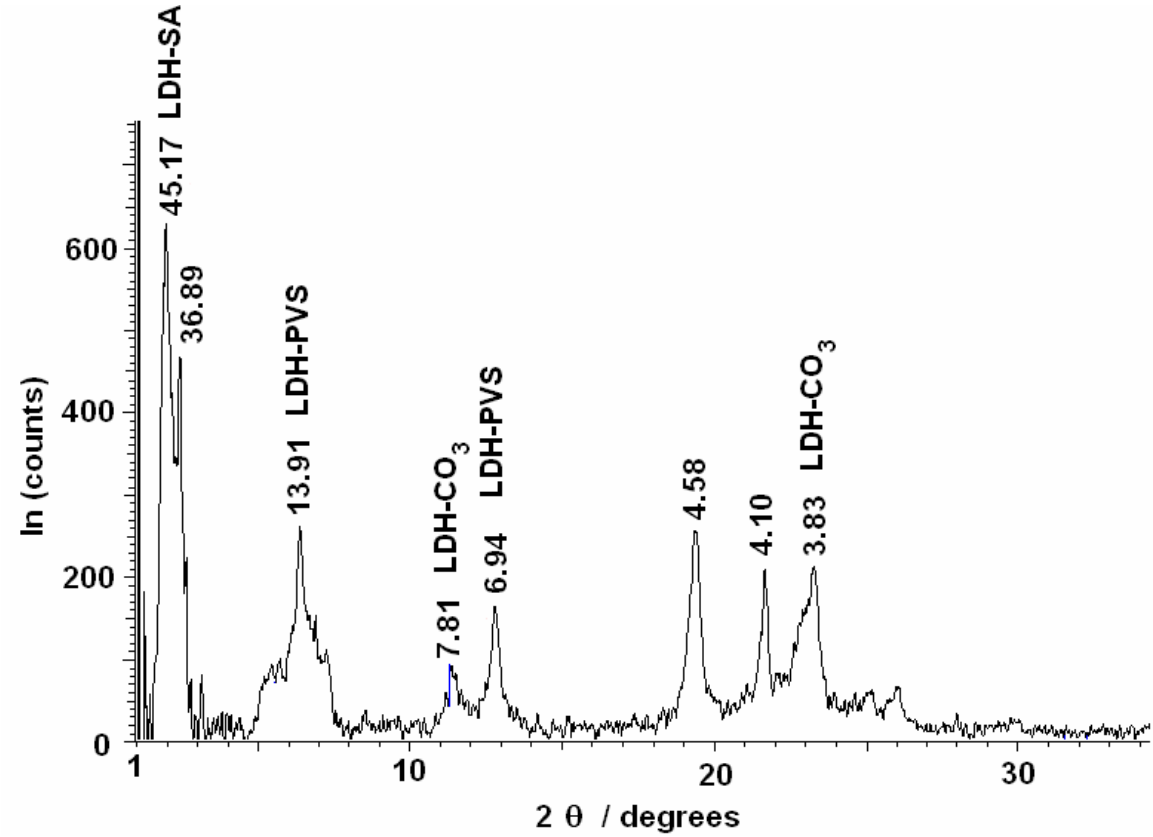

Figure 3-6 X-ray diffractogram of the dried PVS-SA-LDH reaction mixture, showing that the LDH-SA reflections diminished and LDH-PVS appeared at around 13,91 Å. The peaks are broad and of low intensity, attesting that the products are less crystalline.

3.3.4. SEM results

The FTIR results showed that sodium stearate had formed. It was originally thought that the gelling was caused by formation of sodium stearate within the PVS-SA-LDH mixture. When the microstructures of sodium stearate (Fig. 3-7A) and the clear part of the gel (Fig. 3-7B) are compared, this is clearly not the case. The latter shows a spaghetti-like structure approximately 200 nm in diameter and several micrometers in length. Fig. 3-7C is the SEM micrograph of the white part of the gel, which shows large plate-like structures of the LDH (> 10 μm diameter), which are similar to the structures obtained by Itoh *et al*. [9] for stearate intercalated LDHs. The SA and PVS stabilize this plate-like structure above the usual sand-rose – intergrown particulates – structure of LDH-CO_3 (Fig. 3-7D) [13]. The SEM micrograph (Fig. 3-7E) of the freeze-dried suspension of the mixture diluted with deionized water consisted of large thin plate-like structures (> 20 μm diameter). When the diluted mixture was allowed to air dry, the plate-like structures seemed to role up into tubes of diameter 0,5 – 1 μm (Fig. 3-7F). When freeze-dried, the rolling up could not take place and the large, thin plates remained in their original state. Dispersing these plate-like structures, of which the thickness is in the sub-micrometre region, into polymer matrices could lead to the formation of nanocomposites.

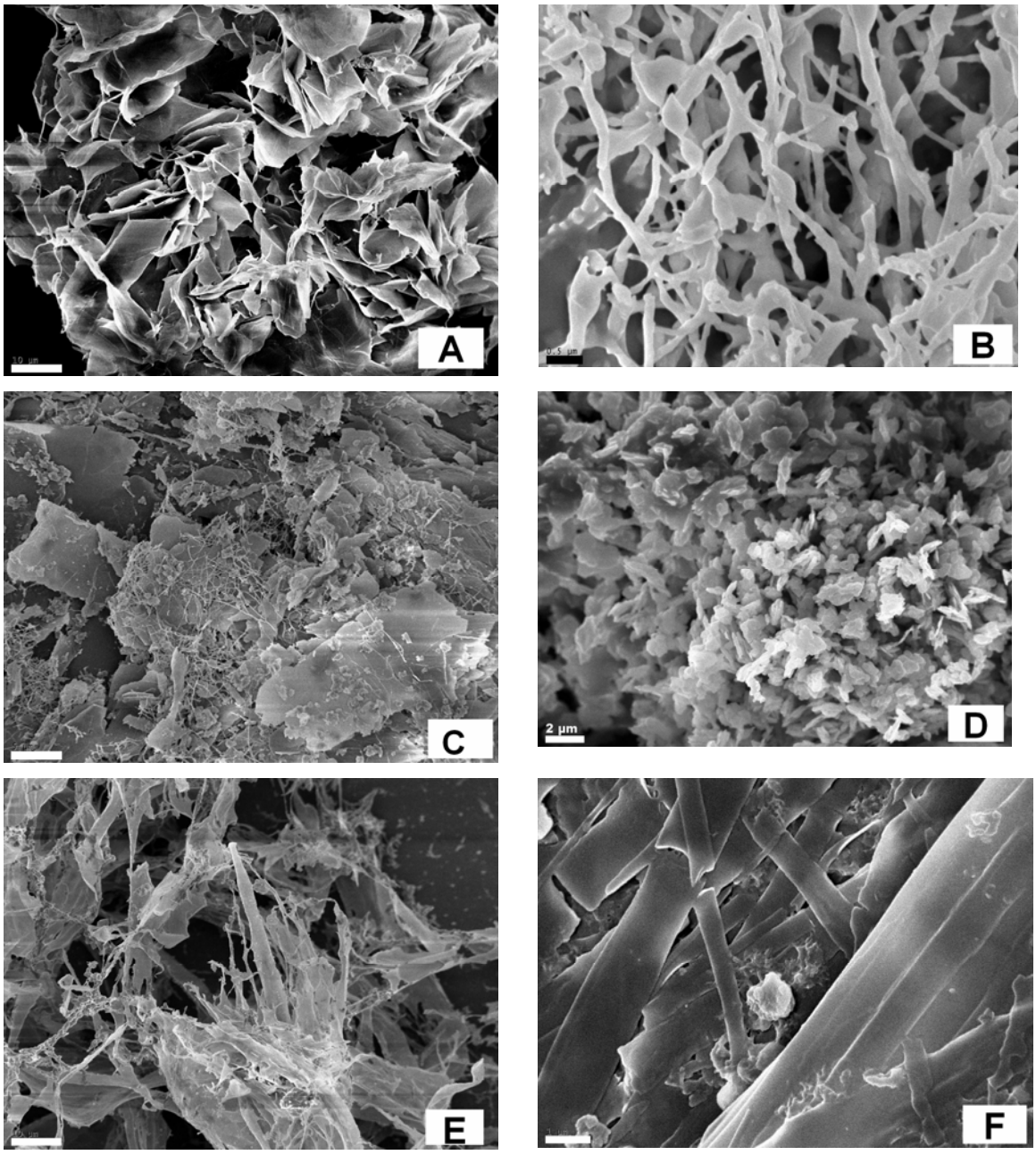

Figure 3-7 Scanning electron micrographs of

(A) Freeze-dried sodium stearate gel, bar is 10 µm.
(B) Freeze-dried clear part of the gel of the PVS-SA-LDH reaction mixture, bar is 500 nm.
(C) Freeze-dried white part of the gel of the PVS-SA-LDH reaction mixture, bar is 5 µm.
(D) The sand-rose microscopic structure of the LDH-CO_3, bar is 2 µm.
(E) Freeze-dried sample of the diluted PVS-SA-LDH suspension, bar is 10 µm.
(F) Air-dried sample of the diluted PVS-SA-LDH suspension, bar is 1 µm.
(G)

3.3.5. TEM results

The TEM images of the tap and deionized water diluted air-dried samples showed the presence of long fibers or tubes (Figs. 8A and B, > 10 μm long and 1 μm wide, possibly the same as was seen in Fig. 3-7F), small unreacted particulates (black, less than 1 μm in size) and large plate-like structures (approximately 10 μm diameter, Figs. 8C and D). In the case of diluting with tap water, the fibers looked more etched, as if it reacted (Fig. 3-8B). Upon drying, the plate-like structures seemed to crack (Fig. 3-8C). It might be that this cracking phenomenon led to the formation of the fiber- or tube-like structures; or perhaps the large plates rolled up to form long, thin tubes. The fibers seem to be of the same length as the diameter of the flat layers (10-20 μm, Figs. 7C, 7E and 8D). Tube-like and fiber-like features were reported by Leontidis *et al.* [14,15] for PEO-SDS-acetate-Pb-sulfide containing systems as well as by Ogata *et al.* [16] for $Zn(OH)_2$-carboxylic acid systems, which are both similar to the current system (layered inorganic substances in combination with carboxylic acids). The fact that the plates are so thin attests to the fact that the sand-rose morphology was broken down to a large extent and that the stearate and PVS stabilized the structure at a few layers. It is possible that exfoliation took place some extent as well. Moujahid *et al.* [5] found that LDH-Cl exfoliated in excess polystyrene sulfonate and possibly the same happened for LDH-SA in excess PVS, which also explains the almost featureless X-ray diffractogram (Fig. 3-6).

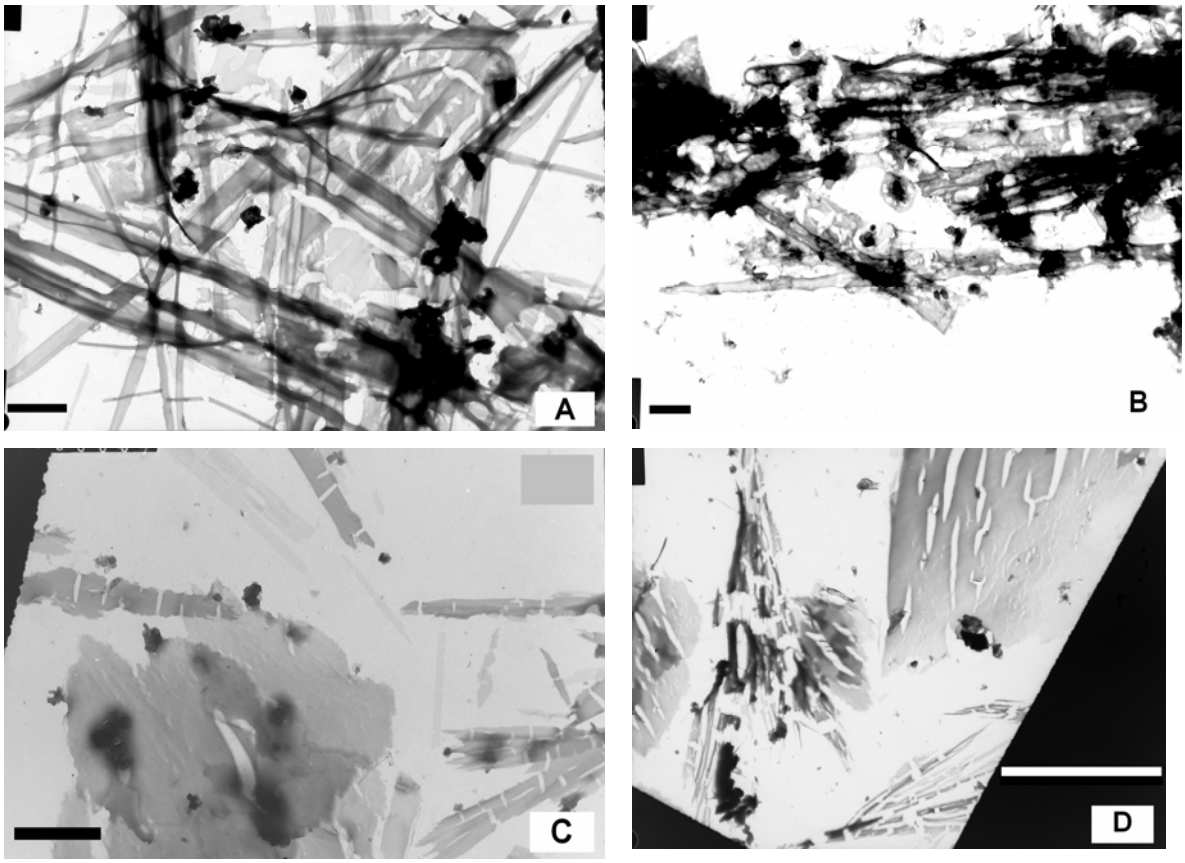

Figure 3-8 Transmission electron micrographs of

(A) Deionized water diluted PVS-SA-LDH reaction mixture dried in air, showing smooth fibers or tubes. Bar is 2 μm.

(B) Tap water diluted PVS-SA-LDH reaction mixture dried in air, showing etched (reacted) fibers or tubes. Bar is 2 μm.

(C) Deionized water diluted PVS-SA-LDH reaction mixture dried in air, showing large, plate-like structures. Bar is 3 μm.

(D) Deionized water diluted PVS-SA-LDH reaction mixture dried in air, showing cracked plate-like structures. Bar is 10 μm.

3.4. Conclusions

The stearic acid reacted with all of the carbonate in the interlayer (FTIR results). XRD showed that the PVS had intercalated and the amount of LDH-SA had diminished. The stearate and PVS anions exchanged to form sodium stearate. The process might be driven by the increase in entropy due to the disassembly of the stearate bilayer. Calcination was not necessary to successfully intercalate the stearate and PVS into the LDH-CO_3; therefore the LDH platelets could keep their original crystallinity. No N_2 atmosphere was needed, probably because the LDH-SA is of similar stability than the LDH-CO_3. The layered mineral or clay is sometimes modified by a surfactant in a separate step before introducing the polymer [2], but in the current system the surfactant modification and polymer incorporation takes place in one pot. In most other instances the polymer intercalated LDHs is prepared by synthesizing (coprecipitating) the LDH in the presence of the polymer; a procedure which requires a N_2 atmosphere. The current process is more environmentally friendly (no calcination, single batch), cheap (LDH-CO_3 starting reagent) and upscalable (no N_2 atmosphere).

The intercalated PVS appears to be stabilized and protected from oxidative or UV degradation (Fig. 3-2). This reaction could possibly be carried out simultaneously with emulsion polymerization of polymers in order to ensure good dispersion of the LDH into the polymers, which could lead to the formation of nanocomposites. The PVS intercalation could also be a model for intercalation of other anionic polymers, like DNA, by the same method.

References

1 C.O. ORIAKHI, I.V. FARR, M.M. LERNER, *J. Mater. Chem.* **6** (1996) 103.

2 F. LEROUX, J.-P. BESSE, *Chem. Mater.* **13** (2001) 3507.

3 P.B. MESSERSMITH, S.I. STUPP, *Chem. Mater.* **7** (1995) 454.

4 S. MIYATA and T. KUMURA, *Chem. Lett.* (1973) 843.

5 E.M. MOUJAHID, J.-P. BESSE, F. LEROUX, *J. Mater. Chem.* **12** (2002) 3324.

6 J.-H. CHOY, S.-Y. KWAK, J.-S. PARK, Y.-J. JEONG, J. PORTIER, *J. Am. Chem. Soc.* **121** (1999) 1399.

7 T.A. KERR, F. LEROUX, L.F. NAZAR, *Chem. Mater.* **10** (1998) 2588.

8 E.L. CREPALDI, J. TRONTO, L.P. CARDOSO, J.B. VALIM, *Colloids Surf. A* **211** (2002) 103.

9 T. ITOH, N. OHTA, T. SHICHI, T. YUI, K. TAKAGI, *Langmuir* **19** (2003) 9120.

10 G.T.D. SHOULDICE, P.Y. CHOI, B.E. KOENE, L.F. NAZAR, A. RUDIN, *J. Polym. Sci.* Part A: Polym. Chem. **33** (1995) 1409.

11 J.T. KLOPROGGE, L. HICKEY, R.L. FROST, *J. Mater. Sci. Lett.* **21** (2002) 603.

12 M. BORJA, P.K. DUTTA, *J. Phys. Chem.* **96** (1992) 5434.

13 M. ADACHI-PAGANO, C. FORANO, J.-P. BESSE, *Chem. Commun.* (2000) 91.

14 E. LEONTIDIS, T. KYPRIANIDOU-LEODIDOU, W. CASERI, K.C. KYRIACOU, *Langmuir* **15** (1999) 3381.

15 E. LEONTIDIS, T. KYPRIANIDOU-LEODIDOU, W. CASERI, P. ROBYR, F. KRUMEICH, K.C. KYRIACOU, *J. Phys. Chem. B* **105** (2001) 4233.

16 S. OGATA, H. TAGAYA, M. KARASU, J. KADOKAWA, *J. Mater. Chem.* **10** (2000) 321.

Chapter 4

Stearate intercalated layered double hydroxides: effect on the physical properties of dextrin-alginate films

Expanded version of article submitted to *Journal of Materials Science*.

Abstract

The effect of stearate intercalated layered double hydroxides (LDH-SA) on the water vapour permeability (WVP) and mechanical properties of glycerol plasticized dextrin-alginate films were tested. The LDH $Mg_4Al_2(OH)_{12}CO_3{\cdot}3H_2O$ and stearic acid (SA) were reacted in different mass ratios within the film solutions. The filler (SA and LDH) concentration was fixed at 16% m/m of the dried films. Infrared spectroscopy verified that the SA did indeed intercalate. WVP measurements showed a broad range of minima around filler compositions of 50-80% SA (and 50-20% LDH). The Young's moduli of the films showed a maximum increase of 213% around the filler composition of 60% SA (40% LDH). From the interlayer distances and intensities of the basal reflections of the LDH-SA (as determined from X-ray diffraction, XRD) and the increased Young's moduli it was concluded that delamination and exfoliation of the LDH-SA took place. A layered and oriented microscopic structure was seen by scanning electron microscopy (SEM).

Keywords: Layered double hydroxides, stearic acid, intercalation, starch, dextrin, alginate, edible films, water vapour permeability, Young's modulus, exfoliation, delamination, cross-linking

4.1. Introduction

Edible films are used to protect foodstuff from water vapour and oxygen in their environment and to prevent water moving from one part to another in multi-component foodstuffs, for example to separate the filling or sauce from the dough of pizzas or pies. Most edible film-forming polymers or hydrocolloids (such as starch, sodium alginate, and sodium caseinate) are hydrophilic and pose no barrier against water vapour, and becomes soggy in contact with water. Lipid films are good barriers against water, but have little structural integrity. This problem has been overcome using laminates of hydrocolloid and wax films and also by making emulsions of the wax or lipid within the hydrocolloid solution. Waxes such as beeswax and stearic acid are emulsified within the surface-active sodium alginate or sodium caseinate and their blends with starch. [1,2,3]

Polymer-layered clay nanocomposites are filled polymers in which at least one of the dimensions of the filler is in the nanometre range (less than 100 nm). Nanocomposites in general have increased modulus, strength and heat resistance, as well as decreased gas permeability and flammability in comparison to the pristine polymer. [4] Studies were done on preparing composites of starch with kaolin [5], Ca^{2+} hectorite [6] and kaolinite, hectorite, layered double hydroxide (LDH) and brucite [7]. These studies focused mainly on the mechanical properties and microstructure of the composites as well as determining whether exfoliation took place by means of X-ray diffraction. These platelet fillers, however, can ideally be used to reduce the WVP of hydrophilic polymers such as starch or alginate.

The water vapour permeability (WVP) and also the permeability to large organic molecules (or pharmaceuticals) of sodium alginate and sodium caseinate films can be reduced by cross-linking with polyvalent cations, e.g. Ca^{2+}. This can be done by immersing films in solutions of Ca^{2+} salts [3] or by *in situ* leaching Ca^{2+} ions from insoluble $CaCO_3$ by acids [8]. This mechanism might play a role in the

current system that is composed of an insoluble layered double hydroxide and stearic acid.

Hydrotalcite is an anionic clay mineral with the composition $Mg_6Al_2(OH)_{16}CO_3.4H_2O$. It has the same layered structure as brucite [$Mg(OH)_2$] but with some of the Mg^{2+} ions substituted by Al^{3+} ions. The presence of the Al^{3+} ions gives rise to a residual positive charge in the layers. This positive charge is balanced by anions such as CO_3^{2-}, Cl^- and NO_3^- or organic anions in the interlayer. [9] A range of compositions is possible in terms of bivalent and trivalent cations and of their relative amounts. These types of compounds are more generally referred to as layered double hydroxides (LDHs).

In the present study a combination of an LDH [$Mg_4Al_2(OH)_{12}CO_3{\cdot}3H_2O$] and stearic acid (SA) was used to reduce the WVP of glycerol-plasticized dextrin-alginate films. Ideally the SA would intercalate into the LDH structure to form LDH-SA during the film solution preparation. Stearate and other surfactant intercalated LDHs have large, plate-like microscopic structures [10,11] and this extended plate-like structures would lower the WVP of the dextrin-alginate films depending on their relative orientation within the films.

4.2. Experimental

4.2.1. Materials

The materials used, their source of origin, and their respective roles are given in Table 4-1.

Table 4-1 Components of the films and their roles.

Component name	From	Role
Dextrin, Stydex 074030	African Products (Pty.) Ltd, South Africa.	Biodegradable polymer
Sodium Alginate (E401), Manugel GMB, viscosity of 1% solution is 185 cps.	Kelco International Limited	Biodegradable polymer, film former, emulsion stabilizer (due to high viscosity), prevent agglomeration of LDH-SA
99% Glycerol	Merck, UNILAB®	Plasticizer
85% Stearic acid	Merck	Hydrophobic, intercalate into LDH.
LDH, $Mg_4Al_2(OH)_{12}CO_3{\cdot}3H_2O$ Particle size distribution by Mastersizer 2000 (Malvern Instruments): d(0,1): 0,694 μm; d(0,5): 5,062 μm and d(0,9): 23,925 μm. The XRF analysis is given in Appendix B.	Chamotte Holdings (Pty.) Ltd., South Africa	Filler, intercalated by SA.
Talc	Sigma-Aldrich, < 10 micron, $3MgO.4SiO_2.H_2O$	Filler, cannot be intercalated by SA. Coated and dispersed by SA.
Bentonite Ocean Clear	Boland Base Minerals, South Africa	Filler, cannot be intercalated by SA, coated and dispersed by SA.
Foamaster 8034	Cognis	Prevent foam formation due to CO_2 release.
Deionised water or tap water		Solvent
Ethanol, rectified 96%	Dana Chemicals	Solvent

4.2.2. Film production procedure

Wu *et al*. [1] attempted to lower the WVP of starch-alginate films by using, amongst others, SA. Their recipe was followed (Table 4-2) except that lecithin (emulsifier) was not used. The LDH, $Mg_4Al_2(OH)_{12}CO_3{\cdot}3H_2O$, was used additionally to the recipe of Wu *et al.* [1]. The ratio of SA and LDH was varied to determine its effect on WVP and Young's modulus. The SA and LDH together are referred to as the filler, which can consist of 100% SA, 100% LDH or any ratio in between. This filler content was kept constant at 16.56% m/m of the dried film, which is similar to the amount used by Wu *et al.* [1]. Films are referred to in terms of the SA content of the filler in the Figures and by annotations such as 60SA/40LDH for a film where the filler consists of 60% SA and 40% LDH by mass. CO_2 is released during the intercalation of stearate into LDH and this necessitated the use of a defoamer.

Table 4-2 Relative amounts of the different components in the films solutions and dry films.

Constituent	Typical amounts / g	% in film solution	% in dried film
Dextrin	2,5	2,78	41,39
Sodium alginate	1	1,11	16,56
Glycerol	1,4	1,55	23,18
SA	0 - 1	0 - 1,11	0 - 16,56
LDH	1 - 0	1,11 - 0	16,56 - 0
Defoamer	0,14	0,16	2,32
Water	60	66,64	-
Ethanol	24	26,65	-

Dextrin, sodium alginate and the LDH were mixed and crushed in a mortar and pestle. This procedure broke the LDH particles down by shear forces. The presence of the LDH also prevented the alginate from forming lumps during dissolution. The powdered mixture was slowly added to the water, ethanol, glycerol and SA solution at 78°C. A reaction time of one hour was used

throughout. Although the defoamer was effective, the mixtures were ultrasonicated in warm water to ensure release of all trapped bubbles still present. 8 g portions of the solutions were cast into metal rings of approximately 67 mm diameter (Fig. 4-1) to prepare samples for WVP analyses. 45 g portions were cast into 150 mm square metal holders that were placed on a non-stick silicone sheet (Silicone zone®). The samples were left to dry at room temperature and then removed by peeling. The films were cut into 45 mm diameter circles for WVP tests or punched into dumbbell shapes (6 mm wide, 35 mm gauge length, 115 mm total length) for tensile testing. Samples were conditioned for two weeks at 23 ± 2 °C, 75 % RH (saturated NaCl solution [12]) prior to analysis.

One film was made with tap water to determine whether the Ca^{2+} ions would have a negative effect (by reducing the alginate solubility) or a positive effect (by cross-linking the alginate) on the WVP.

Figure 4-1 Casting of film solution into metal rings.

4.2.3. Characterization

4.2.3.1. *Fourier Transform Infrared spectroscopy (FTIR)*

A Perkin Elmer Spectrum RX I FT-IR System was used to scan the infrared transmittance through a KBr (Uvasol, potassium bromide, Merck) pellet 32 times at a resolution of 2 cm^{-1}. The averaged spectrum was background-corrected using a pure KBr pellet run under similar conditions. The pellets were prepared with approximately 2 mg of sample and 100 mg of KBr. The 2 mg powder samples were obtained by diluting the film solution with excess deionised water in order to release the insoluble LDH-SA. It was subsequently recovered by centrifugation, dried and ground. This was done in order to enable the observation of carboxylate vibrations of the intercalated stearate, which is otherwise overshadowed by the carboxylate peaks of the sodium alginate.

4.2.3.2. *X-ray Diffraction (XRD)*

The XRD analyses were done on a Siemens D500 X-ray system equipped with a 2.2 kW Cu long fine focus tube, variable slit and secondary graphite monochromator. The system is computer controlled using SIEMENS DIFFRAC ^{Plus} software. The goniometer was set to reflection mode. The films were placed on a no-background silicon (Si) wafer before placing it onto the aluminium sample holder to prevent aluminium peaks from being seen. Samples were scanned from 1 to 40° 2θ with Cu K_α radiation (1.5418 Å) at a speed of 0.02° 2θ, with a recording time of 2 s per step and generator settings of 40 kV and 30 mA.

4.2.3.3. *Scanning Electron Microscopy (SEM)*

The film samples were freeze fractured by dipping into liquid nitrogen and then breaking the brittle film. The broken cross-sections of the films were studied. These were coated with chromium in a high resolution ion beam coater, Gatan model 681 (Warrendale, PA, USA) to prevent charge build-up due to its low conductivity. Samples were then studied with the JSM-6000F field emission scanning electron microscope (JEOL, Tokyo, Japan).

4.2.3.4. Optical microscopy

A drop of the film solution was placed between two microscope slides and studied under 40 times magnification with a Leica DME optical microscope with built-in digital camera.

4.2.3.5. *Water Vapour Permeability (WVP)*

The cast and dried films were cut into discs of appropriate size for the WVP cups. A Mitutoyo Digimatic Indicator was used to determine the thickness of each disc at 9 positions. The measured thicknesses varied between 130 and 140 μm. Additional films were prepared in order to determine the effect of thickness on WVP of films of differing compositions. In all cases at least four discs per formulation were tested. Film discs were mounted on cups filled with dried silica gel (Fig. 4-2) and placed in a desiccator filled with saturated NaCl solution in contact with excess NaCl to obtain 75% relative humidity (RH) at 23 ± 2 °C [12]. Films derived from emulsions always have a shiny side (bottom) and a dull side due to accumulation of lower density wax (or fatty acid) at the top. Therefore, the measured WVP depended on which side faced which relative humidity. [3] Care was taken to always place the shiny (more hydrophilic) side facing the 0% RH side.

A WVP test of the best performing film was carried out at 38 °C/90 %RH in order to determine its performance (good, moderate or poor) according to the classification scheme of Krochta *et al.* [13]

Figure 4-2 Water vapour permeability test setup.

4.2.3.6. *Tensile properties*

Films were allowed to condition for at least two weeks before testing, so that results would be comparable in terms of the age of the samples. The thickness of the samples were tested at three positions within the middle portion of the dumbbells and averaged. The measured thicknesses ranged from 110 to 130 μm. Samples were tested at a strain rate of 1 mm/min on a LRX Plus instrument from Lloyd Instruments, and results were analysed using Nexygen software. The software calculated the Young's moduli. Tests were performed at 25 °C at ambient humidity (30-50% RH). Three samples of each formulation were tested and averaged.

4.3. Results and Discussion

4.3.1. Fourier Transform Infrared spectroscopy (FTIR)

The FTIR spectrum of the LDH-SA intercalates obtained from the 60SA/40LDH film (Fig. 4-3) revealed that all the stearic acid reacted because the ν(C=O) stretching vibration at 1702 cm^{-1} was absent. The carboxylate (COO-)

asymmetric stretching vibrations were at 1539 cm^{-1}, 1554 cm^{-1} and 1576 cm^{-1}, which correlates well with the carboxylate asymmetric stretching vibrations (1542 cm^{-1}, 1557 cm^{-1} and 1589 cm^{-1}) obtained by Borja *et al.* [14] for meristate intercalated Mg_3Al-LDH. The weak peak at 1725 cm^{-1} was also seen by Borja *et al.* [14] at 1720 cm^{-1} and can be attributed to the intercalation of the acid (COOH). Therefore, the same intercalation product was obtained in these aqueous film solutions as was obtained by the ion exchange of the Cl^- ion in LDH-Cl by fatty acids in ethanol [14], and not the Mg/Al salt of the fatty acid. The presence of a peak at 1366 cm^{-1}, attested to the fact that all the carbonate counter-ions did not react. Some unreacted carbonate remained no matter how large an amount of SA was used to react with the carbonate species.

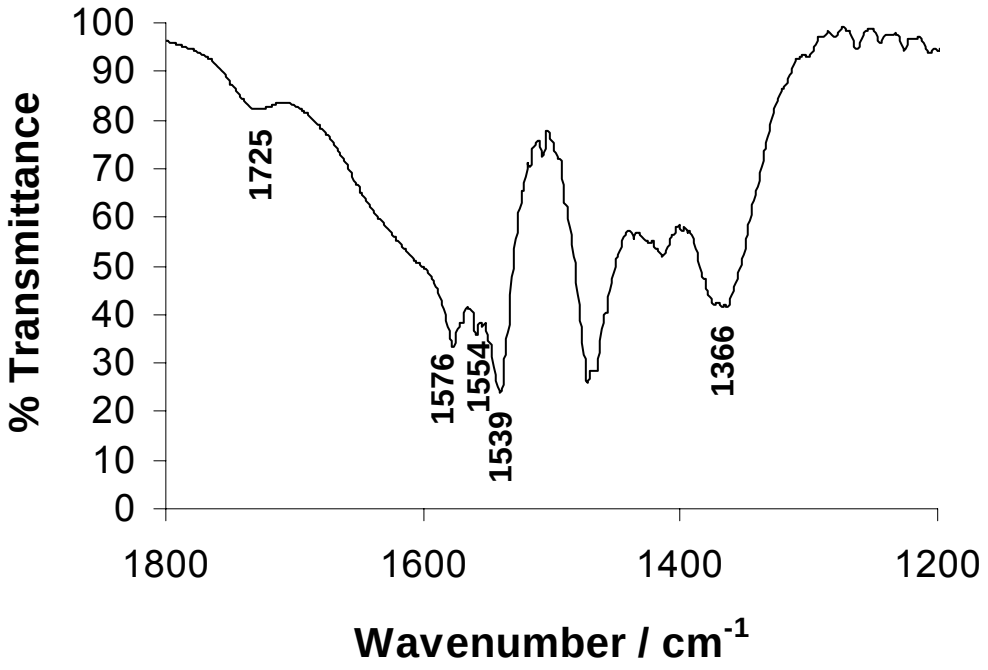

Figure 4-3 FTIR spectrum of the LDH-SA intercalates isolated from the 60SA/40LDH film solution, indicating complete ionisation and intercalation of SA together with some carbonate anions (1366 cm^{-1}).

4.3.2. Water Vapour Permeability (WVP)

The water permeability of hydrophilic films depends on the films moisture content. In the WVP experiment the film separates a region of high humidity from one of low humidity. Therefore there is also a gradient in the moisture content across the film. Owing to concentration polarization, this gradient depends on the film thickness. The consequence is that, unlike hydrophobic polymer films, the WVP of hydrophilic films depends on film thickness. This was previously noted by McHugh *et al.* [15].

Fig. 4-4 shows the WVP of several films. The WVP of blank films (only dextrin, alginate and glycerol, no LDH or SA) as well as the films with only SA or only LDH were thickness dependent and the values fell on the same straight line (WVP = 0.187x + 1.01, R^2 = 0.9928, Fig. 4-4). The WVP of films with a combination of LDH and SA, however, was independent of the thickness. Therefore, the combination of LDH and SA was more successful in producing films with hydrophobic characteristics (water vapour barrier properties) than SA alone. The raw data and calculations relating to Figure 4-4 can be seen in Table A-4 and A-5 in Appendix D. The method for calculating the WVP is also described in Appendix D.

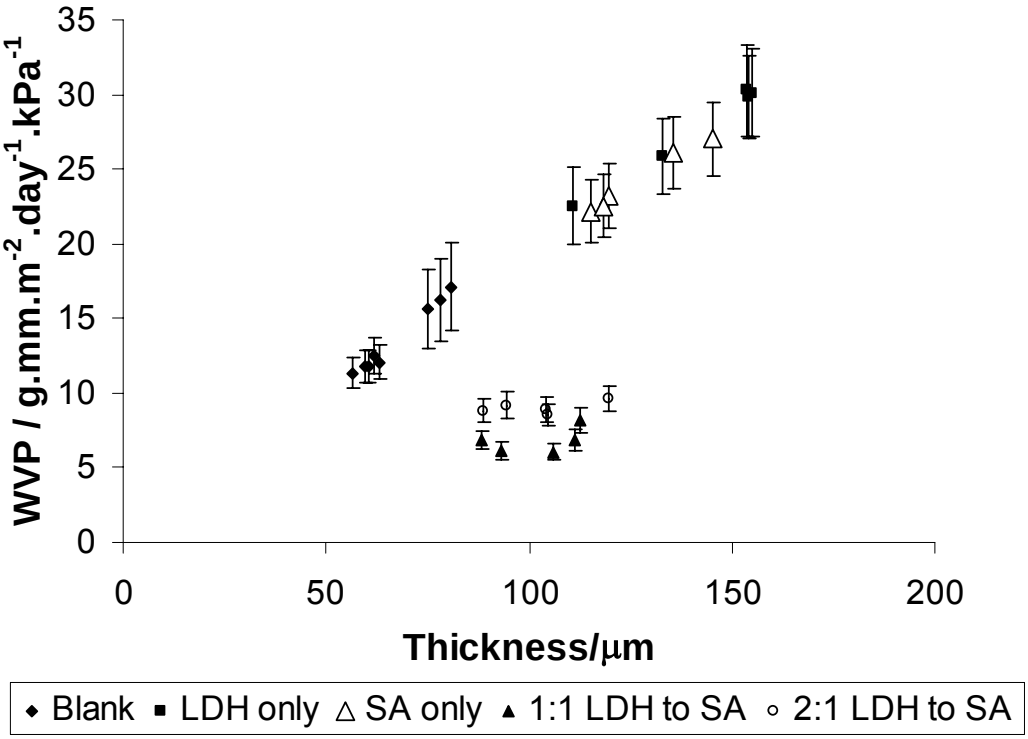

Figure 4-4 Thickness dependence of WVP of films with no filler, SA only or LDH only showing hydrophilic tendencies and those with combinations of SA and LDH showing hydrophobic tendencies.

For the films with constant thickness and amount of filler, a broad minimum in the WVP is observed at filler compositions ranging from 80SA/20LDH to 50SA/50LDH (Fig. 4-5). These results were explained and corroborated by SEM, XRD and tensile (Young's modulus) data. The raw data and calculations relating to Figure 4-5 can be seen in Table A-6 and A-7 in Appendix D.

The film with 100% SA in the filler, showed only a 17% decrease in the WVP. This is in good agreement with the results obtained by Wu *et al*. [1] for meat patties wrapped in starch/alginate/glycerol/SA films in relation to starch/alginate/glycerol films. The replacement of only 20% of the SA by the LDH, however, caused the WVP to decrease to 80% of that of the blank film (Fig. 4-5).

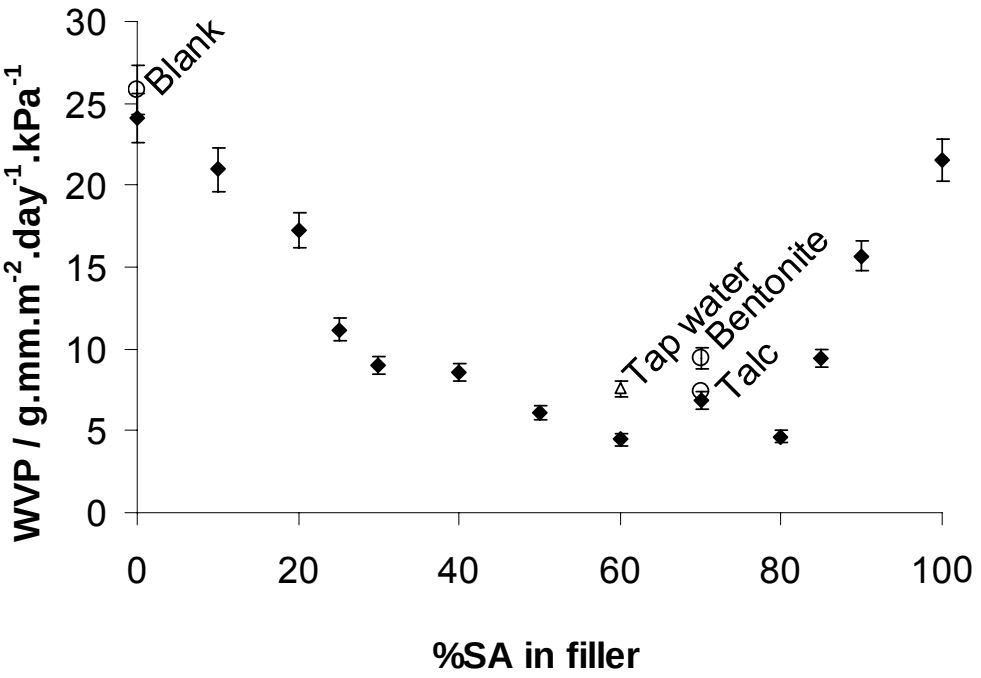

Figure 4-5 WVP measurements of constant-thickness films with fillers varying from 100SA/0LDH to 0SA/100LDH, showing a wide range of filler compositions yielding a minimum in the WVP.

When using tap water, one would expect the Ca^{2+} and Mg^{2+} ions to bind to the alginate, cross-linking it and thus improving the WVP, but the Ca^{2+} ions would decrease the solubility of the alginate which could, in turn, be detrimental to film formation. The use of tap water, however, had no detrimental effects on the results, as the WVP value fell within the variation in WVP seen within the curve (Fig. 4-5). This is beneficial since the water does not have to be demineralised or deionised for large-scale applications.

Films containing other sheet-like fillers at the same mass % dosage level, i.e. talc and bentonite showed a similar WVP (Fig. 4-5). Therefore, the WVP reached a minimum due to the improved dispersion of the LDH, talc and bentonite into the polymer matrices by the SA, a conclusion which is also corroborated by SEM results.

The 60SA/40LDH film which was also tested at 38°C and 90% RH, had a WVP of 13.5 ± 0.5 g.mm.m^{-2}.day^{-1}.kPa^{-1}, which is close to the border between the poor (10-100 g.mm.m^{-2}.day^{-1}.kPa^{-1}) and moderate (0.1-10 g.mm.m^{-2}.day^{-1}.kPa^{-1}) WVP regions according to the categorization of Krochta *et al*. [13]. In order to produce edible films or paper coatings with better performance in terms of WVP, the dextrin, which has poor WVP characteristics, could be replaced by polymers such as methyl cellulose, hydroxypropyl methyl cellulose, corn zein (protein), wheat gluten, poly(lactic acid) or cellulose acetate, which reside in the moderate WVP category according to Krochta *et al.* [13] Sodium alginate could also be replaced by sodium carboxymethyl cellulose in order to increase the hydrophobicity of the films.

4.3.3. Scanning Electron Microscopy (SEM)

The microstructures of the films with filler compositions of 100SA/0LDH through to 0SA/100LDH are shown in Figs. 4-6 (A-L). The SA could not alter the WVP characteristics of the matrix because the SA did not intimately mix with it, but formed dispersed globules (Fig. 4-6B) rather than oriented high aspect ratio sheets. The decrease in WVP (Fig. 4-5) corresponded to the presence of flat (white) plate-like structures (200-1000 nm thick and > 20 μm long) in the microstructure. The LDH-SA intercalates agglomerated in starch or dextrin solutions alone, but the viscous surface-active sodium alginate helped to disperse it into the dextrin-alginate solutions. These structures were first seen at filler composition 80SA/20LDH (Fig. 4-6D), where the reduction in WVP occurs. Beyond the filler composition of 50SA/50LDH (Fig. 4-6G), these structures gradually disappeared and the WVP increased again to higher values. These flat structures are typical of the surfactant intercalated LDHs. [10,11] Long crevices can also be seen where the LDH-SA were pulled out of the matrix due to poor adhesion. Using, for example, 12-hydroxy stearic acid instead of SA could improve the adhesion and compatibility of the intercalated clays with the hydrophilic matrix. The more hydrophobic polymers mentioned previously could

also improve adhesion to the LDH-SA intercalates, reducing pullout and increasing Young's modulus.

The films with bentonite and talc (Figs. 4-6M and 4-6N) also had an oriented structure due to the orientation of the filler particles. Wilhelm *et al*. [6] also observed the orientation of hectorite within fractured starch films. This orientation and dispersion of the fillers, therefore, account for the similar WVP results obtained for films with the same mass % LDH, talc or bentonite and SA.

LDH particles usually have sand-rose structures (Fig. 4-6O). The particles consist of many intergrown smaller particles that reduce accessibility to the surface area as a whole. [11] In Fig. 4-6P a fully intact LDH particulate is shown, which was released from the sand-rose structure and was captured and oriented within the larger plate-like structure of the LDH-SA. Under the influence of the SA the crystallites were aligned and reacted to form the LDH-SA layered structure (thickness ca. 100 nm, Fig. 4-6Q), with increased accessibility to the surfaces of the particles. If completely intercalated, the 100 nm thick plates could be interpreted as 20 layers of the LDH-SA (*ca.* 50 Å interlayer distances according to XRD). If intercalation did not take place, the 100 nm implies 131 layers (7.6 Å interlayer distances). Clearly, exfoliation to single layers did not occur. Single layer exfoliation would not be observable by SEM. According to He *et al.* [16] LDH crystals are only stable when they form stacking structures of approximately 20 layers. According to XRD two phases were present, namely LDH-SA and unreacted LDH-CO_3. Therefore, the plate-like structures probably consist of between 20 and 131 layers.

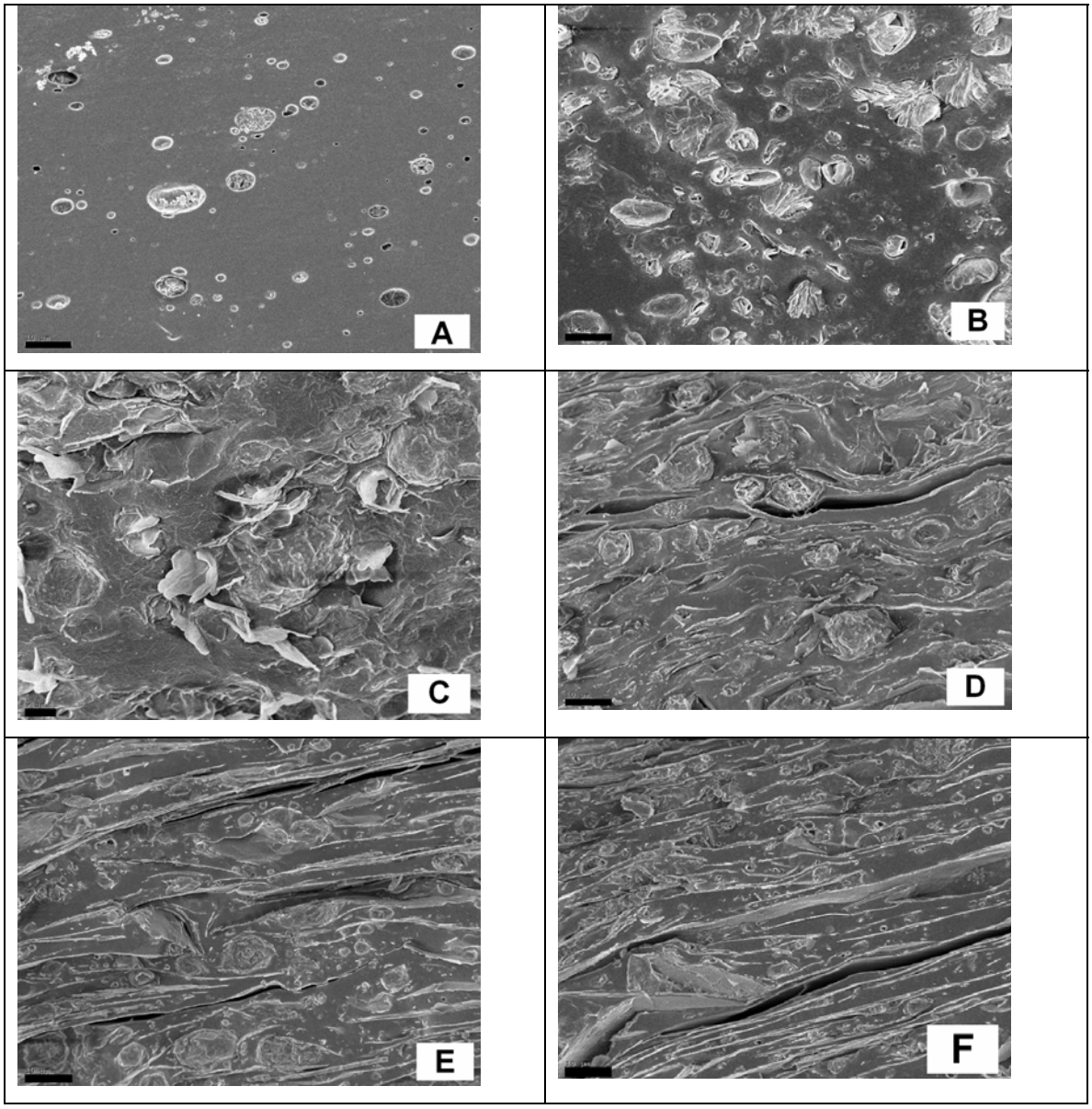

Figure 4-6 Scanning electron micrographs of the films.

A) Blank film. Undissolved alginic acid particles can be seen. Bar is 10 μm.

B) 100SA/0LDH. Some emulsified pockets of stearic acid can be seen. Bar is 10 μm.

C) 90SA/10LDH. Small, unoriented flat products of the SA-LDH reaction can be seen. Bar is 5 μm.

D) 80SA/20LDH. The reaction product of the SA and LDH were larger and more oriented. Bar is 10 μm.

E) 70SA/30LDH. The LDH-SA intercalate formed long, flat structures. Bar is 10 μm.

F) 60SA/40LDH. The LDH-SA intercalate formed long, flat structures. Bar is 10 μm.

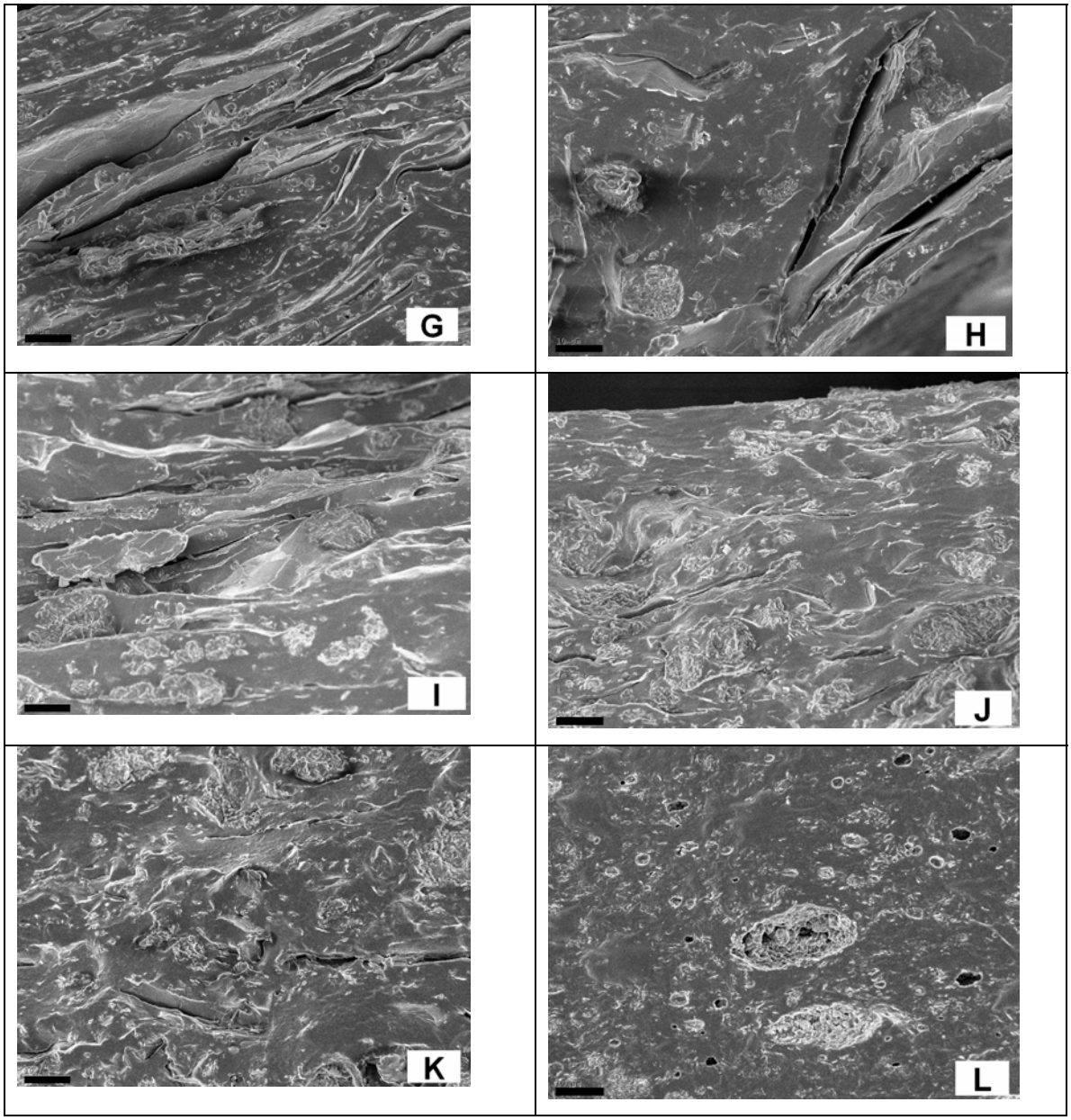

Figure 4-6 Scanning electron micrographs of the films.

G) 50SA/50LDH. The LDH-SA was smaller and less oriented. Bar is 10 μm.

H) 40SA/60LDH. Bar is 10 μm.

I) 30SA/70LDH. Bar is 10 μm.

J) 20SA/80LDH. Bar is 10 μm.

K) 10SA/90LDH. Bar is 10 μm.

L) 0SA/100LDH. Bar is 10 μm.

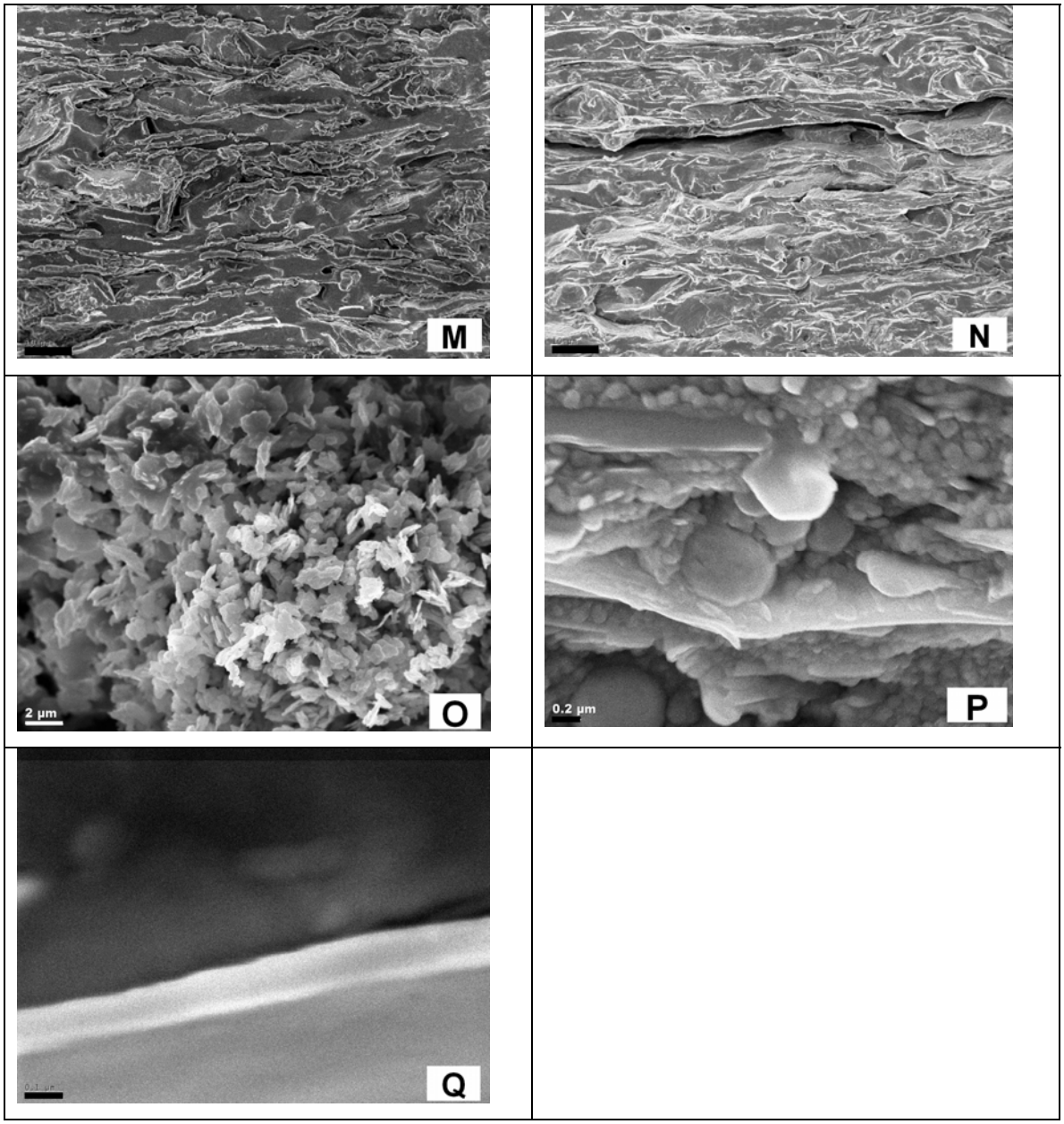

Figure 4-6 Scanning electron micrographs of the films.

M) 70SA/30bentonite. The bentonite is oriented within the film. Bar is 10 μm.

N) 70SA/30talc. The talc is oriented within the film. Bar is 10 μm.

O) Sand-rose structure of the LDH powder. Bar is 2 μm.

P) Large magnification of 80SA/20LDH showing intact LDH particle. Bar is 0,2 μm.

Q) Large magnification of 60SA/40LDH showing thickness of plates. Bar is 0,1 μm.

4.3.4. Optical Microscopy

When looking at film solutions which had a SA/LDH ratio of about 80/20 to 40/60, “needlelike” structures (Fig. 4-7) approximately 20 μm long could be seen. These “needles” are in actual fact plates of *ca*. 20 μm diameter (refer to SEM section) seen from the side. They are transparent from the top. This gives an explanation for why the film solutions are white, but form clear films upon drying. In the solution the large plate-like structures are oriented randomly, scattering the light passing through it, but upon drying, the plate-like structures are all oriented horizontally (as seen by SEM also).

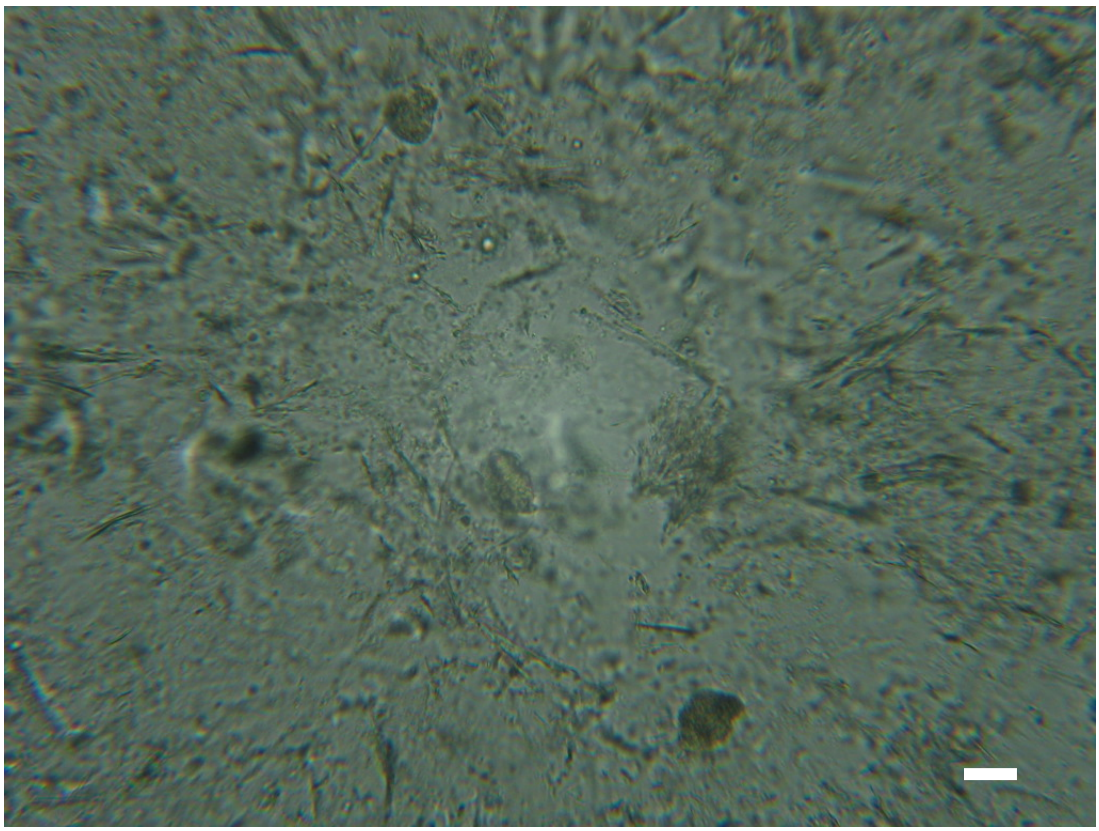

Figure 4-7 Optical microscope photo of the 60SA/40LDH film solution. Bar is 20 μm.

4.3.5. X-Ray Diffraction (XRD)

Depending on the amount of stearate present and the temperature employed, either a monolayer or bilayer could theoretically be intercalated (Fig. 4-8). The interlayer distance would be 32 Å for the monolayer and 52-53 Å for the bilayer. [10,17] Through molecular modelling calculations, Pospíšil *et al.* [18] reported a transition state between mono- and bilayer intercalation of octadecylammonium chloride in montmorillonite, with an interlayer distance of 47.8 Å.

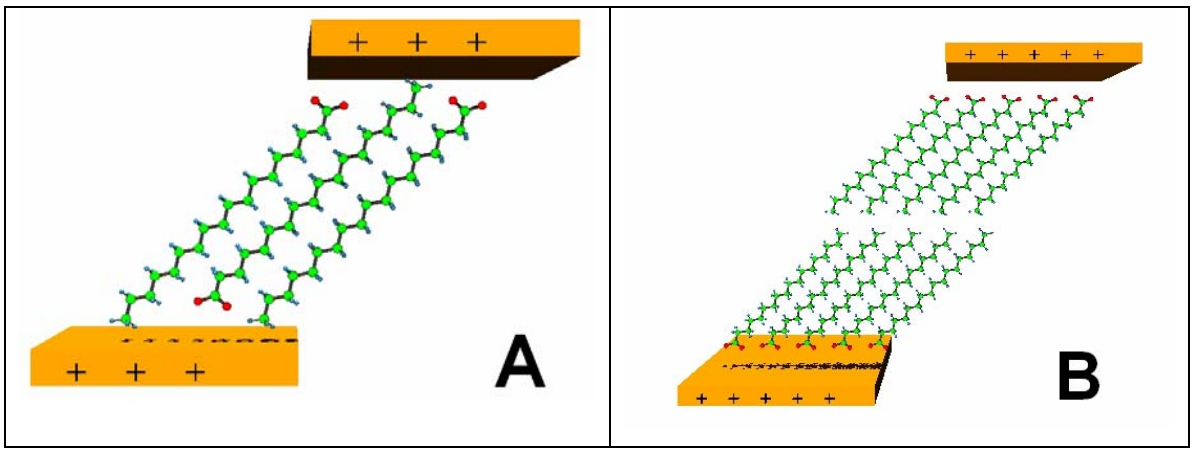

Figure 4-8 Monolayer (A) and bilayer (B) arrangement of stearate intercalated within LDH.

The XRD spectrum of the blank film (no LDH or SA) indicated a completely amorphous structure, with only a broad hump centred around 20° 2θ. The 100SA/0LDH film had a reflection at around 40 Å (due to the unreacted stearic acid bilayer, polymorph C [19]) and a small peak at about 8.1 Å due to the formation of some alginic acid (2-fold screw axis with fiber period of 8.7 Å, [20]). Upon the addition of LDH to the SA in the film, an interlayer distance of 52 Å is reached at the filler composition of 80SA/20LDH. With an increasing amount of LDH the intensity of the basal reflection and the interlayer distance decreased (Figs. 9 and 10), indicating that some exfoliation (delamination) took place at filler compositions in the region of 60SA/40LDH to 70SA/30LDH. The exfoliation behaviour around the middle of the series can be explained in terms of the exfoliation energy. Pospíšil *et al.* [18] calculated the exfoliation energy (total

interaction energy per supercell between two layers) of octadecylammonium chloride intercalated montmorillonite. It was found to decrease dramatically for the bilayer arrangements. In the 60SA/40LDH and 70SA/30LDH films, the interlayer distance should have been the largest (> 54 Å, lowest exfoliation energy), but due to exfoliation the higher interlayer distance reflections disappeared, and a lower interlayer distance phase remained, with a lower intensity. At the filler composition of 50SA/50LDH, the bilayer structure was present once again (basal reflection at 54 Å). Upon further increasing the LDH content (decreasing SA content), the basal spacing decreased again; this time not due to exfoliation but due to a lack of SA. Stearate intercalated to form structures between mono- and bilayers.

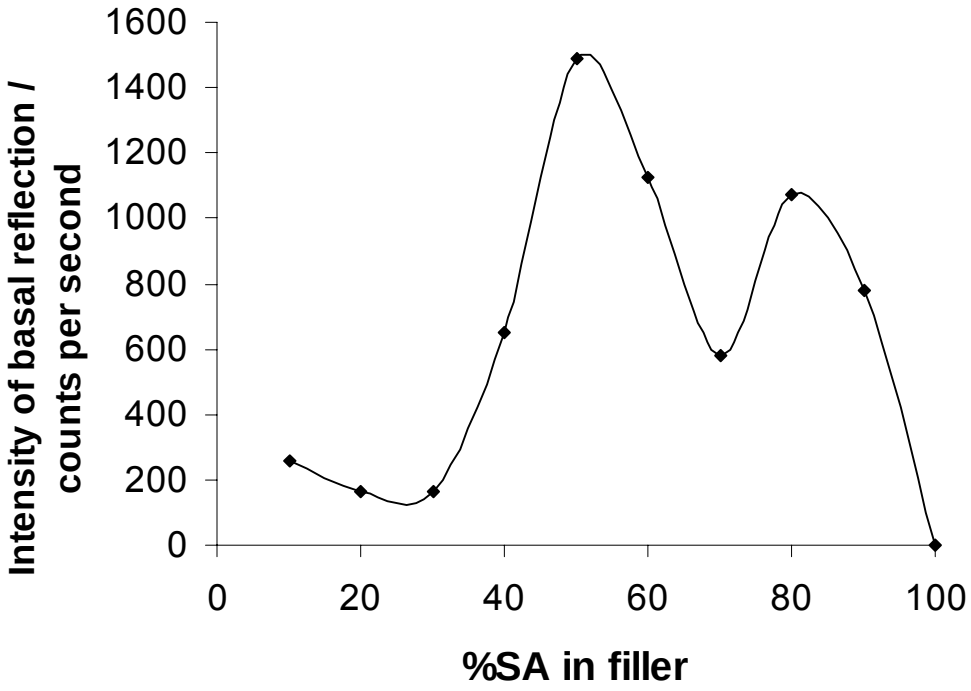

Figure 4-9 Variation in intensity of the basal reflection of the intercalated phase (LDH-SA) as function of filler composition. The dip in intensity indicated that exfoliation (delamination) took place.

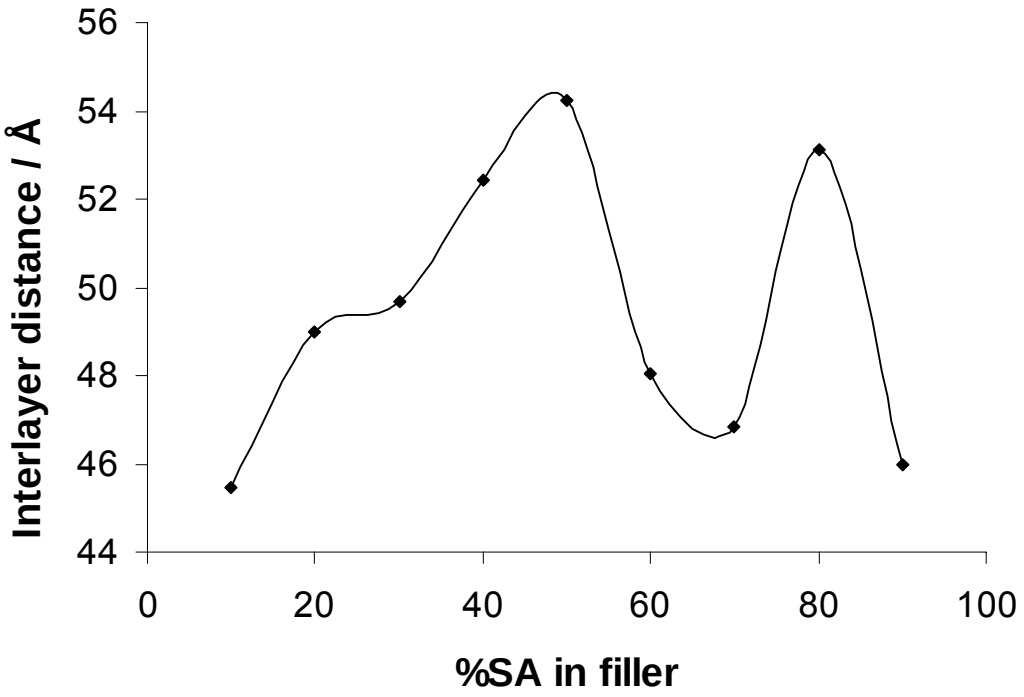

Figure 4-10 Variation of the interlayer distance of the intercalated phase (LDH-SA) as function of the filler composition. The dip in interlayer distance indicated that exfoliation took place, leaving only a phase with smaller interlayer distance.

Fig. 4-11 shows which crystalline phases were present in the 70SA/30LDH film at 10 minutes, 30 minutes and 60 minutes of reaction. At 10 minutes, almost no crystalline phases were present. The LDH basal reflection at 7.7 Å had a low intensity, because the LDH particles were still mostly agglomerated, settling to the bottom and not forming part of the cast film. At 30 minutes the sand-rose structures had broken down and the LDH particulates were suspended in the film solution. The 7.7 Å reflection was the most intense. Some LDH-SA had also formed at 30 minutes (52.2 Å). The 52.2 Å basal reflection had a higher intensity than the 17.9 Å (non-basal) reflection. At 60 minutes, however, the basal reflection reduced in intensity and interlayer distance (to 46.8 Å), with the 17.9 Å reflection being the most intense. This loss of intensity of the basal reflection is a strong indication that exfoliation took place between 30 and 60 minutes. It is

believed that the alginate, being a poly-anionic polysaccharide [21], aided the exfoliation of the LDH-SA without need for high shear mixing.

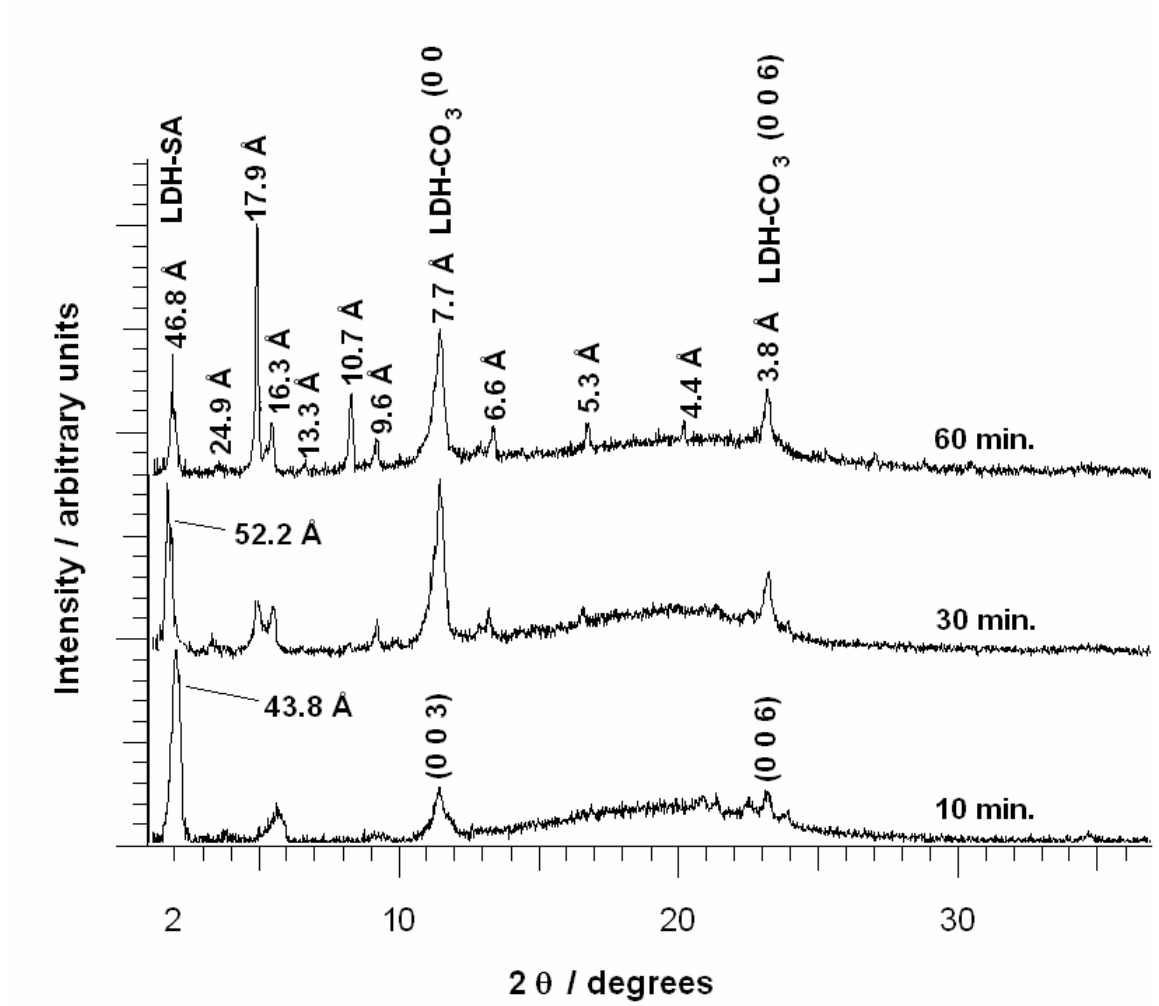

Figure 4-11 The crystalline phases present in the dried film 70SA/30LDH at 10, 30 and 60 minutes of reaction, showing the relative amounts of the LDH-CO_3 and LDH-SA phases and the lower interlayer distance LDH-SA phase remaining after exfoliation.

4.3.6. Tensile properties

Only the film 0SA/100 LDH has a higher tensile strength than the blank film. The other films (which all contain SA as well) are weaker due to the lack of mechanical strength of the SA (Fig. 4-12). All the films are less ductile (lower % strain at break) than the blank film except the film 70SA/30Talc (Fig. 4-13). It is unknown why the talc increased the ductility. The complete set of mechanical properties of these films can be seen in Appendix E.

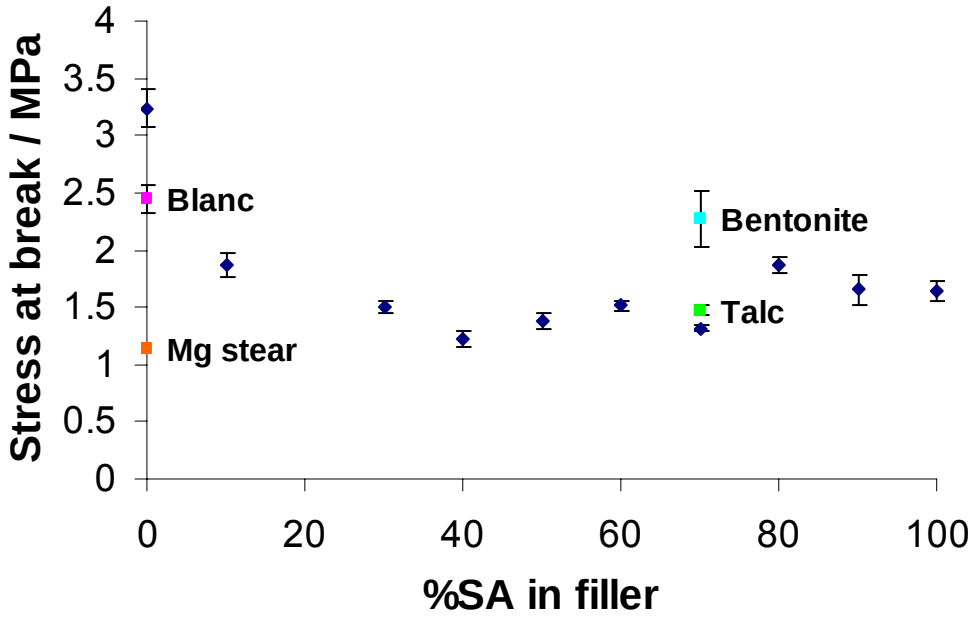

Figure 4-12 Stress at break of films as function of filler composition.

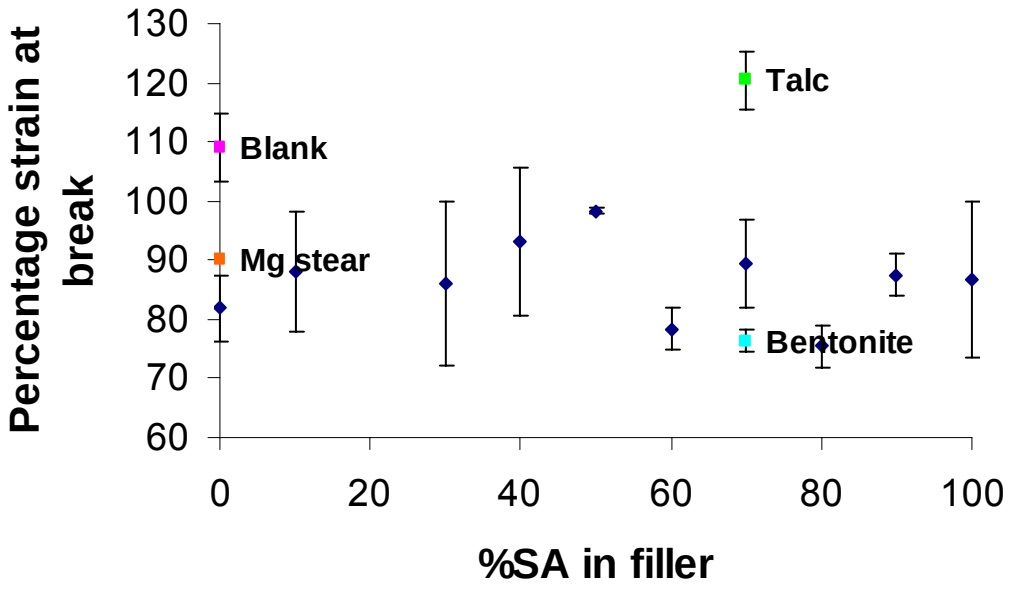

Figure 4-13 Percentage strain at break of films as function of filler composition.

The Young's moduli of our films were an order of magnitude lower and the elongation at break an order of magnitude larger than the starch films of Wilhelm *et al.* [6] because of the presence of the sodium alginate.

Fig. 4-14 shows the Young's moduli of films with different filler compositions. A maximum modulus was achieved at about 60SA/40LDH. This point probably corresponded to the minimum amount of SA needed to effectively break up the sand-rose structure in order to increase the surface area and efficiency of the reinforcing interaction between the LDH and the alginate, and possibly the dextrin. After the 60SA/40LDH point the amount of LDH available became less and thus also the reinforcing capabilities. The talc and bentonite, at the same mass %, did not have the same reinforcing effect (Fig. 4-14). For LDH we obtained a maximum increase in Young's modulus of 213% in comparison to the blank dextrin-alginate film. Wilhelm *et al*. [6] obtained only a 72% increase in modulus at 30% m/m loading of Ca^{2+} hectorite in comparison to pristine thermoplastic starch (glycerol-plasticized). De Carvalho *et al*. [5] observed a 50%

increase in modulus of starch/calcined kaolin composites at 50 phr kaolin (50 parts kaolin per 100 parts thermoplastic starch) in comparison to the pristine thermoplastic starch. Hence, the reinforcing capability of the LDH can probably be attributed to the electrostatic interaction between the positively charged LDH layers and the anionic alginate chains, which is absent in the case of talc and bentonite.

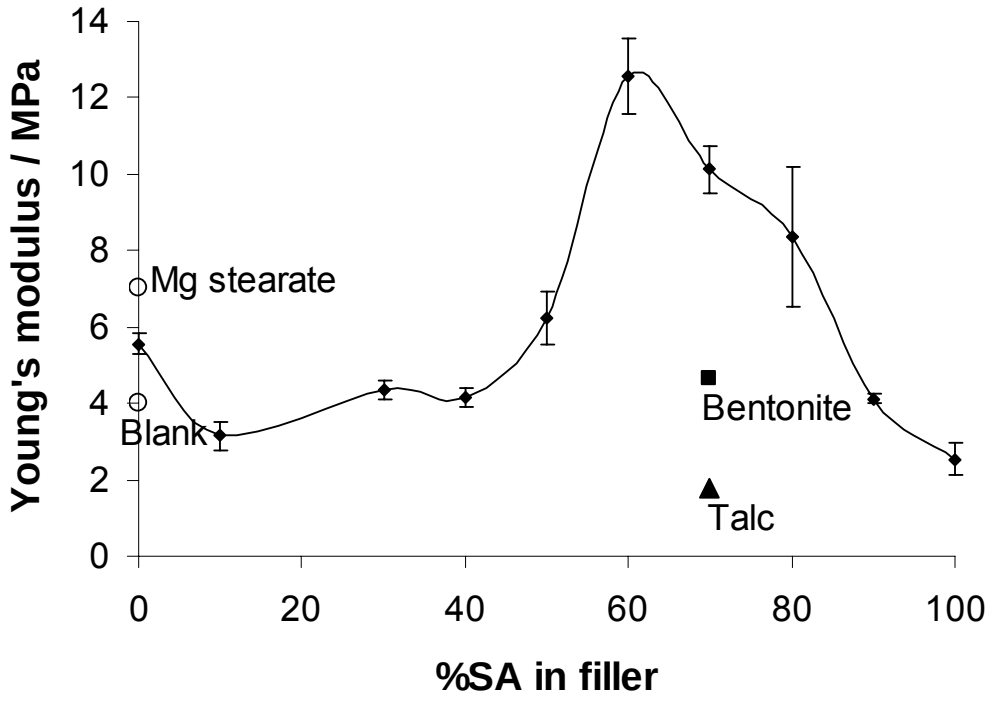

Figure 4-14 Young's moduli of films as function of filler composition.

Leaching of Mg^{2+} from the Mg_2Al-LDH used in this study (due to the presence of the acidic SA) was not expected because Hibino *et al*. [22] found that no leaching of Mg^{2+} cations took place in LDHs with Mg/Al ratio of 2 when treated with aqueous paramolybdate solutions (low pH), whereas substantial leaching took place in LDHs with Mg/Al ratios of 3 and 4. However, the presence of alginate might drive the leaching of some cations. When polymers with carboxylic acid groups (such as alginate) are neutralized with divalent or trivalent metal ions; the viscosity increases due to the formation of cross-links between polymer chains. [21,23,24] However, film solutions containing an equivalent amount of

magnesium stearate had a higher viscosity than LDH-SA containing films, indicating that more Mg^{2+} were available to cross-link the alginate and to increase Young's modulus (Fig. 4-14) [23].

4.3.7. XRD, tensile and WVP results revisited

The WVP, intensity of basal reflection and Young's modulus data show correlated trends (Fig. 4-15). The curve of the intensity of the basal reflection of the LDH-SA and the curve of Young's moduli crossed midway between 50% and 60% SA. Below the 60% SA point in these curves, the intensity of the basal reflection was high, indicating that no exfoliation took place; consequently the modulus dropped drastically. The opposite is true between 60 and 70% SA (the moduli were high and the intensity of the basal reflections were low, indicating exfoliation). Hence, the hypothesis that exfoliation (or delamination) of the LDH-SA caused the increase in Young's modulus was further supported.

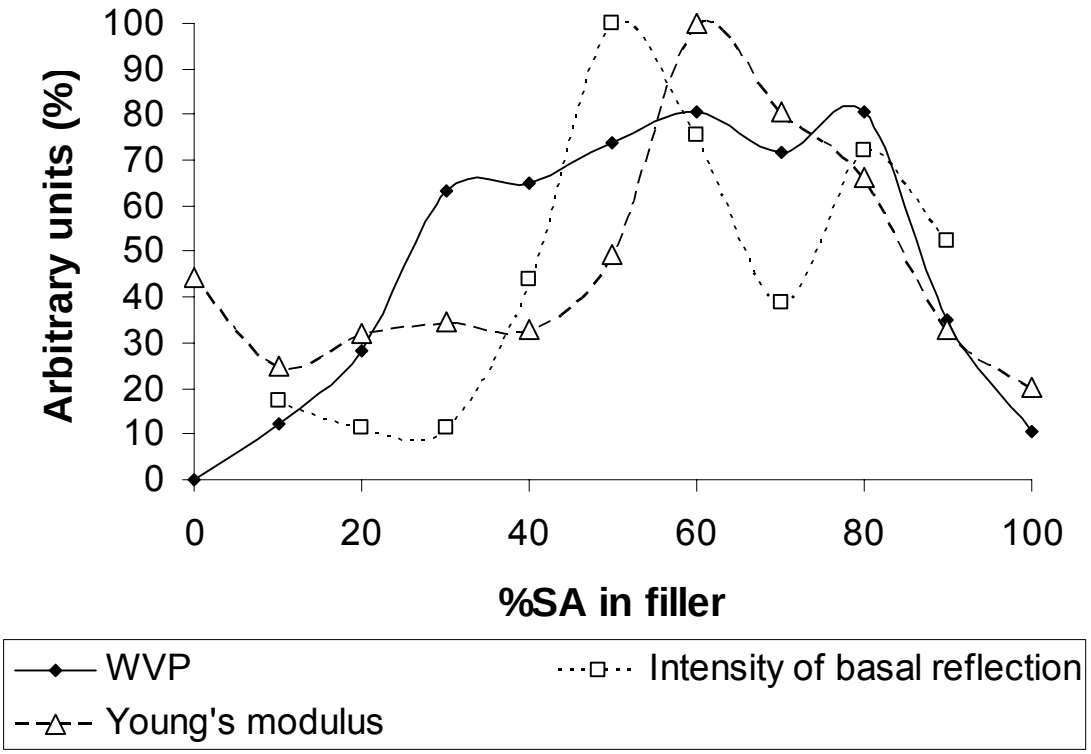

Figure 4-15 Comparison of WVP, Young's modulus and intensity (XRD) data as function of filler composition. WVP values of Fig. 4-4 were subtracted from 100 for this graph.

4.4. Conclusions

The combination of SA and LDH improves the WVP with respect to the use of only SA or only LDH. We believe that the use of the combination of a fatty acid (rather than any other acid) and a LDH is the most beneficial for preparation of films with low WVP because the fatty acid in itself lowers the WVP, it can intercalate into the LDH to form the large plate-like barriers and *in situ* leaching of LDH cations with concomitant cross-linking of the alginate can occur. Also, exfoliation of the LDH-SA by the poly-anionic alginate was evidenced. More research needs to be done in order to determine the contributions of the two mechanisms (exfoliation vs. cross-linking) to the increased Young's modulus (increased stiffness) and decreased WVP, but from qualitative viscosity

observations it seems that cross-linking due to leaching of Mg^{2+} from the LDH plays only a minor role.

References

1 Y. WU, C.L. WELLER, F. HAMOUZ, S. CUPPETT and M. SCHNEPF, *J. Food Sci.* **66** (2001) 486.

2 O.R. FENNEMA, S.L. KAMPER and J.J. KESTER, USP 4 915 971, Method for making an edible film and for retarding water transfer among multi-component food products, 10 April 1990.

3 R.J. AVENA-BUSTILLOS and J.M. KROCHTA, *J. Food Sci*. **58** (1993) 904.

4 M. ALEXANDRE and P. DUBOIS, *Mater. Sci. and Eng. R* **28** (2000) 1.

5 A.J.F. DE CARVALHO, A.A.S. CURVELO and J.A.M. AGNELLI, *Carbohydr. Polym.* **45** (2001) 189.

6 H.-M. WILHELM, M.-R. SIERAKOWSKI, G.P. SOUZA and F. WYPYCH, *Carbohydr. Polym.* **52** (2003) 101.

7 H.-M. WILHELM, M.-R. SIERAKOWSKI, G.P. SOUZA and F. WYPYCH, *Polym. Int.* **52** (2003) 1035.

8 D.W.S. WONG, K.S. GREGORSKI, J.S. HUDSON and A.E. PAVLATH, *J. Food Sci.* **61** (1996) 337.

9 S. MIYATA and T. KUMURA, *Chem. Lett.* (1973) 843.

10 T. ITOH, N. OHTA, T. SHICHI, T. YUI and K. TAKAGI, *Langmuir* **19** (2003) 9120.

11 M. ADACHI-PAGANO, C. FORANO and J.-P. BESSE, *Chem. Commun.* (2000) 91.

12 A. WEXLER, in “Handbook of Physics and Chemistry”, 79th edition, edited by D.R. Lide (CRC Press, Boca Raton, 1998) p. ***15***-25.

13 J.M. KROCHTA and C. DE MULDER-JOHNSTON, *Food Technol.* **51** (1997) 61.

14 M. BORJA and P.K. DUTTA, *J. Phys. Chem.* **96** (1992) 5434.

15 T. HABIG McHUGH, R. AVENA-BUSTILLOS and J.M. KROCHTA, *J. Food Sci.* **58** (1993) 899.

16 J.X. HE, S. YAMASHITA, W. JONES and A. YAMAGISHI, *Langmuir* **18** (2002) 1580.

17 T. KANOH, T. SHICHI and K. TAKAGI, *Chem. Lett.* (1999) 117.

18 M. POSPÍŠIL, P. ČAPKOVÁ, Z. WEISS, Z. MALÁČ and J. ŠIMONÍK, *J. Colloid Interface Sci.* **245** (2002) 126.

19 J.F. MEAD, R.B. ALFIN-SLATER, D.R. HOWTON and G. POPJÁK, in "Lipids: Chemistry, Biochemistry and Nutrition" (Plenum Press, New York, 1986) p. 53.

20 W.T. ASTBURY, *Nature* **155** (1945) 167.

21 R.L. WHISTLER and J.N. BeMILLER, in "Carbohydrate Chemistry for Food Scientists" (Eagan Press, St. Paul, Minnesota, 1997) p. 196.

22 T. HIBINO and A. TSUNASHIMA, *Chem. Mater.* **9** (1997) 2082.

23 M. FUJIYAMA, K. YAMANE, K. AYAMA and H. INATA, *J. Appl. Polym. Sci.* **86** (2002) 2887.

24 F. YOKOYAMA, E.C. ACHIFE, M. MATSUOKA, K. SHIMAMURA, Y. YAMASHITA and K. MONOBE, *Polymer* **32** (1991) 2911.

Chapter 5

Conclusions and Recommendations

This section describes some general conclusions regarding the success of this research; more specific conclusions are given within each chapter.

5.1. Conclusions

A technique for intercalating stearate anions into $Mg_4Al_2(OH)_{12}CO_3 \cdot 3H_2O$ (LDH-CO_3) was developed. The intercalation reaction mechanism consisted of an acid-base exchange between stearic acid (or any other fatty acid) and the carbonate anion of the LDH-CO_3. The use of surfactants was beneficial, preventing agglomeration during the reaction and in cases where LDO (calcined LDH) was used, the surfactant improved the yield of the stearate intercalated LDH (LDH-SA) and prevented the formation of Mg/Al salts of the fatty acids. The newly developed method gave better intercalation results in comparison to some well-known literature methods.

The anionic polymer poly(vinyl sulfonate) intercalated into LDH-CO_3 in the presence of stearic acid. The stearic acid intercalated as stearate anions, which was exchanged by the polymeric anion. This is an easy and facile way to produce nanocomposites. The anionic polymer and LDH interacts on the molecular level and the thicknesses of the resulting plate-like structures are in the nanometre range.

The stearate intercalated LDH (LDH-SA) successfully reduced the water vapour permeability of dextrin-alginate based films. In addition the Young's modulus increased, showing that the LDH-SA plate-like structures (which had thicknesses in the range of 100 nm), had reinforcing interactions with the polymer chains.

5.2. Recommendations for future research

During this research project aqueous film-forming solutions were used and tested as paper coatings. The solutions tended to penetrate deep into the fibrous matrix of the paper, requiring a high loading of solution before forming a continuous barrier film on the paper. This problem could be overcome by forming a thermoplastic starch-alginate blend filled with the LDH-SA. The thermoplastic blend could be prepared in the method developed by Souza *et al*. [1]. The intercalation reaction would then take place *in situ* between the molten SA and the LDH as in the method developed by Carlino *et al* [2,3]. The thermoplastic blend could then be used for melt paper coating.

The intercalation reaction of stearic acid into the LDH-CO_3 could also be done *in situ* during the emulsion polymerization of polymers such as polystyrene, methyl methacrylate, polyvinyl chloride and many more, which could lead to the formation of exfoliated nanocomposites. Furthermore, the system of the PVS ion exchanging with stearate to intercalate, could be used as a model of intercalating other poly-anionic species, such as DNA into the LDH layers, where it could be protected and used as carriers for gene therapy.

References

1 R.C.R. SOUZA, C.T. ANDRADE, *J. Appl. Polym. Sci.* **81** (2001) 412.

2 S. CARLINO and M.J. HUDSON, *J. Mater. Chem.* **4** (1994) 99.

3 S. CARLINO, M.J. HUDSON, S. WAQIF HUSAIN and J.A. KNOWLES, *Solid State Ionics* **84** (1996) 117.

Appendices

Appendix A

List of patents, publications and conference proceedings emanating from this research

1. Provisional patent

A provisional patent with title "Carboxylic acid intercalated layered double hydroxides" was filed in the Republic of South Africa on 6April 2005. The preliminary reference number is V16742.

2. Submitted articles

2.1. Landman EP, Focke WW, **Stearate Intercalated Layered Double Hydroxides: a Comparison of Methods**, *Journal of Materials Science*.

2.2. Landman EP, Focke WW, **Stearate Intercalated Layered Double Hydroxides: Effect on the Physical Properties of Dextrin-Alginate Films**, *Journal of Materials Science*.

2.3. Landman EP, Focke WW, **Poly(vinyl sulfonate) Intercalation into Stearate Intercalated Layered Double Hydroxides**, *Journal of Colloid and Interface Science.*

3. Conference Contributions

3.1. Invited Paper

Landman EP and Focke WW, **Modification of Hydrotalcite for use in Starch Nanocomposites – Exploring Alternatives**, proceedings of the *37th National Convention of the South African Chemical Institute*, Pretoria, 4-9 July 2004, p 138.

3.2. Poster

Landman EP, Focke WW, **Modification of Hydrotalcite for use in Starch Nanocomposites**, proceedings of the *2nd International Conference of the African Materials Research Society*, Johannesburg, 8-11 December 2003, p38.

Appendix B

XRF analysis of the layered double hydroxide

Table A-1 gives the XRF analysis of the LDH used in this study. It shows that the Mg/Al atomic ratio is 2.

Table A-1 XRF analysis of the LDH used in this study.

Oxide species	**%**	**Oxide species**	**%**
MgO	34,54	**K_2O**	0,00
Al_2O_3	21,78	**P_2O_5**	0,00
SiO_2	0,98	**Cr_2O_3**	0,00
TiO_2	0,00	**NiO**	0,08
Fe_2O_3	0,16	**V_2O_5**	0,00
MnO	0,01	**ZrO_2**	0,01
CaO	0,47	**LOI**	41,97
Na_2O	0,00	**Total**	100,01

Appendix C

XRD raw data for internal standard analyses

Each method was repeated twice. For each sample an XRD analysis was done in order to determine the intensity (in counts per second) of the reflections at around 50 Å (LDH-SA), 7,6 Å (LDH-CO_3) and 9,3 Å (talc). The intensity ratio of 50 Å/9,3 Å and 7,6 Å/9,3 Å was determined for each sample. The two intensity ratios for the two samples of the same method were averaged. The standard deviation of the average was calculated by dividing the standard deviation of the two intensity ratios by the square root of 2 (amount of repetitions of each method). The raw data, calculated averages and standard deviations are given in Table A-2 (for the 50 Å phase) and Table A-3 (for the 7,6 Å phase).

Table A-2 XRD intensity data for the amount of the 50 Å phase (LDH-SA) present in the products of the different methods.

Method	$I_{50\ Å}$*	$I_{9,3\ Å}$**	$I_{50\ Å}/ I_{9,3\ Å}$	Average $I_{50\ Å}/ I_{9,3\ Å}$	Standard deviation of average $I_{50\ Å}/ I_{9,3\ Å}$
Water	3849	1189	3,2	4,0	0,8
Water	4948	1026	4,8		
Calcined-Water	5951	2029	2,9	3,2	0,3
Calcined-Water	4122	1170	3,5		
Ethanol-water	2908	1077	2,7	3,0	0,3
Ethanol-water	3475	1053	3,3		
Ethanol	0	1147	0	0	0
Ethanol	0	1265	0		
SDS-water	8360	1433	5,8	5,0	0,8
SDS-water	4683	1115	4,2		
SDS-water-24 h	12457	1483	8,4	7,6	0,8
SDS-water-24 h	9010	1327	6,8		
Calcined-SDS-water	8123	979	8,3	7,6	0,7
Calcined-SDS-water	7245	1048	6,9		
Calcined-SDS-water-24 h	16104	2013	8	8	0,8
Calcined-SDS-water-24 h		1564			
Glycerol-water	1624	1146	1,4	1,2	0,2
Glycerol-water	1708	1612	1,0		
Calcined-glycerol-water	2867	1326	2,2	2,3	0,1
Calcined-glycerol-water	2855	1181	2,4		
Calcined-Na stearate	412	1003	0,41	0,4	0,1
Calcined-Na stearate	516	1322	0,39		
Carlino melt	1086	976	1,1	1,2	0,1
Carlino melt	1215	934	1,3		
Reference	0	1405	0	0	0
Reference	0	1293	0		

* Intensity of the reflection in the region of 50 Å.

** Intensity of the talc reflection at 9,3 Å.

Table A-3 XRD intensity data for the amount of the 7,6 Å phase (LDH-CO_3) present in the products of the different methods.

Method	$I_{7,6\ Å}$	$I_{9,3\ Å}$*	$I_{7,6\ Å}/ I_{9,3\ Å}$	Average $I_{7,6\ Å}/ I_{9,3\ Å}$	Standard deviation of average $I_{7,6\ Å}/ I_{9,3\ Å}$
Water	2021	1189	1,7	1,9	0,2
Water	2153	1026	2,1		
Calcined-Water	137	2029	0,0675	0,0679	0,0003
Calcined-Water	80	1170	0,0683		
Ethanol-water	1509	1077	1,4	1,7	0,3
Ethanol-water	2110	1053	2,0		
Ethanol	4245	1147	3,7	3,4	0,3
Ethanol	3919	1265	3,1		
SDS-water	2577	1433	1,8	2,1	0,3
SDS-water	2675	1115	2,4		
SDS-water-24 h	1630	1483	1,1	1,3	0,2
SDS-water-24 h	1989	1327	1,5		
Calcined-SDS-water	105	979	0,11	0,09	0,02
Calcined-SDS-water	76	1048	0,07		
Calcined-SDS-water-24 h	118	2013	0,06	0,08	0,02
Calcined-SDS-water-24 h	159	1564	0,10		
Glycerol-water	1029	1146	0,90	0,86	0,04
Glycerol-water	1327	1612	0,82		
Calcined-glycerol-water	28	1326	0,02	0,03	0,01
Calcined-glycerol-water	53	1181	0,04		
Calcined-Na stearate	148	1003	0,15	0,13	0,02
Calcined-Na stearate	143	1322	0,11		
Carlino melt	1466	976	1,5	1,4	0,1
Carlino melt	1213	934	1,3		
Reference	3229	1405	2,3	2,0	0,3
Reference	2197	1293	1,7		

* Intensity of the talc reflection at 9,3 Å.

Appendix D

Water vapour permeability raw data and equations

Origin of the data in Chapter 4, Figure 4:

5 Films of each formulation were tested. The thicknesses of the films are given in Table A-4 (*T1-T13*). The average thickness (*T*) of each film was calculated as well as the standard deviation (*s(T)*) and the relative standard deviation of the average thickness (*rs(T)*, Equation E1).

$$rs(T) = \frac{s(T)}{T} \qquad \text{E1}$$

The masses (*m1-m9*) of the cups, filled with dry silica gel and sealed with the films, were measured at different time intervals (Table A-5). The mass was plotted as a function of time. The slope (*S*, Equation E2) and the standard deviation of the slope (*s(S)*, Equation E3) of the mass vs. time plot were determined with the *linest* function of Microsoft Excel® (E2 and E3). The relative standard deviation in the slope was determined in the same way as in Equation E1 for the relative standard deviation in the thickness.

S = index(linest(y values, x values),1) E2

s(S) = index(linest(y values, x values,true,true),2) E3

The water vapour permeability (WVP_x) of the individual films was determined by Equation E4. The *WVP*s of the 5 individual films of each formulation was averaged (*Av WVP*).

$$WVP_x = \frac{S \times T}{A \times P} = \frac{S \times T}{\Pi R^2 \times P} \qquad \text{E4}$$

Where A = 0,0018 m^2 (Area of the opening of the cup)
And $P = p_o - p_i$ = 2,3768 kPa[a,b].

P is the difference in the water vapour pressure on the outside (p_o) and the inside (p_i) of the cup. The relative humidity (*RH*) is assumed to be 0% on the inside (silica gel) and 75% on the outside (excess NaCl in contact with saturated solution of NaCl). The actual *RH*s were not measured. The relationship between the water vapour pressure (p) at a certain temperature and the *RH* is given by Equation E5.

$$p = \frac{RH \times p_w}{100} \qquad \text{[a]} \qquad \text{E5}$$

Where p_w = 3.1690 kPa, the water vapour pressure at 25 °C for pure water.

[a] A. WEXLER, in "Handbook of Physics and Chemistry", 79th edition, edited by D.R. Lide (CRC Press, Boca Raton, 1998) p. ***15***-25.
[b] Vapor pressure of water from 0 to 370 °C, "Handbook of Physics and Chemistry", 79th edition, edited by D.R. Lide (CRC Press, Boca Raton, 1998) p. ***6***-8.

The error in the WVP (E_x) for the individual films was calculated by Equation E6, which was derived from the general Equation E7 on the propagation of errors [c]. The pooled error (*PE*) of the *Av WVP* was determined by Equation E8.

$$E_x = \sqrt{WVP^2 \times \{rs(S)^2 + rs(T)^2 + 4ru(R)^2\}} \qquad \text{E6}$$

Where

R = 0,024 m (radius of the opening of the cup)

$u(R)$ = 0,001 m (uncertainty in the radius measurement, measured with a ruler)

$ru(R) = u(R)/R$ = 0,04 (relative uncertainty in the radius measurement)

$$E_x^2 = (\frac{\partial WVP}{\partial S})^2 \times s(S)^2 + (\frac{\partial WVP}{\partial T})^2 \times s(T)^2 + (\frac{\partial WVP}{\partial R})^2 \times u(R)^2 \qquad \text{[c]} \qquad \text{E7}$$

In Equation E7 the contribution of the error in the difference in the water vapour pressure (*P*) is assumed to be zero because the actual water vapour pressures and the errors therein were not measured.

$$PE = \frac{\sqrt{E_1^2 + E_2^2 + E_3^2 + E_4^2 + E_5^2}}{\sqrt{5}} \qquad \text{E8}$$

The same calculations were done for the films of which the *WVP* data are shown in Chapter 4, Figure 5. The thickness and mass data and calculated values are shown separately in Tables A-6 and A-7 because of the different time intervals of taking measurements. A different cup size was also used and the relevant constants are as follows:

R = 0,0181 m

$u(R)$ = 0,0005 m (measured with a vernier)

$ru(R)$ = 0,027

A = 0,0010 m^2

[c] H.D. YOUNG, Statistical Treatment of Experimental Data, (McGraw-Hill Book Company, New York, 1962) p. 96-98.

For the sample tested at 38 °C/90% *RH* p_o-p_i is 5,9668 kPa[a,b] and p_w is 6,6298 kPa at 38 °C and A = 0,0010 m^2.

Table A-4 Thickness data for films relating to Chapter 4, Figure 4.

	***T1*/mm**	***T2*/mm**	***T3*/mm**	***T4*/mm**	***T5*/mm**	***T6*/mm**	***T7*/mm**	***T8*/mm**	***T9*/mm**	***T10*/mm**	***T11*/mm**	***T12*/mm**	***T13*/mm**	***T*/mm**	***s(T)*/mm**	***rs(T)***
Blank																
1	0,061	0,061	0,059	0,056	0,051	0,052	0,056	0,057	0,055	0,058	0,053	0,056	0,058	0,056	0,00087	0,015
2	0,059	0,063	0,066	0,065	0,064	0,065	0,062	0,060	0,063	0,062	0,064	0,066	0,064	0,063	0,00059	0,009
3	0,061	0,060	0,064	0,064	0,065	0,060	0,057	0,060	0,064	0,061	0,063	0,064	0,062	0,062	0,00065	0,010
4	0,060	0,060	0,058	0,057	0,058	0,057	0,060	0,061	0,058	0,066	0,058	0,058	0,061	0,059	0,00067	0,011
5	0,061	0,063	0,062	0,058	0,059	0,057	0,061	0,062	0,059	0,063	0,062	0,059	0,063	0,061	0,00057	0,009
LDH alone																
1	0,089	0,113	0,075	0,077	0,108	0,157	0,120	0,134	0,108	0,122	0,092	0,132	0,111	0,111	0,00651	0,059
2	0,155	0,156	0,127	0,153	0,152	0,147	0,147	0,173	0,165	0,146	0,158	0,161	0,163	0,154	0,00313	0,020
3	0,130	0,150	0,136	0,152	0,153	0,165	0,167	0,151	0,163	0,138	0,161	0,180	0,170	0,155	0,00402	0,026
4	0,175	0,176	0,148	0,130	0,164	0,185	0,136	0,138	0,153	0,185	0,133	0,132	0,141	0,154	0,00579	0,038
5	0,135	0,114	0,126	0,163	0,145	0,130	0,133	0,129	0,118	0,133	0,145	0,140	0,119	0,133	0,00367	0,028
SA alone																
1	0,144	0,134	0,128	0,126	0,134	0,131	0,147	0,145	0,132	0,133	0,129	0,139	0,142	0,136	0,00193	0,014
2	0,136	0,143	0,145	0,138	0,143	0,153	0,163	0,153	0,136	0,136	0,145	0,147	0,152	0,145	0,00227	0,016
3	0,109	0,100	0,106	0,112	0,118	0,125	0,131	0,127	0,107	0,122	0,109	0,115	0,116	0,115	0,00254	0,022
4	0,115	0,109	0,110	0,123	0,110	0,124	0,127	0,137	0,119	0,118	0,120	0,116	0,125	0,119	0,00219	0,018
5	0,118	0,118	0,114	0,112	0,115	0,118	0,122	0,133	0,121	0,121	0,107	0,117	0,123	0,118	0,00173	0,015
1:1 LDH:SA																
1	0,103	0,097	0,102	0,115	0,123	0,126	0,132	0,098	0,119	0,160	0,098	0,098	0,091	0,112	0,00538	0,048
2	0,111	0,086	0,100	0,088	0,085	0,077	0,071	0,085	0,097	0,086	0,136	0,115	0,074	0,093	0,00511	0,055
3	0,086	0,090	0,085	0,087	0,079	0,082	0,085	0,090	0,082	0,092	0,100	0,106	0,083	0,088	0,00211	0,024
4	0,167	0,131	0,105	0,085	0,113	0,119	0,149	0,105	0,084	0,095	0,103	0,095	0,093	0,111	0,00690	0,062
5	0,095	0,118	0,088	0,096	0,091	0,096	0,113	0,093	0,113	0,130	0,101	0,124	0,122	0,106	0,00397	0,037
2:1 LDH:SA																
1	0,082	0,118	0,109	0,116	0,101	0,103	0,075	0,073	0,076	0,077	0,092	0,116	0,093	0,095	0,00471	0,050
2	0,079	0,082	0,103	0,100	0,091	0,087	0,088	0,085	0,081	0,080	0,095	0,087	0,094	0,089	0,00212	0,024
3	0,095	0,112	0,102	0,126	0,107	0,108	0,102	0,102	0,106	0,104	0,100	0,101	0,094	0,105	0,00225	0,022
4	0,133	0,092	0,097	0,093	0,103	0,132	0,106	0,097	0,108	0,092	0,097	0,100	0,106	0,104	0,00377	0,036
5	0,106	0,103	0,112	0,120	0,126	0,146	0,130	0,107	0,114	0,115	0,134	0,122	0,120	0,120	0,00339	0,028

Table A-5 Mass increase data and calculations for films relating to Chapter 4, Figure 4.

	***t*/day**	0	0,1	0,2	0,9	1,0	2,0	3,0	4,0	7,0							
		***m1*/g**	***m2*/g**	***m3*/g**	***m4*/g**	***m5*/g**	***m6*/g**	***m7*/g**	***m8*/g**	***m9*/g**	***Sl*(g/day)**	***s(S)*/(g/day)**	***rs(S)***	***WVP$_x$l* (g.mm.m^{-2}.day^{-1}.kPa^{-1})**	***E$_x$***	***Av WVP***	***PE***
Blank	**1**	139,3552	139,4242	139,4811	140,2618	140,3950	141,4589	142,3971	143,1735	145,2979	0,87	0,0337	0,04	11	1	12	1
	2	139,2650	139,3264	139,3768	140,133	140,2557	141,2504	142,1510	142,8899	144,8819	0,83	0,0327	0,04	12	1		
	3	139,2010	139,2737	139,3324	140,1499	140,2855	141,3015	142,2811	143,0597	145,1734	0,88	0,0348	0,04	13	1		
	4	139,2622	139,3393	139,3971	140,2343	140,3704	141,4012	142,3324	143,0798	145,1268	0,86	0,0377	0,04	12	1		
	5	136,8620	136,9333	136,9908	137,8023	137,9309	138,9457	139,8624	140,5899	142,5820	0,84	0,0370	0,04	12	1		
LDH alone	**1**	139,4256	139,5167	139,5940	140,4959	140,6331	141,6984	142,6654	143,4380	145,4351	0,88	0,0450	0,05	23	3	28	3
	2	140,3237	140,3925	140,4495	141,2445	141,3808	142,3624	143,2521	144,0026	146,0535	0,84	0,0328	0,04	30	3		
	3	140,4868	140,5627	140,6284	141,4686	141,5977	142,6143	143,5011	144,2244	146,2302	0,84	0,0379	0,05	30	3		
	4	140,2640	140,3444	140,4171	141,2742	141,4027	142,3702	143,2850	144,0579	146,1224	0,86	0,0355	0,04	30	3		
	5	140,0224	140,1078	140,1814	141,0032	141,1408	142,1541	143,0556	143,7822	145,7727	0,84	0,0384	0,05	26	3		
SA alone	**1**	137,1115	137,1200	137,225	138,0179	138,1360	139,1042	140,0090	140,7353	142,7846	0,83	0,0325	0,04	26	2	24	2
	2	139,9684	140,0236	140,0771	140,8523	140,9787	141,9294	142,7860	143,5004	145,4594	0,81	0,0323	0,04	27	3		
	3	139,9268	140,0015	140,0691	140,9022	141,0331	142,0171	142,9162	143,6497	145,6274	0,84	0,0374	0,04	22	2		
	4	140,1941	140,2665	140,3300	141,1496	141,284	142,2798	143,1811	143,9231	145,9461	0,84	0,0358	0,04	23	2		
	5	140,2950	140,3668	140,4312	141,2147	141,3395	142,3173	143,1955	143,9281	145,9365	0,83	0,0331	0,04	23	2		
1:1 LDH:SA	**1**	139,7316	139,7411	139,7512	139,9302	139,9608	140,2381	140,5555	140,851	141,9580	0,315	0,0092	0,03	8	1	7	1
	2	140,0043	140,0151	140,0257	140,2194	140,2500	140,5334	140,8203	141,0871	141,9858	0,284	0,0025	0,01	6	1		
	3	139,3577	139,2721	139,3856	139,6194	139,6563	139,9716	140,3181	140,6289	141,6933	0,339	0,0052	0,02	7	1		
	4	139,3222	139,3320	139,3434	139,5163	139,5450	139,8020	140,0908	140,3572	141,1830	0,268	0,0029	0,01	7	1		
	5	137,1644	137,1729	137,1827	137,3484	137,3746	137,6031	137,8575	138,0961	138,8862	0,246	0,0031	0,01	6	1		
2:1 LDH:SA	**1**	140,0288	140,0458	140,0636	140,3463	140,3917	140,8017	141,2405	141,6597	142,9410	0,419	0,0034	0,01	9	1	9	1
	2	139,3650	139,3795	139,3947	139,6615	139,7032	140,1085	140,5687	140,9926	142,3636	0,431	0,0066	0,02	9	1		
	3	140,1331	140,1462	140,1606	140,3972	140,4349	140,7748	141,1478	141,4882	142,6018	0,354	0,0036	0,01	9	1		
	4	140,0244	140,0380	140,0519	140,3019	140,3421	140,7019	141,0646	141,4494	142,6036	0,370	0,0039	0,01	9	1		
	5	139,5315	139,5426	139,5557	139,7699	139,8042	140,1187	140,4883	140,8465	141,9530	0,347	0,0060	0,02	10	1		

Table A-6 Thickness data for films relating to Chapter 4, Figure 5.

100SA/0LDH	***T1*/mm**	***T2*/mm**	***T3*/mm**	***T4*/mm**	***T5*/mm**	***T6*/mm**	***T7*/mm**	***T8*/mm**	***T9*/mm**	***T*/mm**	***s(T)*/mm**	***rs(T)***
1	0,139	0,147	0,136	0,132	0,138	0,147	0,147	0,137	0,144	0,141	0,00187	0,013
2	0,123	0,137	0,141	0,134	0,144	0,144	0,137	0,135	0,137	0,137	0,00212	0,015
3	0,143	0,136	0,132	0,126	0,130	0,138	0,143	0,135	0,14	0,136	0,00194	0,014
4	0,119	0,125	0,131	0,13	0,129	0,121	0,124	0,128	0,118	0,125	0,00162	0,013
90SA/10LDH												
1	0,143	0,141	0,136	0,134	0,141	0,145	0,149	0,146	0,147	0,142	0,00167	0,012
2	0,131	0,125	0,117	0,124	0,127	0,126	0,134	0,135	0,129	0,128	0,00184	0,014
3	0,141	0,135	0,132	0,144	0,135	0,139	0,146	0,147	0,144	0,140	0,00180	0,013
4	0,141	0,133	0,139	0,138	0,145	0,144	0,145	0,142	0,15	0,142	0,00164	0,012
80SA/20LDH												
1	0,126	0,109	0,111	0,135	0,13	0,118	0,124	0,131	0,131	0,124	0,00309	0,025
2	0,132	0,147	0,141	0,102	0,144	0,15	0,142	0,114	0,132	0,134	0,00536	0,040
3	0,139	0,158	0,156	0,106	0,148	0,163	0,147	0,122	0,15	0,143	0,00613	0,043
4	0,15	0,179	0,149	0,142	0,172	0,195	0,188	0,153	0,161	0,165	0,00628	0,038
70SA/30LDH 10 min												
1	0,123	0,132	0,137	0,129	0,141	0,134	0,136	0,134	0,134	0,133	0,00170	0,013
2	0,132	0,14	0,132	0,126	0,152	0,137	0,132	0,133	0,14	0,136	0,00249	0,018
3	0,128	0,13	0,132	0,126	0,14	0,136	0,143	0,132	0,14	0,134	0,00198	0,015
4	0,12	0,116	0,112	0,117	0,115	0,116	0,126	0,121	0,122	0,118	0,00142	0,012
70SA/30LDH 30 min												
1	0,15	0,144	0,133	0,141	0,152	0,152	0,148	0,145	0,15	0,146	0,00206	0,014
2	0,156	0,105	0,111	0,147	0,125	0,131	0,155	0,157	0,152	0,138	0,00676	0,049
3	0,135	0,132	0,119	0,125	0,124	0,136	0,136	0,136	0,145	0,132	0,00266	0,020
4	0,116	0,122	0,120	0,119	0,123	0,123	0,121	0,121	0,124	0,121	0,00082	0,007
70SA/30LDH 60 min												
1	0,131	0,141	0,128	0,123	0,131	0,135	0,132	0,127	0,135	0,131	0,00175	0,013
2	0,133	0,14	0,129	0,128	0,131	0,132	0,136	0,134	0,132	0,133	0,00121	0,009
3	0,138	0,132	0,127	0,128	0,129	0,133	0,134	0,137	0,136	0,133	0,00133	0,010
4	0,12	0,127	0,114	0,111	0,121	0,122	0,125	0,117	0,128	0,121	0,00192	0,016

Table A-6 continued Thickness data for films relating to Chapter 4, Figure 5.

	***T1*/mm**	***T2*/mm**	***T3*/mm**	***T4*/mm**	***T5*/mm**	***T6*/mm**	***T7*/mm**	***T8*/mm**	***T9*/mm**	***T*/mm**	***s(T)*/mm**	***rs(T)***
60SA/40LDH												
1	0,126	0,125	0,12	0,116	0,121	0,13	0,128	0,118	0,124	0,123	0,00156	0,013
2	0,134	0,131	0,121	0,125	0,128	0,134	0,132	0,129	0,126	0,129	0,00146	0,011
3	0,132	0,136	0,138	0,129	0,136	0,135	0,136	0,131	0,139	0,135	0,00111	0,008
4	0,131	0,137	0,136	0,132	0,135	0,135	0,137	0,133	0,139	0,135	0,00087	0,006
50SA/50LDH												
1	0,12	0,124	0,132	0,131	0,142	0,124	0,126	0,131	0,127	0,129	0,00214	0,017
2	0,116	0,12	0,13	0,131	0,132	0,123	0,124	0,126	0,128	0,126	0,00178	0,014
3	0,121	0,127	0,126	0,12	0,123	0,129	0,128	0,123	0,129	0,125	0,00115	0,009
4	0,111	0,115	0,11	0,111	0,114	0,113	0,113	0,113	0,111	0,112	0,00055	0,005
40SA/60LDH												
1	0,117	0,114	0,115	0,117	0,116	0,121	0,12	0,116	0,116	0,117	0,00075	0,006
2	0,121	0,12	0,122	0,121	0,129	0,125	0,129	0,126	0,127	0,124	0,00118	0,009
3	0,122	0,122	0,125	0,121	0,127	0,124	0,124	0,124	0,13	0,124	0,00093	0,007
4	0,126	0,118	0,127	0,126	0,13	0,123	0,13	0,132	0,131	0,127	0,00148	0,012
30SA/70LDH												
1	0,117	0,116	0,127	0,121	0,123	0,12	0,117	0,124	0,12	0,121	0,00121	0,010
2	0,13	0,13	0,132	0,134	0,127	0,13	0,134	0,133	0,132	0,131	0,00076	0,006
3	0,125	0,126	0,126	0,133	0,131	0,13	0,134	0,131	0,13	0,130	0,00107	0,008
4	0,128	0,129	0,121	0,12	0,123	0,13	0,129	0,123	0,126	0,125	0,00126	0,010
20SA/80LDH												
1	0,133	0,122	0,132	0,135	0,135	0,128	0,133	0,138	0,135	0,132	0,00158	0,012
2	0,129	0,122	0,119	0,13	0,132	0,126	0,131	0,132	0,133	0,128	0,00163	0,013
3	0,125	0,118	0,132	0,125	0,126	0,126	0,126	0,134	0,132	0,127	0,00163	0,013
4	0,105	0,105	0,114	0,114	0,118	0,113	0,11	0,113	0,114	0,112	0,00145	0,013
10SA/90LDH												
1	0,12	0,132	0,117	0,106	0,114	0,143	0,127	0,118	0,133	0,123	0,00379	0,031
2	0,131	0,136	0,13	0,128	0,141	0,14	0,138	0,135	0,142	0,136	0,00169	0,012
3	0,113	0,118	0,121	0,122	0,123	0,126	0,129	0,128	0,131	0,123	0,00191	0,015
4	0,117	0,129	0,132	0,134	0,139	0,135	0,135	0,142	0,14	0,134	0,00248	0,019

Table A-6 continued Thickness data for films relating to Chapter 4, Figure 5.

	***T1*/mm**	***T2*/mm**	***T3*/mm**	***T4*/mm**	***T5*/mm**	***T6*/mm**	***T7*/mm**	***T8*/mm**	***T9*/mm**	***T*/mm**	***s(T)*/mm**	***rs(T)***
0SA/100LDH												
1	0,133	0,13	0,146	0,15	0,138	0,139	0,137	0,147	0,140	0,140	0,00220	0,016
2	0,117	0,137	0,133	0,125	0,135	0,133	0,124	0,122	0,126	0,128	0,00225	0,018
3	0,132	0,126	0,133	0,130	0,137	0,135	0,135	0,133	0,137	0,133	0,00117	0,009
4	0,131	0,135	0,135	0,132	0,14	0,135	0,135	0,138	0,137	0,135	0,00093	0,007
0SA/0LDH Blank												
1	0,135	0,138	0,134	0,132	0,14	0,14	0,143	0,145	0,147	0,139	0,00170	0,012
2	0,143	0,147	0,141	0,136	0,153	0,148	0,148	0,131	0,137	0,143	0,00235	0,016
3	0,13	0,139	0,12	0,123	0,136	0,138	0,134	0,127	0,133	0,131	0,00221	0,017
4	0,138	0,142	0,144	0,145	0,153	0,146	0,151	0,152	0,152	0,147	0,00176	0,012
70SA/30Bent Bentonite												
1	0,126	0,126	0,129	0,124	0,12	0,144	0,123	0,147	0,12	0,129	0,00331	0,026
2	0,123	0,115	0,112	0,113	0,111	0,118	0,122	0,102	0,103	0,113	0,00246	0,022
3	0,124	0,132	0,138	0,127	0,132	0,13	0,128	0,145	0,131	0,132	0,00209	0,016
4	0,117	0,113	0,116	0,136	0,122	0,124	0,145	0,137	0,146	0,128	0,00425	0,033
70SA/30Talc												
1	0,151	0,142	0,151	0,155	0,16	0,16	0,135	0,142	0,165	0,151	0,00332	0,022
2	0,144	0,164	0,16	0,17	0,172	0,161	0,146	0,15	0,176	0,160	0,00385	0,024
3	0,172	0,124	0,153	0,149	0,14	0,177	0,158	0,142	0,136	0,150	0,00568	0,038
4	0,169	0,104	0,123	0,141	0,148	0,142	0,127	0,133	0,127	0,135	0,00606	0,045
70SA/30LDH Tap water												
1	0,145	0,141	0,128	0,127	0,132	0,142	0,143	0,137	0,139	0,1371	0,00221	0,016
2	0,129	0,138	0,127	0,128	0,144	0,136	0,137	0,14	0,143	0,136	0,00213	0,016
3	0,128	0,131	0,123	0,133	0,134	0,133	0,134	0,133	0,141	0,132	0,00162	0,012
4	0,12	0,121	0,117	0,11	0,122	0,125	0,124	0,119	0,124	0,120	0,00154	0,013
70SA/30LDH 38°C/90% RH												
1	0,122	0,131	0,127	0,122	0,125	0,124	0,127	0,125	0,124	0,125	0,00094	0,008

Table A-7 Mass increase data and calculations for films relating to Chapter 4, Figure 5.

	***t*/day**	0	0,104	0,188	0,271							
	***t*/h**	0	2,5	4,5	6,5							
100SA/0LDH		***m1***	***m2***	***m3***	***m4***	***S*/(g/day)**	***s(S)*/(g/day)**	***rs(S)***	***WVP*$_x$/ (g.mm.m^{-2}. day^{-1}.kPa^{-1})**	***E*$_x$**	***Av WVP***	***PE***
1		18,239	18,277	18,306	18,341	0,374	0,01017	0,027	21	1	22	1
2		18,087	18,12	18,145	18,172	0,313	0,00289	0,009	17	1		
3		18,234	18,278	18,312	18,35	0,426	0,00648	0,015	24	1		
4		18,442	18,49	18,527	18,567	0,460	0,00446	0,010	23	1		

	***t*/day**	0	0,094	0,177	0,260							
	***t*/h**	0	2,25	4,25	6,25							
90SA/10LDH		***m1***	***m2***	***m3***	***m4***	***S*/(g/day)**	***s(S)*/(g/day)**	***rs(S)***	***WVP*$_x$/ (g.mm.m^{-2}. day^{-1}.kPa^{-1})**	***E*$_x$**	***Av WVP***	***PE***
1		19,295	19,315	19,332	19,35	0,211	0,00152	0,007	12	1	16	1
2		18,617	18,652	18,682	18,714	0,371	0,00301	0,008	19	1		
3		18,331	18,356	18,377	18,399	0,260	0,00194	0,007	15	1		
4		18,287	18,313	18,336	18,36	0,280	0,00189	0,007	16	1		

	***t*/day**	0	0,104	0,188	0,271							
	***t*/h**	0	2,5	4,5	6,5							
80SA/20LDH		***m1***	***m2***	***m3***	***m4***	***S*/(g/day)**	***s(S)*/(g/day)**	***rs(S)***	***WVP*$_x$/ (g.mm.m^{-2}. day^{-1}.kPa^{-1})**	***E*$_x$**	***Av WVP***	***PE***
1		18,426	18,437	18,444	18,453	0,098	0,00312	0,032	5,0	0,3	4,6	0,4
2		18,193	18,203	18,21	18,218	0,092	0,00166	0,018	5,0	0,4		
3		18,183	18,192	18,197	18,204	0,076	0,00356	0,047	4,5	0,4		
4		17,988	17,995	17,999	18,005	0,0616	0,00297	0,048	4,2	0,3		

	***t*/day**	0	0,083	0,146	0,229							
	***t*/h**	0	2	3,5	5,5							
70SA/30LDH 60 min		***m1***	***m2***	***m3***	***m4***	***S*/(g/day)**	***s(S)*/(g/day)**	***rs(S)***	***WVP*$_x$/ (g.mm.m^{-2}. day^{-1}.kPa^{-1})**	***E*$_x$**	***Av WVP***	***PE***
1		18,485	18,494	18,5	18,512	0,116	0,00743	0,064	6,2	0,5	6,8	0,5
2		18,359	18,369	18,376	18,389	0,130	0,00717	0,055	7,0	0,6		
3		18,39	18,401	18,408	18,421	0,134	0,00593	0,044	7,2	0,5		
4		18,521	18,532	18,539	18,553	0,138	0,00803	0,058	6,8	0,6		

	***t*/day**	0	0,104	0,188	0,271							
	***t*/h**	0	2,5	4,5	6,5							
60SA/40LDH		***m1***	***m2***	***m3***	***m4***	***S*/(g/day)**	***s(S)*/(g/day)**	***rs(S)***	***WVP*$_x$/ (g.mm.m^{-2}. day^{-1}.kPa^{-1})**	***E*$_x$**	***Av WVP***	***PE***
1		18,33	18,338	18,344	18,352	0,080	0,00347	0,043	4,0	0,3	4,5	0,4
2		18,294	18,302	18,309	18,318	0,088	0,00508	0,058	4,6	0,4		
3		18,236	18,244	18,251	18,26	0,088	0,00508	0,058	4,8	0,4		
4		18,056	18,063	18,069	18,078	0,080	0,00672	0,084	4,4	0,4		

	***t*/day**	0	0,104	0,188	0,271							
	***t*/h**	0	2,5	4,5	6,5							
50SA/50LDH		***m1***	***m2***	***m3***	***m4***	***S*/(g/day)**	***s(S)*/(g/day)**	***rs(S)***	***WVP*$_x$/ (g.mm.m^{-2}. day^{-1}.kPa^{-1})**	***E*$_x$**	***Av WVP***	***PE***
1		18,374	18,39	18,4	18,411	0,135	0,00506	0,037	7,1	0,5	6,1	0,4
2		18,124	18,138	18,147	18,156	0,118	0,00493	0,042	6,0	0,4		
3		18,27	18,281	18,289	18,299	0,106	0,00306	0,029	5,4	0,3		
4		18,292	18,307	18,316	18,327	0,128	0,00483	0,038	5,9	0,4		

	***t*/day**	0	0,094	0,177	0,260							
	***t*/h**	0	2,25	4,25	6,25							
40SA/60LDH		***m1***	***m2***	***m3***	***m4***	***S*/(g/day)**	***s(S)*/(g/day)**	***rs(S)***	***WVP*$_x$/ (g.mm.m^{-2}. day^{-1}.kPa^{-1})**	***E*$_x$**	***Av WVP***	***PE***
1		18,282	18,298	18,312	18,327	0,172	0,00176	0,010	8,2	0,5	8,6	0,5
2		18,053	18,069	18,083	18,095	0,162	0,00445	0,027	8,2	0,5		
3		17,894	17,911	17,924	17,939	0,171	0,00347	0,020	8,7	0,5		
4		18,707	18,723	18,737	18,753	0,176	0,00379	0,022	9,1	0,6		

	***t*/day**	0	0,083	0,167	0,25							
	***t*/h**	0	2	4	6							
30SA/70LDH		***m1***	***m2***	***m3***	***m4***	***S*/(g/day)**	***s(S)*/(g/day)**	***rs(S)***	***WVP*$_x$/ (g.mm.m^{-2}. day^{-1}.kPa^{-1})**	***E*$_x$**	***Av WVP***	***PE***
1		18,196	18,208	18,222	18,234	0,154	0,00339	0,022	7,6	0,5	9,0	0,5
2		18,199	18,214	18,229	18,243	0,176	0,00208	0,012	9,5	0,5		
3		18,588	18,603	18,618	18,634	0,184	0,00208	0,011	9,7	0,6		
4		18,155	18,17	18,184	18,2	0,179	0,00317	0,018	9,2	0,5		

	***t*/day**	0	0,104	0,188	0,271							
	***t*/h**	0	2,5	4,5	6,5							
20SA/80LDH		***m1***	***m2***	***m3***	***m4***	***S*/(g/day)**	***s(S)*/(g/day)**	***rs(S)***	***WVP*$_x$/ (g.mm.m^{-2}. day^{-1}.kPa^{-1})**	***E*$_x$**	***Av WVP***	***PE***
1		18,141	18,174	18,2	18,228	0,320	0,00347	0,011	17	1	17	1
2		18,379	18,412	18,44	18,473	0,345	0,01288	0,037	18	1		
3		18,002	18,035	18,062	18,092	0,331	0,00707	0,021	17	1		
4		18,061	18,098	18,126	18,158	0,356	0,00612	0,017	16	1		

	***t*/day**	0	0,104	0,188	0,271							
	***t*/h**	0	2,5	4,5	6,5							
10SA/90LDH		***m1***	***m2***	***m3***	***m4***	***S*/(g/day)**	***s(S)*/(g/day)**	***rs(S)***	***WVP*$_x$/ (g.mm.m^{-2}. day^{-1}.kPa^{-1})**	***E*$_x$**	***Av WVP***	***PE***
1		18,346	18,383	18,409	18,439	0,341	0,00623	0,018	17	1	21	1
2		18,329	18,37	18,398	18,433	0,380	0,01010	0,027	21	1		
3		18,001	18,049	18,084	18,124	0,451	0,00721	0,016	23	1		
4		18,411	18,456	18,488	18,525	0,418	0,00743	0,018	23	1		

	***t*/day**	0	0,104	0,188	0,271							
	***t*/h**	0	2,5	4,5	6,5							
0SA/100LDH		***m1***	***m2***	***m3***	***m4***	***S*/(g/day)**	***s(S)*/(g/day)**	***rs(S)***	***WVP*$_x$/ (g.mm.m^{-2}. day^{-1}.kPa^{-1})**	***E*$_x$**	***Av WVP***	***PE***
1		18,382	18,43	18,464	18,505	0,450	0,01007	0,022	26	2	24	1
2		18,252	18,294	18,324	18,361	0,398	0,01024	0,026	21	1		
3		18,328	18,376	18,41	18,451	0,450	0,01007	0,022	24	1		
4		18,361	18,409	18,444	18,486	0,457	0,01033	0,023	25	2		

	***t*/day**	0	0,083	0,167	0,25							
	***t*/h**	0	2	4	6							
0SA/0LDH Blank		***m1***	***m2***	***m3***	***m4***	***S*/(g/day)**	***s(S)*/(g/day)**	***rs(S)***	***WVP*$_x$/ (g.mm.m^{-2}. day^{-1}.kPa^{-1})**	***E*$_x$**	***Av WVP***	***PE***
1		18,101	18,138	18,173	18,215	0,452	0,01218	0,027	26	2	26	2
2		18,15	18,186	18,223	18,259	0,437	0,00170	0,004	25	1		
3		18,187	18,224	18,262	18,301	0,456	0,00379	0,008	24	1		
4		17,86	17,898	17,936	17,975	0,460	0,00208	0,005	28	2		

	***t*/day**	0	0,083	0,146	0,229							
	***t*/h**	0	2	3,5	5,5							
70SA/30Bent Bentonite		***m1***	***m2***	***m3***	***m4***	***S*/(g/day)**	***s(S)*/(g/day)**	***rs(S)***	***WVP*$_x$/ (g.mm.m^{-2}. day^{-1}.kPa^{-1})**	***E*$_x$**	***Av WVP***	***PE***
1		18,763	18,778	18,788	18,805	0,182	0,00593	0,033	9,6	0,7	9,4	0,7
2		17,846	17,867	17,88	17,901	0,238	0,00574	0,024	11,0	0,7		
3		18,419	18,428	18,434	18,444	0,108	0,00315	0,029	5,8	0,4		
4		18,351	18,369	18,381	18,401	0,216	0,00631	0,029	11,4	0,8		

	***t*/day**	0	0,104	0,188	0,271							
	***t*/h**	0	2,5	4,5	6,5							
70SA/30Talc		***m1***	***m2***	***m3***	***m4***	***S*/(g/day)**	***s(S)*/(g/day)**	***rs(S)***	***WVP*$_x$/ (g.mm.m^{-2}. day^{-1}.kPa^{-1})**	***E*$_x$**	***Av WVP***	***PE***
1		18,329	18,343	18,35	18,363	0,122	0,00868	0,071	7,5	0,7	7,3	0,6
2		18,013	18,022	18,027	18,035	0,079	0,00437	0,055	5,2	0,4		
3		18,214	18,228	18,237	18,249	0,127	0,00437	0,034	7,8	0,6		
4		17,959	17,976	17,988	18,003	0,161	0,00437	0,027	8,9	0,7		

	***t*/day**	0	0,083	0,167	0,25							
	***t*/h**	0	2	4	6							
70SA/30LDH 10 min		***m1***	***m2***	***m3***	***m4***	***S*/(g/day)**	***s(S)*/(g/day)**	***rs(S)***	***WVP*$_x$/ (g.mm.m^{-2}. day^{-1}.kPa^{-1})**	***E*$_x$**	***Av WVP***	***PE***
1		18,256	18,275	18,297	18,322	0,26	0,01138	0,04	14	1	15	1
2		18,294	18,311	18,332	18,353	0,24	0,00831	0,03	13	1		
3		18,14	18,161	18,183	18,203	0,25	0,00317	0,01	14	1		
4		18,1	18,128	18,157	18,19	0,36	0,00982	0,03	17	1		

	***t*/day**	0	0,083	0,167	0,25							
	***t*/h**	0	2	4	6							
70SA/30LDH 30 min		***m1***	***m2***	***m3***	***m4***	***S*/(g/day)**	***s(S)*/(g/day)**	***rs(S)***	***WVP*$_x$/ (g.mm.m^{-2}. day^{-1}.kPa^{-1})**	***E*$_x$**	***Av WVP***	***PE***
1		18,354	18,37	18,383	18,403	0,19	0,01138	0,06	11,5	0,9	10,5	0,8
2		18,035	18,048	18,06	18,078	0,17	0,01119	0,07	9,5	0,9		
3		18,062	18,077	18,091	18,109	0,19	0,00710	0,04	10,0	0,7		
4		18,236	18,253	18,271	18,291	0,22	0,00575	0,03	10,9	0,7		

	***t*/day**	0	0,083	0,167	0,25							
	***t*/h**	0	2	4	6							
60SA/40LDH Tap water		***m1***	***m2***	***m3***	***m4***	***S*/(g/day)**	***s(S)*/(g/day)**	***rs(S)***	***WVP*$_x$/ (g.mm.m^{-2}. day^{-1}.kPa^{-1})**	***E*$_x$**	***Av WVP***	***PE***
1		18,18	18,192	18,204	18,215	0,14	0,00208	0,01	7,9	0,5	7,6	0,5
2		18,336	18,346	18,357	18,369	0,13	0,00379	0,03	7,3	0,5		
3		18,548	18,557	18,569	18,581	0,13	0,00624	0,05	7,2	0,5		
4		18,606	18,619	18,632	18,646	0,16	0,00208	0,01	7,8	0,5		

	***t*/day**	0	0,104	0,292								
	***t*/h**	0	2,5	7								
60SA/40LDH 38 C/90% RH		***m1***	***m2***	***m3***	***m4***	***S*/(g/day)**	***s(S)*/(g/day)**	***rs(S)***	***WVP*$_x$/ (g.mm.m^{-2}. day^{-1}.kPa^{-1})**	***E*$_x$**	***Av WVP***	***PE***
1		18,039	18,105	18,231		0,66	0,01021	0,02	13,5	0,5	-	-

Appendix E

Tensile data

Table A-8 gives the thickness data of the film tested. The width of the tensile specimens (at the middle of the dumbbells) were 6,2 mm and the gage length were 35 mm in all cases. These values were used by the Nexygen program from Lloyd Instruments to calculate the different parameters in Table A-9. The stress at break, % strain at break and the Young's modulus of samples of the same composition were averaged and the standard deviations of the averages were calculated in order to plot the graphs in Figures 12-14 (Chapter 4).

Table A-8 Thickness data for films shown in Figures 12-14 (Chapter 4).

Film composition	Sample number	*T1*/mm	*T2*/mm	*T3*/mm	*T*/mm
100SA/0LDH	1	0,154	0,113	0,169	0,145
	2	0,171	0,167	0,168	0,169
90SA/10LDH	1	0,121	0,114	0,114	0,116
	2	0,115	0,113	0,118	0,115
	3	0,116	0,113	0,118	0,116
80SA/20LDH	1	0,090	0,132	0,138	0,120
	2	0,119	0,130	0,105	0,118
	3	0,135	0,126	0,129	0,130
70SA/30LDH	1	0,118	0,123	0,120	0,120
	2	0,118	0,112	0,112	0,114
	3	0,106	0,110	0,104	0,107
60SA/40LDH	1	0,126	0,126	0,123	0,125
	2	0,127	0,124	0,118	0,123
	3	0,123	0,122	0,120	0,122
	4	0,121	0,127	0,130	0,126
50SA/50LDH	1	0,119	0,123	0,132	0,125
	2	0,122	0,129	0,133	0,128
	3	0,127	0,127	0,145	0,133
40SA/60LDH	1	0,137	0,131	0,134	0,134
	2	0,128	0,127	0,128	0,128
	3	0,104	0,110	0,130	0,115
30SA/70LDH	1	0,126	0,131	0,127	0,128
	2	0,123	0,128	0,111	0,121
	3	0,126	0,110	0,096	0,111
	4	0,131	0,129	0,13	0,130
10SA/90LDH	1	0,086	0,105	0,107	0,099
	2	0,121	0,119	0,128	0,123
	3	0,121	0,121	0,127	0,123
0SA/100LDH	1	0,093	0,078	0,090	0,087
	2	0,097	0,080	0,118	0,098
	3	0,115	0,098	0,106	0,106
Blank	1	0,169	0,161	0,165	0,165
	2	0,158	0,163	0,150	0,157
	3	0,159	0,160	0,158	0,159
	4	0,160	0,149	0,159	0,156
70SA/30 Bentonite	1	0,102	0,096	0,096	0,098
	2	0,109	0,106	0,093	0,103
	3	0,096	0,108	0,106	0,103
70SA/30 Talc	1	0,13	0,124	0,133	0,129
	2	0,122	0,128	0,126	0,125
	3	0,117	0,112	0,120	0,116
Mg stearate*	1	0,143	0,164	0,151	0,153
	2	0,121	0,175	0,177	0,158
	3	0,137	0,142	0,126	0,135

* Mass % of Mg stearate in film is same as sum of SA and LDH

Table A-9 Various parameters calculated by the Nexygen software from Lloyd Instruments for the films shown in Figures 12-14 (Chapter 4).

Film composition	Sample number	Max Load/N	Deflection at Max Load/mm	Stress at Max Load/MPa	% Strain at Max Load	Work to Max Load/J	Stiffness/ (N/m)
100SA/0LDH	1	1,730	25,705	1,924	73,443	0,022	76,519
	2	1,802	34,210	1,720	97,743	0,031	63,276
90SA/10LDH	1	1,092	28,469	1,531	81,340	0,016	87,969
	2	1,444	32,694	2,007	93,410	0,023	81,120
	3	1,463	30,130	1,967	86,086	0,021	87,202
80SA/20LDH	1	1,548	25,785	2,080	73,672	0,022	142,204
	2	1,606	28,639	2,195	81,827	0,025	133,865
	3	1,565	24,390	1,942	69,686	0,022	275,982
70SA/30LDH	1	1,057	33,533	1,495	95,810	0,019	192,018
	2	0,950	28,367	1,432	81,049	0,015	203,714
60SA/40LDH	1	1,318	28,689	1,701	81,968	0,021	295,635
	2	1,317	28,620	1,726	81,772	0,021	235,382
	3	1,154	23,623	1,526	67,495	0,016	324,472
	4	1,385	27,553	1,773	78,723	0,021	248,483
50SA/50LDH	1	1,085	33,916	1,400	96,901	0,021	129,356
	2	1,206	34,131	1,520	97,516	0,023	157,327
	3	1,390	34,561	1,686	98,746	0,026	137,983
40SA/60LDH	1	1,121	37,242	1,349	106,407	0,023	109,635
	2	1,181	36,461	1,488	104,176	0,024	93,644
	3	0,872	23,578	1,223	67,366	0,012	75,461
30SA/70LDH	1	1,377	34,483	1,735	98,524	0,024	82,955
	3	1,105	24,928	1,606	71,222	0,015	99,109
10SA/90LDH	1	1,180	23,537	1,922	67,248	0,013	62,112
	2	1,755	34,777	2,301	99,364	0,028	69,010
	3	1,514	33,507	1,985	95,735	0,024	59,174
0SA/100LDH	1	2,030	28,099	3,763	80,283	0,027	92,840
	2	1,964	25,084	3,233	71,670	0,023	95,477
	3	2,493	31,625	3,793	90,356	0,036	96,515

Film composition	Sample number	Max Load/N	Deflection at Max Load/mm	Stress at Max Load/MPa	% Strain at Max Load	Work to Max Load/J	Stiffness/ (N/m)
Blank	1	2,824	42,433	2,761	121,236	0,048	102,815
	2	2,705	37,802	2,779	108,006	0,040	112,979
	3	2,941	39,267	2,983	112,193	0,046	121,961
	4	2,274	32,712	2,351	93,464	0,029	114,249
70SA/30 Bentonite	1	1,697	25,704	2,793	73,440	0,022	94,945
	3	1,442	27,319	2,258	78,054	0,020	69,240
70SA/30 Talc	1	1,326	42,225	1,657	120,642	0,026	39,624
	2	1,324	44,070	1,708	125,915	0,028	38,144
	3	1,107	37,835	1,539	108,101	0,020	37,683
Mg stearate*	1	1,101	34,950	1,161	99,857	0,023	221,533
	2	1,058	27,158	1,080	77,594	0,017	191,039
	3	1,303	31,532	1,556	90,091	0,022	145,907

* Mass % of Mg stearate in film is same as sum of SA and LDH

Table A-9 continued Various parameters calculated by the Nexygen software from Lloyd Instruments for the films shown in Figures 12-14 (Chapter 4).

Film composition	Sample number	Young's Modulus/MPa	Load at Break/N	Deflection at Break/mm	Stress at Break/MPa	% Strain at Break	Work to Break/J
100SA/0LDH	1	2,979	1,557	25,773	1,732	73,639	0,022
	2	2,114	1,622	34,938	1,548	99,822	0,032
90SA/10LDH	1	4,318	0,983	28,710	1,378	82,030	0,017
	2	3,948	1,299	32,982	1,807	94,233	0,024
	3	4,102	1,317	30,224	1,770	86,355	0,021
80SA/20LDH	1	6,690	1,393	25,908	1,872	74,023	0,022
	2	6,404	1,445	28,808	1,975	82,309	0,025
	3	11,984	1,408	24,558	1,747	70,165	0,022
70SA/30LDH	1	9,509	0,951	33,902	1,346	96,862	0,019
	2	10,748	0,855	28,683	1,289	81,950	0,015
60SA/40LDH	1	13,351	1,186	29,107	1,531	83,163	0,022
	2	10,803	1,185	29,011	1,554	82,888	0,021
	3	15,014	1,039	23,967	1,373	68,476	0,016
	4	11,133	1,246	27,685	1,595	79,101	0,021
50SA/50LDH	1	5,842	0,976	34,097	1,260	97,420	0,021
	2	6,939	1,086	34,345	1,368	98,128	0,023
	3	5,857	1,251	34,720	1,518	99,200	0,026
40SA/60LDH	1	4,619	1,009	37,359	1,214	106,740	0,024
	2	4,130	1,063	36,544	1,340	104,410	0,024
	3	3,704	0,785	23,911	1,101	68,318	0,012
30SA/70LDH	1	3,659	1,240	35,021	1,562	100,060	0,025
	3	5,040	0,995	25,299	1,445	72,283	0,015
10SA/90LDH	1	3,542	1,062	23,780	1,730	67,942	0,014
	2	3,167	1,579	35,106	2,071	100,304	0,029
	3	2,716	1,362	33,582	1,787	95,949	0,024
0SA/100LDH	1	6,024	1,827	29,124	3,387	83,213	0,029
	2	5,500	1,768	25,104	2,910	71,727	0,023
	3	5,140	2,244	31,698	3,414	90,565	0,036

Film composition	Sample number	Young's Modulus/MPa	Load at Break/N	Deflection at Break/mm	Stress at Break/MPa	% Strain at Break	Work to Break/J
Blank	1	3,518	2,542	42,501	2,485	121,431	0,048
	2	4,062	2,434	37,871	2,501	108,202	0,041
	3	4,330	2,647	39,361	2,685	112,461	0,046
	4	4,134	2,047	32,892	2,116	93,977	0,030
70SA/30 Bentonite	1	5,469	1,527	26,035	2,513	74,385	0,023
	3	3,795	1,298	27,428	2,032	78,365	0,020
70SA/30 Talc	1	1,734	1,193	42,976	1,492	122,788	0,027
	2	1,723	1,191	44,665	1,537	127,613	0,028
	3	1,834	0,996	38,882	1,385	111,092	0,021
Mg stearate*	1	8,174	0,991	35,511	1,045	101,461	0,023
	2	6,826	0,952	27,477	0,972	78,505	0,017
	3	6,101	1,172	31,725	1,401	90,643	0,022

* Mass % of Mg stearate in film is same as sum of SA and LDH